

Design Optimization of Vehicle Structures for Crashworthiness Improvement

Hesham Kamel Ibrahim

A Thesis

In the Department

of

Mechanical and Industrial Engineering

Presented in Partial Fulfillment of the Requirements

For the Degree of Doctor of Philosophy at

Concordia University

Montreal, Quebec, Canada

August 2009

©Hesham Kamel Ibrahim, 2009

CONCORDIA UNIVERSITY
SCHOOL OF GRADUATE STUDIES

This is to certify that the thesis prepared

By: **Hesham Kamel**

Entitled: **Design Optimization of Vehicle Structures for Crashworthiness Improvement**

and submitted in partial fulfillment of the requirements for the degree of

DOCTOR OF PHILOSOPHY (Mechanical & Industrial Engineering)

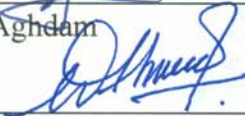
complies with the regulations of the University and meets the accepted standards with respect to originality and quality.

Signed by the final examining committee:


_____ Chair
Dr. E. Doedel


_____ External Examiner
Dr. M. El-Gindy


_____ External to Program
Dr. A. Aghdam


_____ Examiner
Dr. A.K.W. Ahmed



_____ Examiner
Dr. S.V. Hoa


_____ Thesis Co-Supervisor
Dr. R. Sedaghati


_____ Thesis Co-Supervisor
Dr. M. Medraj

Approved by 
_____ Dr. P. Wood-Adams, Graduate Program Director

August 14, 2009


_____ Dr. Robin A.L. Drew, Dean
Faculty of Engineering & Computer Science

Abstract

Design Optimization of Vehicle Structures for Crashworthiness Improvement

Hesham Kamel Ibrahim, Ph.D.

Concordia University, 2009

The complicated nature of the physical crash processes of complex vehicle structures makes design optimization for crashworthiness a very challenging task. Moreover, large scale and highly nonlinear nature of crashworthiness simulations of vehicle structure make it impractical to conduct direct optimization on the full nonlinear model of the structure. The main objective of the thesis is to present a systematic and practical methodology to conduct vehicle crashworthiness design optimization efficiently at early stages of design. The thesis includes four main parts. In the first part, an efficient and practical methodology for design optimization of vehicle structures under frontal impact for crashworthiness improvement is presented. The proposed methodology is based on identifying the main vehicle structural part contributing most to the total amount of impact energy absorbed in the whole vehicle structure. The computationally efficient surrogate model of expensive nonlinear finite element simulation of this major vehicle part is developed and then integrated with gradient based optimization algorithm to maximize its absorbed impact energy while guarding against increase in its weight. In the second part, a methodology for deriving the important relation between minimum structural weight and maximum impact energy is presented. The proposed methodology is based on the principle of the Pareto front and multiobjective optimization. The methodology enables the designer to evaluate the crashworthiness performance of any suggested design easily and effectively. Moreover, the methodology provides different optimum designs from which the designer can easily select the optimum design variables to improve the performance

of the initial design. In the third part, the crashworthiness behavior of simple thin walled structures and vehicle structural components made of magnesium due to its light weight is examined and a new methodology for material design optimization is presented. The proposed methodology adds material type as design variables to formal size design variables. Direct optimization using the genetic algorithm is conducted to find the optimum material combination and part's thicknesses to improve the crashworthiness performance of the vehicle structure. Finally in the fourth part, the effect of imperfection on crush elements performance is studied. Different imperfection configurations are proposed to improve the crashworthiness performance of crush elements. The genetic algorithm is directly combined with nonlinear finite elements models to search for optimum imperfection values. The results show that the crashworthiness performance of crush elements can be greatly improved through introduction of proper imperfection. Using the proposed methodologies, the current research presents a fundamental and systematic study to conduct design optimization of vehicle structures practically and efficiently.

Dedication

To my beloved wife and my two precious jewels, Yasmeen and Sara, I love you all.

Acknowledgments

First and foremost, all praise is to Allah.

I wish to express my sincere and deep gratitude to my supervisors Dr. Sedaghati and Dr. Medraj for their patient guidance and generous support during the whole process of this research. Your patience, understanding and humaneness have been of tremendous value to me. I sincerely wish you peace and happiness.

I also wish to express my appreciation to Dr. Hoa, Dr. Waizuddin Ahmed, Dr. Aghdam and Dr. El-Gindy for reviewing my work and serving on my committee.

Table of Contents

List of Figures	xiii
List of Tables	xvii
Nomenclature	xix
1 Introduction	1
1.1 Problem Statement and Motivation	1
1.2 Literature Review	6
1.2.1 Crash Characteristics	6
1.2.2 Accidents Types	7
1.2.2.1 Frontal Impact	7
1.2.2.2 Side Impact	8
1.2.2.3 Rear Impact	9
1.2.2.4 Rollover Accidents	9
1.2.3 Structural Requirements	9
1.2.4 Stability of the Axial Collapse	11
1.2.5 Crashworthiness Metrics	13
1.2.6 Modeling Simple Vehicle Structural Components	13
1.2.6.1 Analytical Approach	14
1.2.6.2 Empirical Approach	16
1.2.7 Modeling Vehicle Structures	19

1.2.7.1	LMS Models	19
1.2.7.2	Limitations of LMS Models	22
1.2.7.3	FE Models	23
1.2.7.4	Brief History of Nonlinear FE Softwares	25
1.2.7.5	MBD Models	27
1.2.7.6	Hybrid Models	28
1.3	Crashworthiness Improvement	29
1.3.1	Geometry Optimization for Crashworthiness	29
1.3.2	Material Optimization for Crashworthiness	32
1.3.2.1	Steel	32
1.3.2.2	Composite Materials	33
1.3.2.3	Aluminum	33
1.3.2.4	Magnesium	34
1.4	The Aim of the Present Work	35
1.5	Thesis Organization	37
2	Nonlinear Finite Element Modeling	39
2.1	Introduction	39
2.2	Overview of the FE method	40
2.2.1	Differences between Linear and Nonlinear FE Analyses	41
2.2.2	Sources of Nonlinearity	42
2.3	Nonlinear FE for Crashworthiness	42
2.3.1	Governing Equations	43
2.3.2	Direct Integration Methods	46
2.3.2.1	The Implicit Method	46
2.3.2.2	The Explicit Method	47
2.3.2.3	The Central Difference Method	47
2.3.3	Contact Algorithm	49

2.3.4	Friction	49
2.3.5	Shell Elements	49
2.3.5.1	The Belytschko-Lin-Tsay Shell (T2) Element	52
2.3.5.2	The Co-Rotational Method	53
2.3.5.3	Element Limitations	54
2.3.6	Material Models	55
2.3.6.1	Material Strain Rate Sensitivity	55
2.3.7	The Role of Imperfection in Nonlinear FE Analysis	56
2.4	Applications of the Nonlinear FE Analysis	57
2.4.1	Modeling Simple Vehicle Structural Components	57
2.4.2	Modeling Vehicle Structures	58
2.4.3	Modeling Full Vehicle Structure	58
2.4.4	Modeling Occupants	59
2.4.5	Modeling Pedestrians	60
2.5	Simulation of a Square Tube	60
2.5.1	Description of the Nonlinear FE model	61
2.5.2	Results and Discussion	62
2.5.2.1	Mesh Sensitivity Analysis	63
2.5.2.2	The Effect of Using Different Shell Elements	65
2.5.2.3	The Computational Time of Different Shell Elements	66
2.5.2.4	Snapshots of the Deformation History	67
2.5.2.5	The Effect of Imperfection	68
2.5.3	Conclusion	69
3	Optimization for Crashworthiness	70
3.1	Introduction	70
3.2	Meta-model Building	72
3.2.1	Design of Experiments (DOE)	73

3.2.1.1	Factorial	73
3.2.1.2	Koshal	74
3.2.1.3	Central Composite	74
3.2.1.4	D-optimal	74
3.2.1.5	Latin Hypercube Sampling	75
3.2.1.6	Random Numbers	75
3.2.1.7	Remarks on DOE Designs	76
3.2.2	Meta-Model Techniques	77
3.2.2.1	Response Surface Method (RSM)	77
3.2.2.2	Kriging	82
3.2.2.3	Neural Networks (NN)	82
3.2.2.4	Remarks on Meta-Model Techniques	85
3.3	Optimization of a Benchmark Analytic Function	86
3.4	Optimization of a Vehicle S-Rail	88
3.4.1	Problem Statement	88
3.4.2	Solution Approach and Results	89
3.5	Proposed Methodology	95
3.6	Illustrative Example	98
3.6.1	Identification of Major Influencing Components and Construction of Reduced Models (Stage 1)	99
3.6.2	Model Parametrization and Construction of the Approximate Model (Stage 2)	102
3.6.3	Optimization Problem Formulation (Stage 3)	105
3.6.4	Optimization of the Full Model	107
3.6.5	Discussion	108
3.6.6	Remarks	112
3.7	Summary	115

4	Vehicle Design Improvement using the Pareto Front	116
4.1	Introduction	116
4.2	The Pareto Front	117
4.3	Finding the Pareto Front	118
4.4	Proposed Methodology	122
4.5	Design Improvement of a Thin Walled Tube Using the Pareto Front	123
4.5.1	The Anti Pareto Front (APF)	129
4.6	Design Improvement of a Vehicle Chassis Frame Using the Pareto Front	131
4.7	Summary	136
5	Magnesium for Crashworthiness Improvement	138
5.1	Introduction	138
5.2	Design Optimization of a Thin Walled Tube	140
5.2.1	Material Variation of a Thin Walled Tube	143
5.2.2	Thickness and Material Optimization of a Thin Walled Tube	145
5.2.3	Thickness Optimization of a Thin Walled Tube	147
5.2.4	Comparing the Solutions of a Thin Walled Tube	149
5.3	Design Optimization of a Vehicle Chassis Frame	150
5.3.1	Material Variation of a Vehicle Chassis Frame	151
5.3.2	Thickness and Material Optimization of a Vehicle Chassis Frame	154
5.4	Summary	157
6	Investigation of Imperfection in Crush Elements	158
6.1	Introduction	158
6.2	Methodology	161
6.3	Results and Discussion	165
6.3.1	Manual Design of the (1C) Configuration	166

6.3.2	The Deformation States	167
6.4	Summary	170
7	Summary, Contributions, and Future Work	171
7.1	Summary and Conclusions	171
7.2	Contributions	173
7.3	Future Work	174
	References	176

List of Figures

1.1	Axial collapse mode	11
1.2	Bending collapse mode	11
1.3	Kamal’s LMS model	20
1.4	The static crush setup	21
1.5	A LMS model for frontal impact	21
1.6	Comparison between physical test results and a LMS model	22
1.7	A LMS model for a vehicle to vehicle impact simulation	22
1.8	The VW-POLO model	25
1.9	An early MBD model	27
1.10	A hybrid model of a side impact test	28
2.1	Shell element	53
2.2	CR kinematic description	54
2.3	View of the FE model of the square tube	61
2.4	Velocity vs time for element T2 using different mesh sizes	64
2.5	Final deformed shapes of the square tube	64
2.6	Deformation vs time for element T2 using different element sizes	65
2.7	Error values between specimen (I21) and simulations for all element types	66
2.8	Recorded computational time for all element types	67
2.9	Different snap shots of the deformation history	68
2.10	Comparison between two deformation profiles	69

3.1	Typical reaction force-time history in a frontal impact	71
3.2	The meta-model building process	72
3.3	A schematic drawing of a neuron	83
3.4	The Sigmoid activation function	83
3.5	A schematic drawing of a NN	84
3.6	View of the S-Rail	89
3.7	Iteration history of the optimization problem of the S-Rail	93
3.8	Iteration history of the constrained optimization problem of the S-Rail	94
3.9	Comparison between Design 1, Design 2 and baseline for Mass, IE and RWFmax	95
3.10	A flow diagram of stage 1	97
3.11	A flow diagram of stage 2	97
3.12	A flow diagram of stage 3	98
3.13	View of the Chevrolet C2500 pickup model	99
3.14	View of the chassis frame	100
3.15	Comparison between IE for major structural components	100
3.16	View of the FE model of the chassis frame	101
3.17	Impact energy absorbed by the chassis in full vehicle model and in the reduced model	101
3.18	Design variables on the chassis frame	102
3.19	Iteration history of the optimization problem of the reduced model	106
3.20	Iteration history of the optimization problem of the full model	108
3.21	Location of B-pillar	109
3.22	Comparison between design variables	110
3.23	Normalized IE versus Mass for the full vehicle	111
3.24	View of the mass response surfaces	112
3.25	The number of elements for modeling a full vehicle over 20 years	113

3.26	Different automobile objectives	114
4.1	A representative drawing of the Pareto Front	117
4.2	A scheme of a typical genetic algorithm	121
4.3	A schematic drawing of the methodology	122
4.4	View of the thin walled tube model	123
4.5	IE vs Mass for the thin walled tube	124
4.6	The PF and the fit for IE vs Mass for the thin walled tube	127
4.7	The PF and the APF for the thin walled tube	130
4.8	The PF of the chassis frame	134
4.9	The PF and the APF of the chassis frame	135
4.10	Comparison between IE and Mass for the two approaches	136
5.1	The design space after using the proposed concept	139
5.2	View of the nonlinear FE model of the thin walled tube	140
5.3	Final deformed shapes of the base, ST and SW designs of thin walled tube	142
5.4	Comparison between max (RWF) for the three configurations of thin walled tube	143
5.5	Comparison between Mass and IE for the different material combinations of the thin walled tube	144
5.6	Normalized IE versus normalized Mass for the genetic algorithm results for the thin walled tube	146
5.7	Iteration history of the thickness optimization problem for thin walled tube	149
5.8	Comparison between SEA for the base, T and TM designs for thin walled tube	150
5.9	Design variables on the chassis frame	150

5.10	Normalized IE versus normalized Mass for material variation for the chassis frame	153
5.11	Normalized IE versus normalized Mass for the genetic algorithm results for the chassis frame	155
6.1	A typical load curve	160
6.2	A view of the 1-C class model	161
6.3	A view of the 4-C class model	162
6.4	A view of the 2-S class model	162
6.5	A view of the 4-S class model	163
6.6	Load vs time of the baseline design	163
6.7	A comparison between <i>RWF</i> and <i>IE</i> for all configurations	166
6.8	A comparison between <i>RWF</i> and <i>IE</i> for different design cases	167
6.9	States of deformation for all configurations	168
6.10	Two deformed states of the (2S_D) configuration: (a) Start of the global bending mode (b) Final deformed state	169
6.11	The reaction force history for the (2S_D) configuration	170

List of Tables

2.1	Shell elements in LS-DYNA	50
3.1	Values of $adjR^2$ for different response surface models of the Rosenbrock function	87
3.2	Full scale and prototype model parameters for the S-Rail	90
3.3	Material properties of the S-Rail	91
3.4	The design matrix of the response surface model for the S-Rail	91
3.5	Values for $adjR^2$ for different RSM models for the S-Rail	92
3.6	FE model parameters of the vehicle model	99
3.7	The design matrix of the response surface model for the chassis frame	103
3.8	Comparisons between $adjR^2$ for different RSM models of the chassis frame	105
3.9	Comparisons between $adjR^2$ for the different RSM models of the full vehicle	107
4.1	Parameters of the nonlinear FE model of the thin walled tube	123
4.2	The design matrix of the response surface model for thin-walled tube	125
4.3	Values for $adjR^2$ for different RSM models for the thin walled tube	126
4.4	Values for Mass, IE and their associated design variables for the PF of the thin walled tube	128
4.5	Values for Mass, IE and associated design variables for the PF of the chassis frame	131

5.1	Model parameters of the nonlinear FE model of the thin walled tube	141
5.2	Comparison between Mass and IE of the base, ST, and SW designs for thin walled tube	142
5.3	Results for material variation for thin walled tube	144
5.4	Design matrix of the RSM model for the thin walled tube	147
5.5	The $adjR^2$ values for the different RSM models for thin walled tube .	148
5.6	Results for material variation for the chassis frame	151
5.7	ΔIE and $\Delta Mass$ and associated design variables for designs A, B and C for the chassis frame	156
6.1	Values for IE, RWF and design variables for the different configurations	165

Nomenclature

Roman symbols

A_0	overall section area defined by the outer circumference [m^2]
$adjR^2$	adjusted coefficient of determination
$ampl$	amplitude of imperfection [m]
b	rectangular tube width [m]
C	square tube edge width [m]
$[C]$	structural damping matrix [$N.sec.m^{-1}$]
$[c]$	element damping matrix [$N.sec.m^{-1}$]
D	Cowper Symonds parameter [sec^{-1}]
$\{D\}$	structural nodal displacements [m]
$\{\dot{D}\}$	structural nodal velocities [$m.sec^{-1}$]
$\{\ddot{D}\}$	structural nodal accelerations [$m.sec^{-2}$]
d	rectangular tube height [m]
$\{d\}$	nodal functions of time
E	Young's modulus of elasticity [Pa]
E_s	specific energy [J/kg]
E_r	Maximum energy that can be absorbed by the structure [J]
\hat{e}_1, \hat{e}_2	inplane unit vectors
\hat{e}_3	normal unit vector
$\{F\}$	vector of element body forces [N]
$f(x)$	polynomial function
IE	impact energy absorbed [J]

$[K]$	structural stiffness matrix [$N.m^{-1}$]
k_p	crippling coefficient
L	summation of squared errors
l	element length [m]
$[M]$	structural mass matrix [kg]
M_0	fully plastic moment [N]
MSE	mean squared errors
$[m]$	element mass matrix [kg]
$[N]$	shape functions of space
P_m	mean crush force [N]
$\{p\}_i$	vector of concentrated loads [N]
q	Cowper Symonds parameter
R	circuclar tube mean radius [m]
RWF	rigid wall force [N]
R^2	coefficient of determination
$\{R^{ext}\}$	vector of structural external forces [N]
$\{r^{int}\}$	vector of element inetrnal forces [N]
r^{ext}	vector of element external forces [N]
$S_e,$	element surface [m^2]
S_{max}	maximum crushing strength [Pa]
SSE	sum of squared errors
SST	sum of total squares
t	tube thickness [m]
$\{u\}$	element displacement field [m]
V_e	element volume [m^3]
V_m	material volume [m^3]
V_s	volume enclosed by the structural section [m^3]

v	axial impact velocity [$m.sec^{-1}$]
v_{ac}	acoustic wave speed through element material [$m.sec^{-1}$]
W	weight [kg]
wvl	wave length of imperfection [m]
X	design matrix
y	true response
\hat{y}	approximate response

Greek symbols

β	vector of unknown coefficients
γ	material strain hardening factor
Δt	time step
$\{\delta\epsilon\}$	vector of element strains
$\delta(U)^e$	element internal energy [J]
$\{\delta u\}$	vector of element displacements [m]
δW^e	external work done on an element [J]
ϵ	error between true and approximate responses
η	structural effectiveness
Γ_0	base configuration
Γ_D	current configuration
Γ_{CR}	Corotational configuration
κ_D	material damping parameter [$N.sec.m^{-1}$]
$\kappa(x)$	stochastic function
ρ	density [$kg.m^{-3}$]
ν	Poisson's ratio

σ_0	average flow stress [Pa]
σ_d	dynamic flow stress [Pa]
σ_u	tensile strength [Pa]
σ_{us}	specific ultimate strength [Pa]
σ_y	yield strength [Pa]
$\{\sigma\}$	vector of element stresses [Pa]
$\{\Phi\}$	vector of prescribed surface tractions [$N.m^{-2}$]
ϕ	relative density

Chapter 1

Introduction

1.1 Problem Statement and Motivation

Each year more than one million people are killed in road accidents [1]. In Canada in 2006, nearly two hundred thousands were injured in road accidents [2], bringing an estimate of \$63 billion in social costs [3]. The majority of fatalities and serious injuries occurred due to frontal vehicle collisions [4].

Consumers have become highly aware of the importance of vehicle safety which has made it a major influencing factor in vehicle sales. Moreover, the competitive nature in the automobile sector makes each company always strive to develop safer vehicles. Considering this, safety is of paramount importance in modern vehicle design and according to Khalil and Du Bois [5], crashworthiness is the first analysis to be completed in modern vehicle design.

The nonlinear finite element method is the state of the art tool in modern vehicle design for safety. This method enables the designer to investigate different designs easily and reliably. This is very important especially at the initial design stages, at which the design is uncertain and different alternatives are to be tested. Another

advantage of the nonlinear finite element method is that, it reduces the total number of prototype testing. This is also very important, since vehicle crash tests are expensive and time consuming. For instance, a physical crash test may take on average 36 hours to prepare and a male dummy costs approximately \$30,000 without instrumentation [6].

The nonlinear finite element method is extremely computationally expensive. This is due to the complex nature of vehicle structures. A typical vehicle structure consists of many parts with complex shapes made of different materials. During an accident, parts go through large deformations and stresses exceed materials elastic limits into plastic regions. Furthermore, parts are pressed against each others under the large forces of impact. This produces contact forces and friction between these parts. Finally, the whole accident occurs during very short time (about 100 ms). Considering this, the nonlinear finite element method requires sophisticated modeling, which in turn demands huge calculations. For example, a simulation of full frontal impact of a full vehicle model may last for more than half a day [7].

In addition to safety, there are numerous design objectives (fuel economy, space, comfort, etc.). An acceptable vehicle design must meet safety requirements and all other design objectives. This means that an ad-hoc approach can no longer be applied to vehicle design, and instead, optimization must be applied. Optimization is a numerical technique that systematically and automatically searches the design space through numerous iterations to find an optimum feasible solution. This constitutes a problem in vehicle design for safety due to the large computational cost of nonlinear finite element analysis. Moreover, the gradient based optimization technique requires gradients of the objective and constraint functions, which cannot be obtained analytically due to the complexity of the problem. Numerical evaluation of these gradients may also fail or generate spurious results due to the high frequency noisy nature of the responses. Also, in the case of using nongradient based algorithms such as genetic

algorithms, a much larger number of iterations is required compared with gradient based techniques. Considering this, applying optimization algorithms directly to the nonlinear finite element model is not practical and an alternative method based on approximation techniques should be investigated.

Approximation techniques are used to create approximate mathematical models of complicated models, and they are sometimes called meta-models (models of models). Basically, the idea is to collect sample points of the design space and then use them to create the approximate models. Design of experiments is used to minimize the number of the required sample points. Approximate models can be used to predict the crash responses instead of performing the complex nonlinear finite element analysis. Moreover, approximate models smooth the captured response by modeling the global behavior and ignoring the high frequency numerical noise which is usually present in typical vehicle crash responses. Subsequently, approximate models can be used with any gradient based optimization technique. They can also be used with nongradient based optimization techniques, since their computational cost is very small compared to the nonlinear finite element model. The Response Surface Method (RSM) is one of the approximation techniques that has been successfully used by many researchers to model the important crash responses.

RSM has been used mainly for vehicle component models. This may cause a problem, since optimizing a component separated from the vehicle does not necessarily guarantee that the optimized component will behave optimally when integrated in the full vehicle. Another problem with RSM design optimization is that, the number of design points required to build RSM models increases rapidly as the number of design variables increases. This is known as the curse of dimensionality [8] which in turn limits the possibility of using RSM with full vehicle nonlinear finite element models. Developing an efficient design optimization technique for full vehicle structures is a challenging task that has not yet received sufficient attention.

Considering the aforementioned issues, the main objective of the present research is to develop an efficient and practical methodology for design optimization of full vehicle nonlinear finite element models. The proposed methodology is based on the efficient and effective integration of optimization algorithm, nonlinear finite element analysis, and approximation methods. Using the proposed methodology, practical approximate models of vehicle structural components are created and then used for design optimization of the full vehicle structure for crashworthiness improvement. Thus, optimum designs can be obtained at a very modest computational cost. This is very useful, especially at initial design stages. Applying optimization at early design stages has been proven to be an efficient means for improving product design at even later design stages [9]. Chen and Usman [10] mention that implementing optimization at early design stages will help in improving the manufacturing process and also in reducing the number of required tests and prototypes, which will ultimately reduce the total product cost.

A problem in modern vehicle design for crashworthiness is the ability to evaluate the performance of a specific design easily and quickly. In modern vehicle design for crashworthiness, the main goal is to maximize the amount of impact energy absorbed in vehicle structure and at the same time minimize its weight. Thus, it is important to find if a design absorbs the maximum amount of impact energy for its current weight or not. In this thesis, a new methodology is proposed to derive the relationship between maximum amount of impact energy absorbed and minimum weight. The methodology is based on the principle of the Pareto front and multiobjective optimization. The derived relationship can then be used to find if a design is optimum or not. The proposed methodology also provides the designer with the optimum design variables that can be used to optimize the performance of any sub-optimum design.

Weight reduction is a very important goal in modern vehicle design. Reducing weight

will lower fuel consumption and consequently carbon emissions. Recently, magnesium has received a considerable attention from automobile manufacturers due to its low density. A considerable amount of research has been published on the development of new magnesium alloys. However, few research has been made on the crashworthiness response of vehicle structural parts made of magnesium alloys. In this thesis, the behavior of vehicle structural parts made of magnesium alloys under dynamic impact loading is analyzed. In addition, a methodology is proposed for including material type as a design variable in design optimization for crashworthiness improvement. This will provide the designer with a wider selection of design solutions than when conducting a conventional design optimization that uses only parts thicknesses as design variables.

Thin walled columns are typically used as add-on crash energy absorbing systems and are usually called crush elements. During a frontal collision, they help in absorbing part of the amount of impact energy and more importantly they reduce the impact forces transmitted to the occupants. This is very important since very large forces can cause irrecoverable brain damage. Thus, crush elements help in reducing the risk of brain injuries and in improving the crashworthiness performance of the whole vehicle. For optimum performance, crush elements must deform in a progressive buckling mode under impact. To initiate this mode of deformation, geometrical imperfections are intentionally introduced to the crush elements shape. This is typically made by simple chamfering. In this thesis, different new configurations are presented and their effect on crush elements performance is systematically studied. To achieve optimum performance of crush elements, design optimization is conducted to find the optimum values of imperfection shape parameters.

1.2 Literature Review

Crashworthiness is an engineering term used to define the ability of vehicle structure to protect its occupants during an impact [11]. Crashworthiness is not limited to automobiles only, it is also applied to other transportation vehicles, such as ships, planes, and trains. In fact, the first systematic and scientific investigation of the subject was applied to railway axles between 1879 to 1890 by Thomas Andrews [12]. In other words, crashworthiness is the process of improving the crash performance of a structure by sacrificing it under impact for the purpose of protecting occupants from injuries [13]. To improve the structure design for crashworthiness, it is required to understand the different factors affecting the crash process. In the following, different fundamental aspects of design for crashworthiness have been described and pertinent works have been reviewed.

1.2.1 Crash Characteristics

Accidents occur in a random manner. An automobile can be impacted from any direction at different speeds. It can also include an automobile impacting another automobile, which in turn can be the same or different from the first automobile. This shows how automobiles affect and being affected by each other in crash situations [6]. An automobile can also impact a rigid barrier, a tree, a light post... etc, which may lead to severe deceleration and high loads, as a rigid body can not deform to absorb part of the impact energy. An automobile can also impact a pedestrian which leads to the importance of design for pedestrian safety as well, and finally an automobile can go into rollover accidents. According to Galganski [14], crashworthiness problems can be characterized by:

1. Displacement and energy: Frontal structure length is being reduced by modern

design styles and at the same time, it is required to absorb most of the impact energy and to minimize intrusion into the compartment.

2. Crash pulse: Crash pulse is the deceleration induced by impact on the human body. Head injury criterion (HIC) is used to measure the damage from crash pulse on the brain, and it should be less than a certain limit by regulations [15].
3. Crash position: The structure should be able to mitigate injuries in different crash positions such as full frontal impact, offset frontal impact, side impact, rear impact, and rollover.
4. Automobile compatibility: With different automobile models, the structure should be able to mitigate injuries resulting from an accident involving two different automobiles, which can differ in size and/or weight.

1.2.2 Accidents Types

1.2.2.1 Frontal Impact

Frontal impact can be realized in two stages: In the first stage, the vehicle strikes a barrier or another vehicle which causes front to end crush and the kinetic energy is dissipated into deformation of the structure. In the second stage, the occupant continues to move freely against the interior if not restrained, or interacts with restraint system, if restrained. The kinetic energy is then transformed into interior deformation of the structure and compression to the occupant's body. Finally, the remaining kinetic energy is dissipated as the occupant decelerates with the vehicle.

Injuries may occur during the second stage in case the impact loading is high enough beyond the safety limits. A good design should ensure that the kinetic energy is dissipated gradually to minimize injuries.

Safety measures, such as using energy absorbing materials to cover the interior parts, seat belts, and air bags are important in reducing injuries due to interaction between the occupant and the interior.

To provide the minimum level of safety, automobile manufacturers are obliged by law to ensure that their designs comply with governmental regulations. Automobile manufacturers must demonstrate that their vehicles are in compliance with safety standards before they are sold. For frontal collisions, vehicle designs are regulated by FMVSS 208 in the U.S., by CMVSS 208 in Canada, and by ECE R-12 in Europe [16–18].

1.2.2.2 Side Impact

Side impact is the second most frequent mode of accidents. It is defined as the incident when a striking vehicle hits a target vehicle in the area of one or more of its pillars, during which the kinetic energy is transformed into deformation of both vehicles. The side impact can be described in two stages as has been described in frontal impact. However, in side impacts, restraint systems play less role in protecting the occupant due to the proximity of the occupant to the interior (doors). The stiffness of the side structure plays a major role in occupant's safety, i.e., it must be strong to resist intrusion. The cross bars are also important in controlling the deformation to protect the occupant. Finally, the inside layout is an important factor as well in minimizing injuries due to interaction between the occupant's body and the vehicle interior. For side impacts, vehicle designs are regulated by FMVSS 214 in the U.S., by CMVSS 214 in Canada, and by ECE R-59 in Europe [16–18].

1.2.2.3 Rear Impact

Although the number of rear impacts is much less than the number of front or side impacts, the whiplash injuries caused by this types of accidents are complicated, hard to recover from, and can cause fatalities [19]. For safety against rear impact, special attention must be given to the structural integrity of the fuel tank and fuel lines, seat resistance especially seat backs, and to head restraints. For rear impacts, vehicle designs are regulated by FMVSS 224 in the U.S., by CMVSS 224 in Canada, and by ECE R-42 in Europe [16–18].

1.2.2.4 Rollover Accidents

In rollover accidents, the whole vehicle structure along with vehicle interior must protect occupants from injuries. Seat belts are particularly important in these accidents and the roof must provide resistance to deformation. During rollover accidents, the doors must not open by themselves and special valves must ensure that fuel lines are closed and fuel ventilation is directed to a charcoal canister to prevent fire hazards [6]. The study of rollover is of special interest to heavy vehicles and trucks since their relatively higher center of gravity makes them more susceptible to this kind of accidents. This type of accidents can be prevented by controlling vehicle dynamic responses during driving and braking performance, as reported by El-Gindy et al. [20, 21]. For rollover accidents, vehicle designs are regulated by FMVSS 201 and 208 in the U.S., by CMVSS 201 and 208 in Canada, and by ECE R-21 in Europe [16–18].

1.2.3 Structural Requirements

By definition, crashworthiness is the measure of the structure’s ability to protect the occupants during impact, therefore the structure must fulfill some requirements, that are summarized in the following:

- The structure must absorb as much impact energy as possible by plastically deforming in a controllable manner to minimize the remaining impact energy which can then be handled by the restraint system.
- The structure must preserve at least the minimum survival space to keep injury and fatality levels as low as possible.

A good design should achieve these two goals simultaneously and at the same time, it must adhere to other design objectives, e.g., comfortabilty, accessibility, weight, fuel consumption,...etc. Thus, the full design process is very complicated and requires high levels of communication between different disciplines.

In order to achieve these goals, a good understanding of the structural deformation process and its mechanism should be maintained. Generally, the deformation (collapse) modes of the structure can be divided in two modes:

1. Axial collapse mode characterized by regular accordion type folding or irregular crumpling of the walls of the structure.
2. Bending collapse mode where discrete plastic hinges are formed and the structure collapses around them in a linkage type fashion.

Pure axial collapse as shown in Figure 1.1 is the most desirable collapse form, as it includes the absorption of the maximum amount of energy. An axial collapse, also called progressive buckling, involves formation of complete folds along the beam/tube. However, it is the most difficult to achieve and it can be realized only during a head on collision, direct front-rear accidents, or slightly off-angle ($5^\circ - 10^\circ$) impacts.

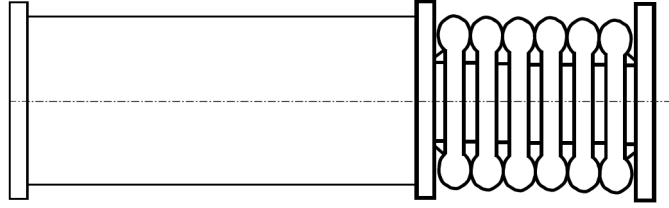


Figure 1.1: Axial collapse mode

On the other hand, the bending collapse mode is the most frequent to occur as it has the least energy path during an impact, and the structure will follow this path unless it is well designed to be forced into the axial collapse mode. As shown in Figure 1.2, this mode involves a global bending initiated by building up of stress concentration at a weak point until yield is exceeded and the structure bends around this point. Therefore, the design must not allow this building up of stress concentration and maintains a uniform deformation along the component length, which leads to the issue of the stability of the axial collapse.

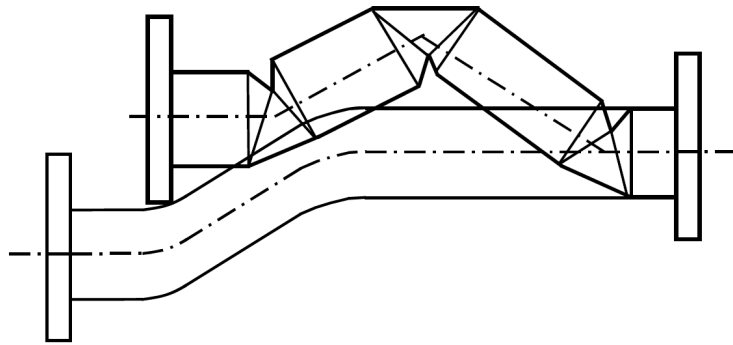


Figure 1.2: Bending collapse mode

1.2.4 Stability of the Axial Collapse

The axial collapse is the most efficient mode of deformation and it is also the most difficult to attain. A structure that starts to deform axially can suddenly buckle in the global bending mode, causing a significant drop in the capacity of the structure to

absorb the impact energy. This behavior may completely alter the crash performance of the structure, hence it is important to understand the mechanics of this transition so that proper measures can be taken to avoid it.

Very few research has been conducted in this area despite its great importance to the subject of design for crashworthiness, which can be explained by the high level of complexity of the subject and due to the many factors involved. It has been shown that the loss of stability can be attributed to the sharp reduction of bending stiffness of the locally deformed portion of the tube, which causes the tube to buckle in a global manner when a certain critical collapsed length is reached [22].

Abramwicz and Jones [22] studied the transition between global bending to progressive buckling of statically and dynamically loaded tubes. This transition is important since the amount of the absorbed impact energy is significantly different in each case. Based on numerous test results, they proposed two empirical formulas for square and circular steel tubes as:

$$\left(\frac{L}{C}\right)_{cr} = 3.423e^{\left(\frac{0.04C}{t}\right)} \quad (1.1)$$

$$\left(\frac{L}{2R}\right)_{cr} = 3.355e^{\left(\frac{0.032R}{t}\right)} \quad (1.2)$$

Eq.(1.1) provides the critical length to width ratio for square tubes while Eq.(1.2) gives the critical length to diameter ratio for circular tubes. If length to mean diameter or edge width of tubes are higher than the above critical values, the tubes will undergo global buckling [22].

1.2.5 Crashworthiness Metrics

Crashworthiness is measured by different metrics depending on the type of analysis being conducted. There are mainly three types of analyses [6]:

Structural analysis, in which the structure response under impact is of engineering concern. In this type of analysis, the amount of Impact Energy (IE) absorbed is of paramount importance as the larger the value, the safer the design. The main objective of the design process is to increase IE. Dividing IE by the structural mass is called the Specific Energy Absorbed (SEA), which represents the amount of energy absorbed with respect to the structural mass. It is basically used to compare the efficiency of different structures. Another important quantity is the peak reaction force achieved during impact. The objective of the design process is to limit peak values since higher peak values can induce large deceleration values which may cause irrecoverable brain damage.

Injury analysis, in which the effect of impact on the occupants is considered. This effect is determined by the injury tolerance limits determined from bio-mechanics. This type of analysis also studies the interaction between occupants and vehicle interior under crash situations, and how restraint systems can limit the level of injury severity.

Pedestrian injury analysis, in which the effect of impact on pedestrians is studied. This type of analysis is concerned with improving the vehicle bumper, hood and windshield designs in order to minimize injuries to pedestrians.

1.2.6 Modeling Simple Vehicle Structural Components

Vehicle structures are mainly composed of thin walled members. Researchers have used both analytical and experimental approaches to study the behavior of simple

thin walled tubes under impact. Brief discussions of these approaches are provided in the following sections.

1.2.6.1 Analytical Approach

The work for developing analytical models of thin walled tubes under axial impact was pioneered by Alexander [23]. He derived a simple analytical equation for calculating the mean impact force needed to plastically deform a thin wall cylindrical tube. He equated the required work to deform the walls of the tube into folds with the mean impact force multiplied by the amount of deformation, and derived the following equation:

$$P_m = Ct^{1.5}\sqrt{D} \quad (1.3)$$

where

P_m	Mean crush force
C	A constant to be determined by experiments
t	Wall thickness
D	Mean diameter

His equation was later improved to model the mechanics and the kinematics of the folding process of the axial collapse mode [24, 25]. The models involved simple relations between the important crash characteristics and the component geometry and material properties. These models were based on simplifying assumptions, such as, the neutral surface does not stretch nor shrink, which limited the models prediction capabilities. Later on, Wierzbicki and Abramowicz [26] developed an analytical approach to the crushing response of thin walled columns, based on the plasticity theory. Using the energy balance between external load and internal work exerted by the deforming parts, they developed an equation for the mean crushing load as:

$$P_m = 38.12M_0C^{1/3}t^{-1/3} \quad (1.4)$$

where

P_m	Mean crush force
$M_o = \sigma_0 t^2 / 4$	Fully plastic moment
$\sigma_0 = (0.9 - 0.95) \sigma_u$	Average flow stress
σ_u	Ultimate tensile strength of the material
$C = (b + d) / 2$	b and d are sides of a rectangular box column
t	Wall thickness

For a square tube, where $C = d = b$, Eq.(1.4) becomes:

$$P_m = 9.53\sigma_0 t^{5/3} b^{1/3} \quad (1.5)$$

and for a circular tube, where R is the mean radius:

$$P_m = 2(\pi t)^{3/2} R^{1/2} \sigma_0 / 3^{1/4} \quad (1.6)$$

In the above equations, the influence of the inertia forces is neglected as they are relatively small in comparison with the static crushing load. It is also assumed that the static flow stress (σ_0) is independent of the strain rate. This latter simplification neglected the fact that some materials exhibit a change in response under impact loading due to the change in the strain rate. This behavior is referred to as material strain rate sensitivity.

Material strain rate sensitivity is the phenomena in which the dynamic flow stress (σ_d) depends on the strain rate ($\dot{\epsilon}$). Cowper and Symonds [27] proposed a constitutive equation to calculate the dynamic flow stress (σ_d) as a function of static flow stress (σ_0), strain rate ($\dot{\epsilon}$), and two material parameters q and D which, can be described as:

$$\sigma_d = \sigma_0 \left[1 + \left(\frac{\dot{\epsilon}}{D} \right)^{1/q} \right] \quad (1.7)$$

Abramwicz and Jones [28] updated Eq.(1.6) to account for strain rate sensitivity using Eq.(1.7) and reached an analytical formula for P_m as:

$$P_m = 2 (\pi t)^{3/2} R^{1/2} \sigma_0 \left[1 + \left(\frac{V}{4RD} \right)^{1/q} \right] / 3^{1/4} \quad (1.8)$$

where V is the axial impact velocity. It is noted that when D approaches infinity for strain rate insensitive materials, Eq.(1.8) reduces to Eq.(1.6). They also introduced another equation for calculating P_m for square tubes as:

$$P_m = 13.05 \sigma_0 t^2 (C/t)^{1/3} \left[1 + \left(\frac{0.33V}{CD} \right)^{1/q} \right] \quad (1.9)$$

1.2.6.2 Empirical Approach

Other researchers followed another approach, instead of purely analytical, they used experimental data of crushed tubes to develop empirical relations. Magee and Thornton [29] used crush test data of different columns (steels ranging in tensile strength from 276 to 1310 MPa, aluminum alloys and composites) of several different section geometries and developed a relationship for the mean crush load for circular tubes as:

$$P_m = \eta \sigma_u \phi A_0 \quad (1.10)$$

where

$\eta = \frac{E_s}{\sigma_{us}}$	Structural effectiveness
$E_s = \frac{E_r}{W}$	Specific energy
E_r	Maximum energy that can be absorbed by the structure
W	Weight
$\sigma_{us} = \frac{\sigma_u}{\rho}$	Specific ultimate strength
σ_u	Ultimate strength
ρ	Density
$\phi = \frac{V_m}{V_e}$	Relative density
V_m	Material volume
V_e	Volume enclosed by the structural section
A_0	Overall section area defined by the outer circumference

For square tubes, where b is the edge width and t is the thickness, the relation is:

$$P_m = 17t^{1.8}b^{0.2}\sigma_u \quad (1.11)$$

Equations (1.10 and 1.11) have a drawback as the material elasticity is not taken into consideration. Thus, for two materials having the same ultimate strength, they exhibit the same mean crush load. Mahmood and Paluszny [30] proved that this contradicts test findings. They developed a quasi-analytical approach, in which they assumed that a thin walled square tube is a composition of plate elements subjected to compression and will buckle locally only when critical stresses are reached. The process starts with local buckling of some elements and finally leads to folding of the tube. The section collapse strength is related to its thickness to width ratio (t/b) and to its material properties. For very small sections, called (non-compact) sections ($t/b = 0.0085 - 0.016$), the collapse mode will be governed by geometry as its local buckling strength is considerably less than its material yield strength [30]. For larger (t/b) values (compact sections), material properties govern the mode of collapse as the local buckling strength exceeds material yield strength. In general, the collapse mode will be governed by a combination of geometry and material properties, in which the

maximum crushing strength of the section (S_{max}) is given by [31]:

$$S_{max} = \left[k_p E (t/b)^{1/2} \right]^n \left[(1 - \nu^2) \gamma \sigma_y \right]^{-n} \sigma_y \quad (1.12)$$

where

- k_p The crippling coefficient and it is a function of the degree of restraint at the longitudinal edges
- n Exponent that is influenced by the degree of warping and lateral bending of the unloaded edges (corners)
- E Young's modulus of elasticity
- σ_y Material yield strength.
- γ Material strain hardening factor

The maximum loading capacity P_{max} of a section can be calculated by multiplying Eq.(1.12) by the cross section area. Hence for a rectangular section with thickness t and sides b and d , the area is $(2tb(1 + \alpha))$, where $\alpha = d/b$ is the aspect ratio and thus P_{max} can be given as:

$$P_{max} = 2 \left[k_p E / \gamma (1 - \nu^2) \right]^{0.43} t^{1.86} b^{0.14} (1 + \alpha) \sigma_y^{0.57} \quad (1.13)$$

For a square steel column ($\alpha = 1$, $k_p = 2.11$, $\nu = 0.3$ and $E = 30 \times 10^6$ psi), Eq.(1.13) yields to:

$$P_{max} = 9425 t^{1.86} b^{0.14} \gamma^{-0.43} \sigma_y^{0.57} \quad (1.14)$$

The expressions for mean crushing stress (S_m) and mean crushing load (P_m) of a square steel tube can be given by [31]:

$$S_m = \left[k_p E (t/b)^2 / (1 - \nu^2) \gamma \right]^{0.43} \sigma_y^{0.57} \quad (1.15)$$

$$P_m = 3270t^{1.86}b^{0.14}\gamma^{-0.43}\sigma_y^{0.57} \quad (1.16)$$

1.2.7 Modeling Vehicle Structures

In the previous section, models of only simple thin walled tubes under axial loading have been presented. However, these simple models cannot be used to predict the behavior of complicated vehicle structures under different loading conditions. The automobile manufacturers have fueled the research for developing reliable models that can accurately predict the behavior of vehicle structures under impact. This is due to the fact that, vehicle safety certification is a complicated process that requires numerous tests. For example, for a car to meet the safety requirements for frontal impact, it must pass a rigid barrier crash at 0, +30 and -30 degrees at 30 mph according to FMVSS 208 [16] and at 35 mph at 0 degrees according to the New Car Assessment Program (NCAP) [32]. These tests are expensive and time consuming and considerable research has been devoted to develop reliable models to reduce the number of required tests. The current modeling techniques can be divided as follows:

1. Lumped Mass Spring (LMS) models
2. Finite Element (FE) models
3. Multi Body Dynamics (MBD) models
4. Hybrid models

In the following sections, a brief overview of each modeling technique is presented.

1.2.7.1 LMS Models

A simple and yet a relatively accurate model was developed by Kamal [33] in 1970. This model became widely known as the Lumped Mass-Spring (LMS) model. This

model succeeded in simulating the response of a full automobile in a full frontal impact with a rigid wall. The model as shown in Figure 1.3, approximates the vehicle by a system of lumped masses and springs.

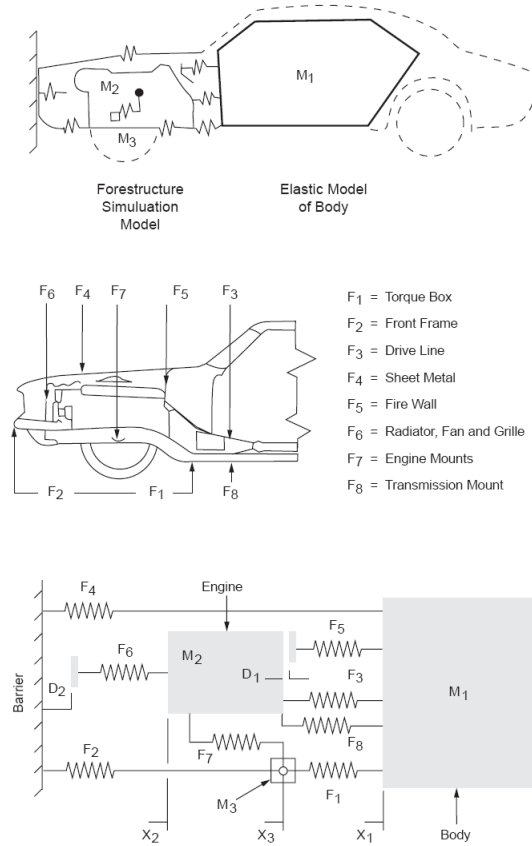


Figure 1.3: Kamal's LMS model [33]

The model is quite simple, however, it requires an extensive knowledge and understanding of structural crashworthiness from the user and also a considerable experience in determining the model parameters and translating the output into design data. Moreover, the model also requires that spring parameters to be determined from physical experiments using the static crush setup as illustrated in Figure 1.4.

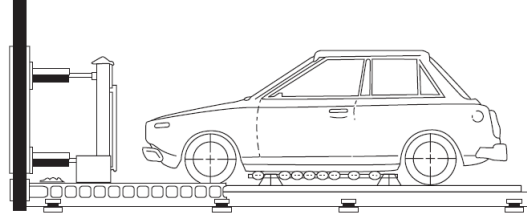


Figure 1.4: The static crush setup [34]

LMS models have been used successfully in the simulations of front, side and rear impact vehicle crashes [35–37]. Figure 1.5 shows a LMS model for simulating a vehicle hitting a rigid wall barrier at 56 km/h. The model parameters were identified from an actual rigid wall test from which masses and springs stiffnesses were tuned in order to achieve the best agreement with test results. Figure 1.6 shows a sample comparison between the acceleration histories of the actual test results and the results from the LMS model. Figure 1.7 also shows a LMS model of a bullet car impacting a target car from the side at 50 km/h.

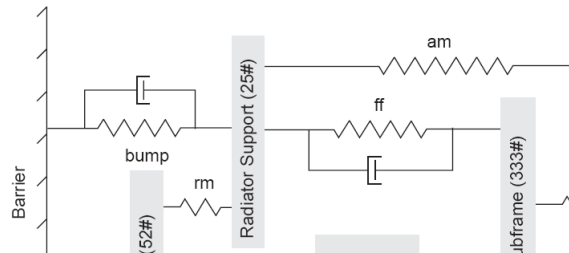


Figure 1.5: A LMS model for frontal impact [38]

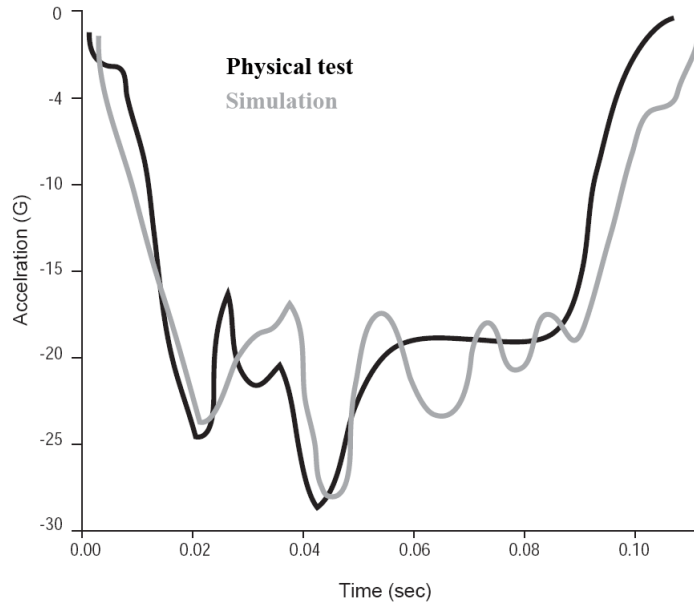


Figure 1.6: Comparison between physical test results and a LMS model [38]

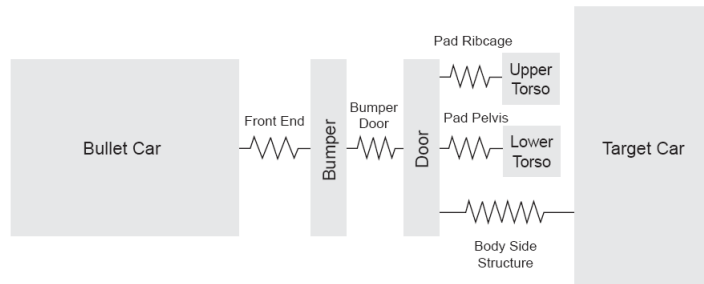


Figure 1.7: A LMS model for a vehicle to vehicle impact simulation [37]

1.2.7.2 Limitations of LMS Models

LMS models are easy tools for developing energy management systems. The designer can use LMS models to develop design guidelines for component placements. LMS models also enable the designer to understand the mechanics and the influencing factors of collision such as impact speed, mass ratio and structural stiffnesses of colliding vehicles. Deceleration time history, amount of energy absorbed by vehicle structure and the amount of deformation can be easily calculated. However, LMS

models have their limitations which can be summarized as follows [39]:

- A prime limitation of the LMS models is that they require a prior knowledge of the spring characteristics of the system, thus they are ineffective for developing new models.
- The development of an accurate model highly depends on the developer experience, skill, and understanding of the crash mechanics.
- LMS models with one degree of freedom for each component are only limited for predicting the behavior in the longitudinal direction. For example, the behavior due to a mis-alignment in the horizontal or in the vertical planes can not be captured. In addition, problems involving offset or angular impact can not be simulated. Three dimensional LMS models have been developed to overcome this restriction [40, 41] .

1.2.7.3 FE Models

The application of the nonlinear FE method in crashworthiness analysis is described in detail in Chapter 2. In the following, an overview of the application of nonlinear FE models to crash problems is presented.

Some research has been conducted to investigate the use of the implicit method in crash simulations. A pioneering article was published in 1981 by Winter et al. [42], in which a head-on collision of a vehicle frontal structure with a rigid wall was simulated using the implicit code DYCAST [43]. In this model, the left half of the vehicle was represented by 504 membrane triangular, beam, bar, and spring elements.

Later in 1983, Haug et al. [44] discussed the development of an implicit-explicit code (PAM-CRASH), which was used to analyze the response of an A-pillar and the right

front quarter of a unit-body passenger vehicle structure. The code incorporated a quasi-static analysis using an iterative incremental force/displacement analysis.

In 1986, Argyris et al. [45] discussed the development of an implicit code for crash analysis. The developed code was used to calculate the response of a frontal vehicle structure under impact with a rigid barrier at an initial velocity of 13.4 m/s. From this point, the application of implicit FE solvers to crash analysis did not proceed any further. This is primarily due to its inability to account for contact and folding of thin sheet metal structures and due to excessive demands on computer hardware storage and speed.

The year 1986 is a landmark in the history of the nonlinear FE method and marks a breakthrough in crash simulations [5]. At that year, Haug et al. [46] published what appears to be the first published work on the application of the explicit FE method in crashworthiness problems. The FE model as shown in Figure 1.8 simulated a Volkswagen Polo hitting a rigid wall barrier at 13.4 m/s and included 2272 shell elements and 106 beam elements. As shown, the model primarily represented the frame structure. The nonlinear behavior of the material was included using an elastoplastic constitutive model with strain hardening. The simulation took four hours to simulate 60 milliseconds of the crash event on a CRAY-1 supercomputer.

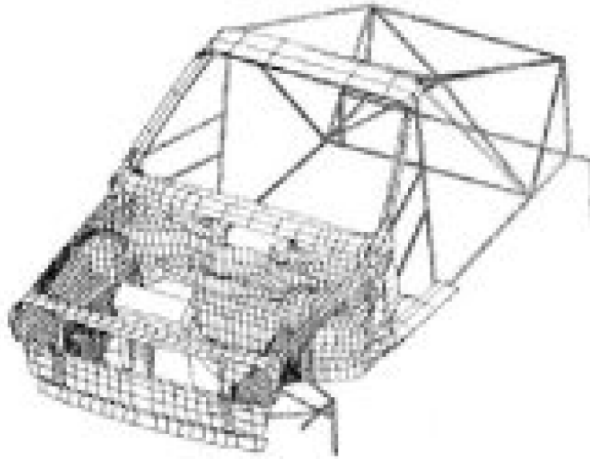


Figure 1.8: The VW-POLO model [46]

This breakthrough was the result of the introduction of vectorized supercomputers that allowed the practical application of the explicit finite element method to crash simulations. From this point onward, nonlinear FE models have been used at an increasing rate due to the rapid advancement in the computational capabilities in terms of speed, memory and storage. Now, nonlinear FE models are widely used for analyzing the behavior of vehicle structures under impact loading. The detailed geometric models of vehicle components are usually established using computer aided design softwares. This has facilitated the development of FE models as these geometric models can be easily imported to the FE codes for meshing. In addition, the improvement of the nonlinear codes for faster computations and more accurate results has encouraged the design community to adopt nonlinear FE models as the state of the art tool for crashworthiness analysis.

1.2.7.4 Brief History of Nonlinear FE Softwares

The birth of the first nonlinear FE software was at the US Lawrence Livermore National Laboratories (LLNL) [47]. The software was named DYNA and it was developed mainly for solving problems that were highly nonlinear and impossible to

solve with existing computational tools. For example, for a military aircraft hitting at 200 m/s a concrete safety containment of a nuclear power plant, 60 elements were used to model the concrete building and the simulation took 33 hours on a VAX 11/780 [48]. The software was developed in an open environment in what resembles today an open source environment. In 1973, the French company ESI Group saw the potentials of using a numerical tool for solving nonlinear problems in commercial applications and began developing its own code and named it PAM-CRASH [49]. In 1985, several developers from the ESI French group founded their own company and developed their own code RADIOSS [50]. In 1989, developers from the US LLNL founded their own company named Livermore Software Technology and called the code LS-DYNA [51]. In 1978, ABAQUS was developed by a group of PhD students from Brown University in the US. At first, it included an implicit solver and later in 1991, the explicit solver was introduced. In 2005, the company was acquired by the French group Dassault Systèmes [52]. Currently LS-DYNA, PAM-CRASH, RADIOSS and ABAQUS are the most widely used nonlinear FE software for crash simulations. The use of nonlinear FE models is not limited only to crash simulations and is applied to many other complex problems involving high nonlinearity such as:

- Occupant simulation [53, 54].
- Evaluating and improving roadside hardware [55–57].
- Improving vehicle design for pedestrian safety [58–62].
- Development of the metal forming processes [63–65].
- Aerospace design [66–68].
- Medical applications [69, 70].

1.2.7.5 MBD Models

In multi body dynamic models, physical components are represented by interconnected bodies with different joint types. In fact, LMS models are special cases of the more general MBD models. The difference is that in MBD models, various joint types with different degrees of freedom can be used and multi bodies can be flexible bodies instead of rigid bodies used in LMS models. MBD models are efficient at capturing the kinematics and the kinetics of interacting bodies, which is an area best suited for analyzing the response of the human body when interacting with the vehicle interior or vehicle exterior [71]. In an early work by McHenry in 1963 [72], he used MBD to model the human body seated with restraint system in a frontal collision as shown in Figure 1.9. In his work, the human body is represented by four rigid bodies connected through pin joints. The model was in good agreement with experimental test results.

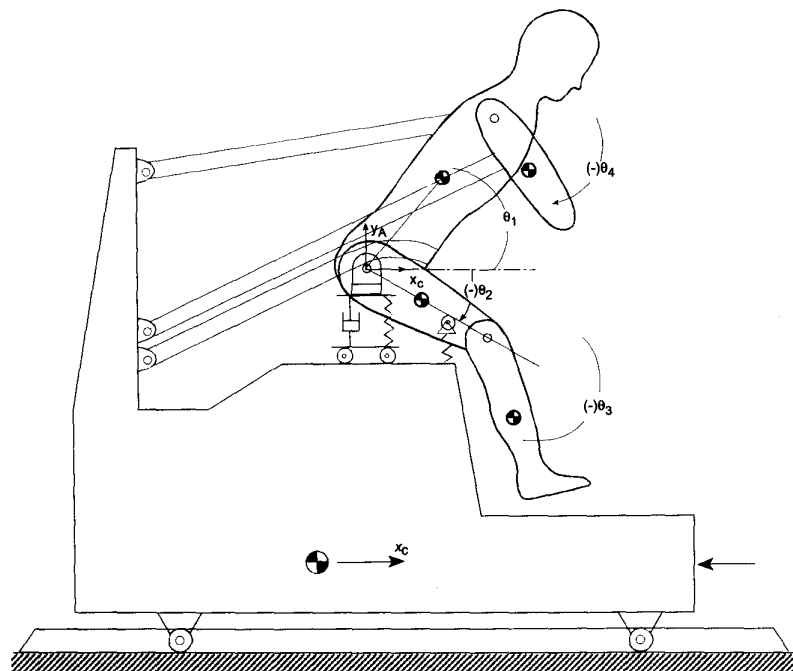


Figure 1.9: An early MBD model [72]

Currently MBD models are mainly used to simulate the interaction between occu-

pants or pedestrians and vehicle structure and also to predict the interacting kinetics between two or more colliding vehicles.

1.2.7.6 Hybrid Models

A hybrid model combines FE and MBD in a single model. Usually, the FE model is used to simulate the vehicle structure where the MBD model is used to simulate human occupants. This configuration allows for computational efficiency, since MBD can model the human body at a comparatively lower computational cost compared to FE models. The model in Figure 1.10 shows a hybrid model for a side impact test. LS-DYNA is used to model the vehicle structure and the rigid barrier, where MADYMO, a MBD commercial software is used to model the occupant.

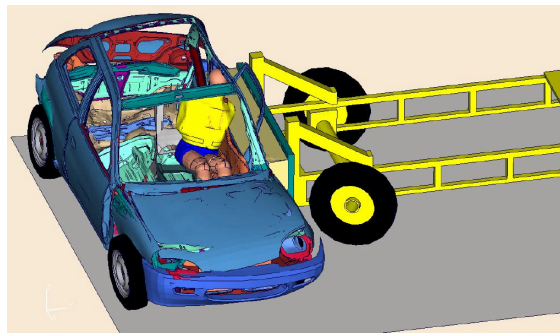


Figure 1.10: A hybrid model of a side impact test [73]

Modeling humans using MBD models has been criticized on the basis that designing a car based on the dummies responses will make the car safe for dummies but not necessarily for humans [74]. Therefore, research has been conducted in this area to use FE models to model the occupants since they can capture more details about the effect on the body, especially the internal organs. The problem with this approach is the evaluation of material properties for human body parts which is not an easy task. Moreover, the resulting FE model becomes exceedingly complex and computationally demanding. For example, a human brain model alone consists of more than 300,000

elements [74]. Nevertheless, some automobile manufacturers have developed their own FE human models, such as Toyota which has developed Total HUMAN Model for Safety (THUMS) [75].

1.3 Crashworthiness Improvement

Having a variety of reliable modeling tools, researchers have used these tools to analyze and improve vehicle designs for safety. Crashworthiness improvement can be approached in two ways: (1) Geometry optimization for crashworthiness and (2) Material optimization for crashworthiness.

1.3.1 Geometry Optimization for Crashworthiness

The automobile is a complicated product with different design (often contradicting) objectives. An intuitive ad-hoc approach can no longer be used to find a feasible solution that can meet all the design objectives and using optimization becomes inescapable. Optimization is a systematic mathematical method for solving problems in which the problem is configured in a way that the objective and the constraints are well specified and defined as functions of the problem variables.

The problem is formulated as the process of finding the set of design variables X that minimizes or maximizes the objective function F within the design constraints G_j , where $j = 1 : n$ and n is the number of constraints. X is usually bounded between X_L (Lower bound) and X_U (Upper bound). A formal optimization problem with a single objective is formally defined as follows:

$$\begin{aligned}
& \text{Find } X \text{ that :} \\
& \text{Minimizes } F \\
& \text{Subject to: } G_j \leq 0 \\
& \text{where, } X_L \leq X \leq X_U
\end{aligned} \tag{1.17}$$

There are numerous numerical approaches for solving optimization problems and they can be classified into two main categories: gradient and nongradient based methods. In gradient based method, analytical or numerical gradients of the objective and constraint functions are required, while nongradient based methods do not require the gradients. Nevertheless, both methods require a considerable number of iterations to find the optimum value of X .

Considering this, applying optimization for crashworthiness design is extremely difficult since analytical gradients are not readily available in nonlinear FE analysis and also numerical evaluation of gradients generate erroneous results due to the inherent complexity of the nonlinear FE method. Moreover, each iteration to evaluate the objective and constraint functions requires running the computationally very expensive nonlinear FE analysis. These complexities prevent the practical application of optimization directly to nonlinear FE analysis.

To overcome these problems researchers have investigated different approximate models, sometimes called meta-models (models of models) [76]. The idea is to build simple and easy to calculate approximations of the complex nonlinear FE model and use these approximations to predict the responses of the model. As these approximations can be calculated at a much less computational cost than the nonlinear FE models, an optimization problem can then be formulated using these meta-models to calculate the values of objective and constraint functions at each iteration, and thus optimization

can be applied effectively. The first application of meta-models for optimization of large scale structural problems was introduced by Schmit and Farshi [77] in 1974. For a comprehensive review of approximate methods for optimization in structure design, one can refer to Ref. [78]. In the following, some pertinent works are presented.

The first published work on the application of meta-models in crashworthiness design appears to have been published by Schoof et al. [79] in 1992. They built approximate models of multi body dynamics models. Then, they applied optimization to the approximate models to minimize the injury criterion for a child seated in a child's seat. Later in 1996, Etman et al. [80] used the RSM to build approximate models of the crash responses of a sedan in frontal impact. They used MADYMO (a multi body dynamic software) to simulate the frontal impact on the occupant side. Schramm et al. [81] used LS-DYNA (a nonlinear finite element software) to model an S-rail under frontal impact. They then used RSM to build approximate models of the impact energy and applied optimization to maximize the value of the impact energy absorbed in the S-rail structure. Yamazaki and Han used RSM to approximate the energy absorbed in circular tubes [82], square tubes [83] and S-rails [84]. They applied optimization to the approximate models, where the objective was to maximize the amount of impact energy absorbed in the tubes and the S-rails. Marklund and Nilsson [85] used RSM to model an air bag that was simulated by LS-DYNA. They applied optimization to the approximate model to find the optimum airbag design variables to minimize occupant injuries in situations where the occupant is not seated in an ideal position. Craig et al. [86] used RSM to create function approximations of an instrument panel and conducted optimization to find the optimum shape design variables to minimize knee injuries of the occupant. Recently, Liu [87, 88] used LS-DYNA to model thin walled square and octagonal tubes under axial impact. He then used RSM to approximate the impact energy absorbed by the tube. Finally, he applied optimization to find the optimum shape variables to maximize the specific

energy absorbed while constraining the maximum crushing force.

1.3.2 Material Optimization for Crashworthiness

Material's role is of paramount importance to crashworthiness. Lighter materials are being developed to reduce automobile's weight for cost and emission reduction. At the same time these lighter materials should maintain the safety of the automobile according to regulations. Significant research work has been conducted to achieve both objectives. The research in this area can be classified according to the type of material into four categories: (1) steel, (2) composite materials, (3) aluminum and (4) magnesium. A brief overview of the published literature is presented in the following:

1.3.2.1 Steel

Steel sheets have been used in vehicle structures for more than one century. Its low production costs, consistent properties and the huge accumulated and available knowledge about its production processes make it the material of choice for automobile manufacturers. Its crashworthiness performance has been studied by several researchers. Van Slycken et al. [89] studied high strength steels potentials for crashworthiness. They showed that high strength steels under dynamic loading experience higher energy absorption capacities and these capacities even increase as the strain rate increases, which is an advantage for crash energy absorption applications. Peixinho et al. [90] examined the crashworthiness behavior of thin walled tubes made of dual phase and transformation induced plasticity (TRIP) steels. TRIP steels are steels containing a metastable austenite that transforms into martensite during plastic deformation, which allows for enhanced strength and ductility [91]. They conducted tensile tests at different strain rates as well as axial crushing tests. Their test results showed that TRIP steels are strain rate sensitive and this can be useful for crash-

worthiness applications. They used LS-DYNA to model the tests, and numerical and experimental results were in good agreement. Hosseinipour et al. [92] studied improving the crash behavior of steel tubes by incorporating annular grooves. They showed that this may lead to a controllable progressive deformation, thus increasing the energy absorption capacity of the tubes.

1.3.2.2 Composite Materials

Composite materials have been investigated for their probable use as impact energy absorbing elements. Some of the composites that have been investigated for use in crashworthiness are random chopped fiber reinforced composites. George et al. [93] studied the crashworthiness performance of random chopped carbon fiber reinforced epoxy composites. They conducted quasi static tests and concluded that they can be used as crash energy absorbers. Mahdi et al. [94] used ABAQUS to simulate corrugated steel tubes filled with cotton fibers embedded into polypropylene. They showed that the energy absorption capacity increases as the number of corrugations increases and decreases as the ratio between diameter to thickness (D/t) increases.

1.3.2.3 Aluminum

Aluminum has been used in some automobile structures due to its low density. In 1993, Audi introduced the aluminum space frame sedan, and in 1999, GM introduced the first all wrought aluminum cradle [95]. Caliskan et al. [96] studied the impact behavior of the frontal structure of a 2005 Ford GT aluminum spaceframe. They conducted a full frontal test and used material properties from actual tests as input data for the LS-DYNA model. They also studied the energy absorption capacity of rails made of a 6063-T6 aluminum alloy and concluded that properties of the Heat Affected Zone (HAZ) affect the rail crash performance and their effect should be

included in future models.

1.3.2.4 Magnesium

Magnesium has recently received a great attention from the automotive industry due to its attractive low density. It is the lightest of all structural metals (78% lighter than steel and 35% lighter than aluminum). Moreover, it is also one of the the most abundant structural materials in Earth's crust and in sea water [97]. Due to its excellent casting properties, it has been used in several automotive components, such as, engine block, engine cradle, transmission case, and instrument panel [98]. Also, it has been used as inner door frames and seats [99]. However, it has not fully replaced steel in vehicle structures due to the following challenges:

- Magnesium has a Hexagonal Closed Packed (HCP) crystal structure and has limited slip systems, mainly in the basal planes, hence it is difficult to form especially at low temperatures.
- Magnesium has high affinity to react with oxygen which causes corrosion, hence expensive treatments are required [100].

There is a considerable amount of research to overcome the challenges that hinder the full use of magnesium alloys in vehicle structures. Nehan et al. [101] presented the development of an instrument panel cross beam made of magnesium AM60B alloy. They mentioned that magnesium improved vehicle safety and at the same time, it minimized the vehicle weight. Newland et al. [102] studied the strain rate behavior of magnesium alloys and concluded that reducing the aluminum content within the alloys improves their strain rate sensitivity and ultimately improves their impact absorbing capacity. Abbott et al. [103] studied magnesium alloys AM60, AS21 and AZ91 and concluded that they can perform very well in crash situations. Recently,

Easton et al. [104] presented the development of a new alloy AM-EX1. They also mentioned that magnesium alloys, specifically AZ31 alloy, can absorb more impact energy than aluminum or steel alloys. They concluded that material models should be improved by incorporating defects, non-uniformity, and materials microstructural characteristics. Despite these efforts, more research is required to understand the crashworthiness performance of vehicle structures made of magnesium alloys. In this study, a new approach is introduced on improving the crashworthiness performance of vehicle structures using magnesium alloys.

1.4 The Aim of the Present Work

The main objective of this research is to develop an efficient and practical methodology for design optimization of vehicle structures. The proposed methodology consists of three main stages and is demonstrated on a nonlinear finite element model of a pickup truck.

In the first stage, a full nonlinear transient dynamic finite element analysis using LS-DYNA is conducted on the full vehicle model under frontal impact. Then, the crash behavior of major structural parts is examined based on their impact energy absorbing characteristics. The major contributing structural part to the total impact energy absorbed in the whole vehicle structure is identified. After that, a separate nonlinear finite element model of the identified structure component is constructed and modified so that its crashworthiness behavior, when treated individually under the same impact scenario, is similar to that in the full vehicle model.

In the second stage, an approximate model of the separate nonlinear finite element of the identified structure component is developed using RSM. Different types of RSM models are tested and the most accurate is used to represent the crashworthiness behavior of the structural component.

In the third stage, the RSM model selected from the second stage is used in an optimization problem. The objective of the optimization problem is to maximize the amount of impact energy absorbed in the identified structural component while maintaining its initial weight. The optimized structural component is then integrated into the full vehicle nonlinear finite element model and simulated. The results are then examined to verify if the crashworthiness performance of the full vehicle has been improved.

Besides the above main objective, other important objectives of the present work are:

Utilizing the developed RSM model to formulate a multiobjective optimization problem.

The goal is to construct the Pareto front, which includes all possible optimal solutions within the design space in order to derive the relation between the optimal amount of impact energy absorbed and optimal weight. The derived relation can then be used as a guideline to the designer to quickly investigate the effectiveness of any design. If the design is not optimal, using the proposed approach, the designer can easily select the proper design variables to achieve an optimum design. This enables the designer to quickly and easily evaluate vehicle designs and select optimum designs.

Crashworthiness improvement using magnesium.

The modified nonlinear finite element model of the chassis frame that was identified previously in the main objective is used to investigate the crashworthiness response of vehicle structural parts made of magnesium. Different combinations between steel and magnesium are also examined. The optimum combination between steel, magnesium and parts thicknesses is also studied using a genetic algorithm directly combined with the modified nonlinear finite element model.

Investigation on add-on crash energy absorbing system.

The system includes a thin walled square tube that acts as an impact energy absorber.

The objective of the system is to absorb as much impact energy as possible and at the same time to reduce the transmitted impact loads to the occupants. To achieve this goal, different imperfections are introduced to the thin walled tubes to trigger the deformation in a controlled manner for optimal performance. The genetic algorithm is also directly combined with the nonlinear finite element model of the thin walled tube to find the optimal values of imperfection.

1.5 Thesis Organization

This thesis consists of seven chapters. The present chapter (chapter 1) provides the problem statement and motivation of the study. In this chapter, a systematic literature review was presented on the subject of crashworthiness with most important and relevant contributions to the field. The chapter concludes by identifying the objectives of the work and the layout of the thesis.

In chapter 2, nonlinear finite element analysis is presented. The differences between linear and nonlinear finite element analyses and the sources of nonlinearity are also discussed. Then, modeling of crashworthiness using the nonlinear finite element method is described in details. After that, a thin walled square tube is modeled and the simulation results are verified against published experimental work. Finally, mesh sensitivity analysis is conducted and different shell element types are simulated and compared.

Chapter 3 begins with an overview of the process of creating approximate models and then different types of meta-model building techniques are presented. The response surface method is described in details along with the other used tools such as design of experiments and regression analysis. After that, optimization using the response surface method is demonstrated with two examples: a benchmark analytic function and an S-rail vehicle component. The proposed methodology is then explained in details

and demonstrated through an illustrative example and finally results are discussed.

Chapter 4 presents a new concept on the process of deriving the relations between optimal crashworthiness responses. Multiobjective optimization and the Pareto front are first reviewed, and then the concept is applied to a simple thin walled tube. Finally, the concept is applied to the chassis structure identified in chapter 3.

Chapter 5 investigates the crashworthiness behavior of vehicle structural components made of magnesium using the modified nonlinear finite element model that was developed in chapter 3 for the identified chassis structure.

Chapter 6 investigates the effect of imperfection on the performance of a crash energy absorbing system. The genetic algorithm is used to find the optimal imperfection values.

Finally, chapter 7 provides a summary and the most important findings and contributions of the present work. Then various recommendations are identified for future work.

Chapter 2

Nonlinear Finite Element Modeling

2.1 Introduction

The work developed in this thesis basically depends on using the nonlinear FE method to model vehicle structures in crashes. Therefore, the theory and the mathematical foundation of the nonlinear FE method are explained in this chapter, which is divided into four main parts. In the first part, an overview of the FE method is presented and the differences between linear and nonlinear FE analyses are stated. This is followed by the description of the sources of nonlinearity in nonlinear FE analysis. In the second part, the nonlinear FE method is described focusing on its implementation in crashworthiness design. The theoretical foundation which includes the development of the governing equations is presented. The time integration algorithms required to solve the nonlinear time dependent equations are also described. Next, the contact algorithm used to handle the contact forces between structural parts under compression and also shell elements and material model types are described. Then finally, a brief discussion on the role of imperfection in nonlinear FE analysis is presented. The third part presents a review over the different applications of the nonlinear FE analysis in vehicle crashworthiness design. The fourth part includes a detailed description

of the modeling process of a thin walled square tube under axial impact loading and results are discussed in details.

2.2 Overview of the FE method

The FE method is a numerical method used for solving complicated engineering problems. Starting from its first application in the analysis of aircraft structures in the mid fifties [105], the FE method has evolved as the state of the art tool for solving complex engineering problems. The basic idea is that, the human mind can not understand the behavior of complex (continuous) physical systems without breaking them down into simpler (discrete) sub-systems [106]. The process of breaking down the continuous system into simpler systems is called *discretization* and the simpler systems are called *finite elements* .

A standard procedure for the FE method has been elaborated over the years and can be summarized as follows:

1. The whole continuous system is discretized into simpler elements of finite sizes interconnected at nodal points.
2. The cause - effect relationship is established over each element. This relation depends on the problem type, e.g., for structural analysis problems, it is a relation between force (cause) and displacement (effect).
3. Equations are assembled (i.e., combining all elements relations) according to continuity considerations and the boundary conditions are applied.
4. The equations are solved using a suitable numerical technique.

2.2.1 Differences between Linear and Nonlinear FE Analyses

There are mainly two types of FE analyses: linear and nonlinear. The two major differences between them can be summarized as [107]:

- In linear FE analysis, the displacements are assumed to be infinitesimally small, where nonlinear FE analysis involves large displacements. The term displacements refers to both linear and rotational motions.
- In linear FE analysis, the material behavior is assumed to be linearly elastic, whereas in nonlinear FE analysis, the material exceeds the elastic limit and/or its behavior in the elastic region is not necessarily linear.

Linear FE problems are considerably easy to solve at a low computational cost compared to nonlinear FE problems. Also, different load cases and boundary conditions can be scaled and superimposed in linear analysis which are not applicable to nonlinear FE analysis. The nonlinear FE analysis can be considered as the modeling of real world systems, while linear FE is the idealization. This idealization can be reasonably satisfactory in some cases, but for special cases nonlinear FE modeling is the only option such as in crashworthiness simulations. The main distinct features of the nonlinear FE method can be summarized as follows [108]:

- The principle of superposition can not be applied.
- The load is analyzed one case at a time.
- The response is dependent on the load history.
- Initial system state is important.

2.2.2 Sources of Nonlinearity

The sources of nonlinearity can be divided as follows [107]:

Geometric nonlinearity; in which the change in geometry is taken into consideration in setting the strain-displacement relations.

Material nonlinearity; in which the material response depends on the current deformation state and possibly past deformation history.

Boundary condition nonlinearity; in which the applied force and/or displacement depends on the deformation of the structure.

2.3 Nonlinear FE for Crashworthiness

Simulation of vehicle accidents is one of the most challenging nonlinear problems in mechanical design as it includes all sources of nonlinearity. A vehicle structure consists of multiple parts with complex geometry and is made of different materials. During crash, these parts experience high impact loads resulting in high stresses. Once these stresses exceed the material yield load and/or the buckling critical limit, the structural components undergo large progressive elastic-plastic deformation and/or buckling. The whole process occurs within very short time durations. Since closed form analytical solutions are not available, using numerical approach specially the nonlinear FE method becomes unavoidable. There are few computer softwares dedicated to nonlinear FE analysis such as ABAQUS, RADIOSS, PAM-CRASH and LS-DYNA. LS-DYNA has been proved to be best suited for modeling nonlinear problems such as crashworthiness problems. In the following section, the theoretical foundation of the nonlinear FE analysis is presented.

2.3.1 Governing Equations

The principle of virtual work can be employed to derive the governing differential equations in finite element form [106]. It states that the work done by external loads is equal to the work done by internal loads. It should be noted that the principle of virtual work can be applied to both linear and nonlinear problems. Now, applying the principle of virtual work to a finite element with volume V_e , we can write [109]:

$$\delta (U)^e = \delta W^e \quad (2.1)$$

where $\delta (U)^e$ is the work done by the internal loads and δW^e is the work done by the external loads. Eq.(2.1) can be expressed as:

$$\begin{aligned} \int_{V_e} \{\delta u\}^T \{F\} dV + \int_{S_e} \{\delta u\}^T \{\Phi\} dS + \sum_{i=1}^n \{\delta u\}_i^T \{p\}_i - \\ \int_{V_e} \left(\{\delta u\}^T \rho \{\ddot{u}\} + \{\delta u\}^T \kappa_D \{\dot{u}\} \right) dV = \int_{V_e} \{\delta \epsilon\}^T \{\sigma\} dV \end{aligned} \quad (2.2)$$

Rearranging the terms in Eq.(2.2), the equations of motion can be written as:

$$\begin{aligned} \int_{V_e} \{\delta u\}^T \{F\} dV + \int_{S_e} \{\delta u\}^T \{\Phi\} dS + \sum_{i=1}^n \{\delta u\}_i^T \{p\}_i = \\ \int_{V_e} \left(\{\delta \epsilon\}^T \{\sigma\} + \{\delta u\}^T \rho \{\ddot{u}\} + \{\delta u\}^T \kappa_D \{\dot{u}\} \right) dV \end{aligned} \quad (2.3)$$

where $\{\delta u\}$, $\{\delta \epsilon\}$ and $\{\sigma\}$ are vectors of displacements, strains and stresses respectively, $\{F\}$ is a vector of body forces, $\{\Phi\}$ is a vector of prescribed surface tractions,

which are nonzero over surface S_e , $\{p\}_i$ is a vector of concentrated loads acting on total n points in the element, $\{\delta u\}_i$ is the displacement at the i^{th} point, ρ is the mass density, and κ_D is the material damping parameter.

The displacement field $\{u\}$ is a function of both space and time and it can be written with its time derivatives as:

$$\{u\} = [N] \{d\} \quad \{\dot{u}\} = [N] \{\dot{d}\} \quad \{\ddot{u}\} = [N] \{\ddot{d}\} \quad (2.4)$$

Eq.(2.4) represents a local separation of variables, where $[N]$ are shape functions of space only and $\{d\}$ are nodal functions of time only. Substituting Eq.(2.4) in Eq.(2.3) yields:

$$\{\delta d\}^T \left[\int_{V_e} [N]^T [B]^T \{\sigma\} dV + \int_{V_e} \rho [N]^T [N] dV \{\ddot{d}\} + \int_{V_e} \kappa_D [N]^T [N] dV \{\dot{d}\} - \int_{V_e} [N]^T \{F\} dV - \int_{S_e} [N]^T \{\Phi\} dS - [N]^T \sum_{i=1}^n \{p\}_i \right] = 0 \quad (2.5)$$

where $\{\epsilon\} = [B] \{u\}$ and Eq.(2.5) can be written in matrix form as:

$$[m] \{\ddot{d}\} + [c] \{\dot{d}\} + \{r^{int}\} = r^{ext} \quad (2.6)$$

where the element mass matrix is defined as:

$$[m] = \int_{V_e} \rho [N]^T [N] dV \quad (2.7)$$

the damping matrix is defined as:

$$[c] = \int_{V_e} \kappa_D [N]^T [N] dV \quad (2.8)$$

the element internal force vector is defined as:

$$\{r^{int}\} = \int_{V_e} [N]^T [B]^T \{\sigma\} dV \quad (2.9)$$

and the external load vector is defined as:

$$r^{ext} = \int_{V_e} [N]^T \{F\} dV + \int_{S_e} [N]^T \{\Phi\} dS + \sum_{i=1}^n \{p\}_i \quad (2.10)$$

The governing equations of motion of a structure consisting of many elements can be derived by expanding Eq.(2.6) as:

$$[M] \{\ddot{D}\} + [C] \{\dot{D}\} + \{R^{int}\} = \{R^{ext}\} \quad (2.11)$$

where $[M]$ and $[C]$ are system structural mass and damping matrices respectively, $\{R^{int}\} = [K] \{D\}$ is the internal load vector, $\{R^{ext}\}$ is the external load vector, $\{D\}$, $\{\dot{D}\}$ and $\{\ddot{D}\}$ are the nodal displacements, velocities and accelerations respectively.

Eq.(2.11) is a system of coupled, second order, ordinary differential equations in time. Thus, it is called a finite element semi-discretization because although displacements $\{D\}$ are discrete functions of space, they are still continuous functions of time. It should be noted that for problems with material and geometry nonlinearity as in crashworthiness problems, the stiffness matrix $[K]$ is not constant and instead is a function of displacement and consequently of time as well.

2.3.2 Direct Integration Methods

Direct integration methods are used to discretize Eq.(2.11) in time to obtain a sequence of simultaneous algebraic equations. The approach is to replace the time derivatives in Eq.(2.11) (i.e. $\{\dot{D}\}$ and $\{\ddot{D}\}$) by approximate differences of displacement $\{D\}$ at various instances of time. First, Eq.(2.11) can be written at a specific instant of time as:

$$[M] \{\ddot{D}\}_n + [C] \{\dot{D}\}_n + \{R^{int}\}_n = \{R^{ext}\}_n \quad (2.12)$$

where, n denotes $n\Delta t$ time and Δt is the time step. There are two methods to solve Eq.(2.12): implicit and explicit.

2.3.2.1 The Implicit Method

In the implicit method, $\{D\}$ is defined as:

$$\{D\}_{n+1} = f \left(\{\dot{D}\}_{n+1}, \{\ddot{D}\}_{n+1}, \{D\}_n, \dots \right) \quad (2.13)$$

Hence, the implicit method requires knowledge of time derivatives of $\{D\}_{n+1}$, which are unknown, thus expensive iterative methods must be used. Every iteration requires the solution of a system of equations involving mass, damping, and stiffness matrices. Depending on the complexity of the model, the number of equations can reach tens of thousands, hence the computational cost can be expensive. The implicit algorithm is unconditionally stable under some conditions, thus it allows for large time steps to be used. This makes it suitable for long-duration structural dynamic problems and not for crash problems with very short durations, where the explicit method should be used [109].

2.3.2.2 The Explicit Method

In the explicit method, $\{D\}$ is defined as:

$$\{D\}_{n+1} = f\left(\{D\}_n, \{\dot{D}\}_n, \{\ddot{D}\}_n, \{D\}_{n-1} \dots\right) \quad (2.14)$$

Hence, the explicit method requires knowledge of the complete history of the information consisting of displacements and their times derivatives at time $n\Delta t$ and earlier to calculate the displacements at time step $n + 1$. The explicit method has been proved to be very suitable for nonlinear transient dynamic problems with very short durations of time such as crash problems.

2.3.2.3 The Central Difference Method

The central difference method is one of the numerical integration techniques and it has been successfully used with the explicit method to solve the equations of motion Eq.(2.12). The central difference method approximates velocity as:

$$\{\dot{D}\}_n = \frac{1}{2\Delta t} (\{D\}_{n+1} + \{D\}_{n-1}) \quad (2.15)$$

and acceleration as:

$$\{\ddot{D}\}_n = \frac{1}{\Delta t^2} (\{D\}_{n+1} - 2\{D\}_n + \{D\}_{n-1}) \quad (2.16)$$

The aforementioned equations are obtained using Taylor series expansion of the terms $\{D\}_{n+1}$ and $\{D\}_{n-1}$ about time $n\Delta t$ as:

$$\{D\}_{n+1} = \{D\}_n + \Delta t \{\dot{D}\}_n + \frac{\Delta t^2}{2} \{\ddot{D}\}_n + \frac{\Delta t^3}{6} \{\ddot{\ddot{D}}\}_n + \dots \quad (2.17)$$

$$\{D\}_{n-1} = \{D\}_n - \Delta t \{\dot{D}\}_n + \frac{\Delta t^2}{2} \{\ddot{D}\}_n - \frac{\Delta t^3}{6} \{\dots\}_n + \dots \quad (2.18)$$

Substituting Eqs.(2.15 and 2.16) in Eq.(2.12) yields:

$$\begin{aligned} & \left[\frac{1}{\Delta t^2} M + \frac{1}{2\Delta t} C \right] \{D\}_{n+1} = \quad (2.19) \\ & \{R^{ext}\}_n - [K] \{D\}_n + \frac{1}{\Delta t^2} [M] (2 \{D\}_n - \{D\}_{n-1}) + \frac{1}{2\Delta t} [C] \{D\}_{n-1} \end{aligned}$$

Eq.(2.19) is a system of linear algebraic equations. All the information in the right hand side are known for time step n . Eq.(2.19) is conditionally stable, which requires the time step Δt to be less than the time needed for the acoustic wave to propagate across one element. If Δt is too large, the explicit method fails and if it is unnecessarily small, the computation becomes too expensive. Δt is bounded by the Courant condition, which can be written as follows:

$$\Delta t \leq \frac{l}{v_{ac}} \quad (2.20)$$

where l is element length and v_{ac} is the acoustic wave speed through the material of the element

The explicit method is ideal for wave propagation problems such as in typical automobile accidents. For example, the acoustic speed in mild steel is $v_{ac} \approx 5000 \text{ m/s}$ and for an element with $l = 5 \text{ mm}$, the time step will be 1 microsecond. In addition, the explicit method can be easily implemented and is capable of solving large problems with minimum computer storage [109]. However, for structural dynamic problems, where the time durations are usually long, the implicit method is more well suited. In LS-DYNA, the explicit method is the default method for solving crash problems

and the central difference method is used for integration [110].

2.3.3 Contact Algorithm

In vehicle crash accidents, contact forces are developed when structural parts are crushed under impact loading. An algorithm is required to handle the transmission of forces between the individual structural parts through contact. There are three types of contact algorithms available in LS-DYNA [110]. The algorithms are: (1) The kinematic constraint algorithm, (2) The distribution parameter algorithm, and (3) The penalty algorithm. The penalty algorithm is the most widely used for vehicle crash simulations [110]. It calculates the contact force on a node by placing normal interface springs between penetrating nodes and the contact surface. For more information on the subject, one can refer to Refs. [108, 110].

2.3.4 Friction

Vehicle crashes involve structural parts sliding against each others or against themselves. It is essential to handle the friction forces between parts accurately. In LS-DYNA, friction between surfaces is based on a Coulomb formulation [110]. One can refer to Ref. [108] for more information.

2.3.5 Shell Elements

Most vehicle structural parts are thin plate like structures that are modeled using shell elements. An overview over the recent shell elements is provided in Ref. [111]. LS-DYNA includes a comprehensive library of element types from which the analyst can select the best element according to the type of problem. There are currently 14 different shell elements in LS-DYNA as provided in Table 2.1.

Table 2.1: Shell elements in LS-DYNA

El #	Element
1	Hughes-Liu
2	Belytschko-Lin-Tsay
3	BCIZ triangular shell
4	C^0 triangular shell
6	S/R Hughes-Liu
7	S/R co-rotational Hughes-Liu
8	Belytschko-Leviathan shell
10	Belytschko-Wong-Chiang Shell
11	Co-rotational Hughes-Liu
16	Fully integrated shell element
17	Fully integrated DKT,triangular shell element
25	Belytschko-Tsay shell with thickness stretch
26	Fully integrated shell with thickness stretch
27	C^0 triangular shell with thickness stretch

A brief description of the different shell elements available in LS-DYNA can be summarized as follows:

1. The Hughes-Liu element (T1) is formulated based on a degenerated solid element [112, 113]. This formulation results in substantially large computational costs, however it is effective when very large deformations are expected. This element uses one-point quadrature at the mid-plane.
2. The Belytschko-Lin-Tsay element (T2) element is the most computationally efficient among all shell elements [114]. The element cannot treat warped configurations accurately and also, it should not be used with coarse meshes [115].

3. The BCIZ Triangular element (T3) is based on a Kirchhoff plate theory [116]. It uses three in-plane integration points which increases its computational cost.
4. The C^0 Triangular element (T4) is based on a Mindlin-Reissner plate theory and uses linear velocity fields [117]. One quadrature point is used in the element formulation. This element is slightly stiffer than the quadrature element as has been pointed out by its developers [117]. Hence, it should be used as a transition between different meshes and not the entire mesh.
5. The S/R Hughes-Liu element (T6) is the same as the Hughes-Liu, however, instead of using one-point quadrature, it uses selectively reduced integration at Gauss quadrature integration points. This feature increases the computational cost.
6. The S/R co-rotational Hughes-Liu element (T7) is the same as the S/R Hughes-Liu except that it uses the co-rotational system [114].
7. The Belytschko-Leviathan element (T8) adds the drilling degree of freedom to the element formulation which inhibits the formation of zero energy modes [118]. It can accurately model the twisted beam, hence it is recommended for warped structures.
8. Belytschko-Wong-Chiang element (T10) is an improvement over the Belytschko-Lin-Tsay element (T2) to solve the twisted beam problem, however, it is relatively computationally expensive (approximately 10% more compared to T2) [119].
9. The co-rotational Hughes-Liu element (T11) uses the co-rotational system, however, it is computationally expensive compared to the Hughes-Liu element (T1).
10. The fully-integrated Belytschko-Tsay element (T16) uses the local element coordinate system defined by two basis vectors parallel to its plane and a third vector

normal to its plane [120]. It is about as 2.5 times slower than the Belytschko-Tsay element (T2) element.

11. The Fully integrated DKT triangular element (T17) is based on the Discrete Kirchhoff Triangular (DKT) formulation developed by Batoz [121] which is an extension to the work made by Morley [122]. The bending behavior of this element is better than the C^0 triangular element.
12. Elements (T25 and T26) are the Belytschko-Tsay element and are fully integrated shell elements with two additional degrees of freedom to allow a linear variation of strain through the thickness. These elements are best suited for metal forming applications.
13. The C^0 triangular shell with thickness stretch element (T27) is the same as element (T4) however, it allows for strain variation along the thickness.

The default element in LS-DYNA is the Belytschko-Lin-Tsay shell (T2) element. It is widely used in crash modeling due to its computational efficiency and acceptable accuracy. Therefore, it is discussed in more details in the following section.

2.3.5.1 The Belytschko-Lin-Tsay Shell (T2) Element

The Belytschko-Lin-Tsay shell element is a quadrilateral element, in which each of the four nodes has 5 degrees of freedom (3 translations and 2 rotations), in which 2 axes of rotation lie within the element plane as shown in Figure 2.1. The four nodes lie within the plane and the unit vectors \hat{e}_1 and \hat{e}_2 are tangent to the shell's mid plane and \hat{e}_3 is in the thickness direction. The sign \hat{e} denotes the local coordinates.

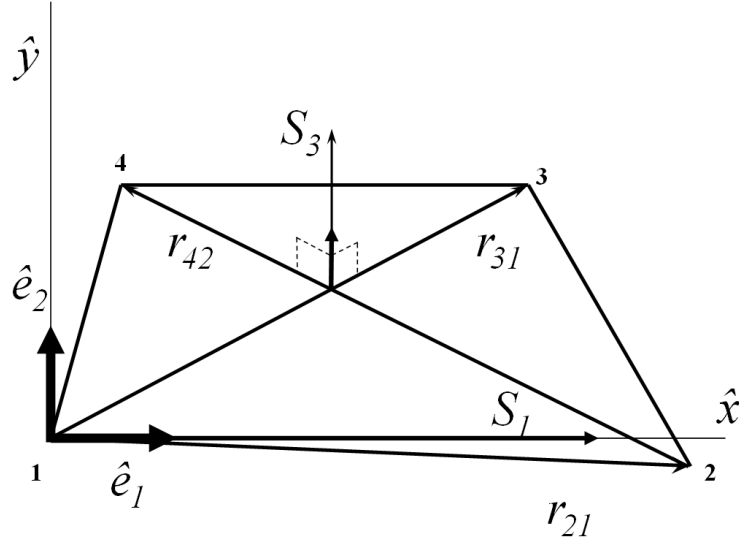


Figure 2.1: Shell element

The Belytschko-Lin-Tsay shell element has been successfully used in industry especially in crash modeling during the past two decades [114]. This is due to its computational efficiency and stability which stems from its efficient formulation. The formulation is based on the Co-Rotational (CR) method, which is briefly explained in the following sections.

2.3.5.2 The Co-Rotational Method

The co-rotational method is the most recent Lagrangian kinematic description for nonlinear FE analysis and has been used successfully by many researchers to solve highly geometrical nonlinear problems [123–126]. The CR method decomposes the motion into rigid body motion and pure rotation. An embedded coordinate system follows the element (like its shadow) during deformation. As illustrated in Figure 2.2, the current configuration Γ_D is a combination of rigid body motion and pure deformation which is obtained through eliminating the rigid body motion by using the base configuration (Γ_0) and the CR configuration (Γ_{CR}). Application of the CR method in shell type structures is very complex and one may refer to Ref. [127] for a

more comprehensive review.

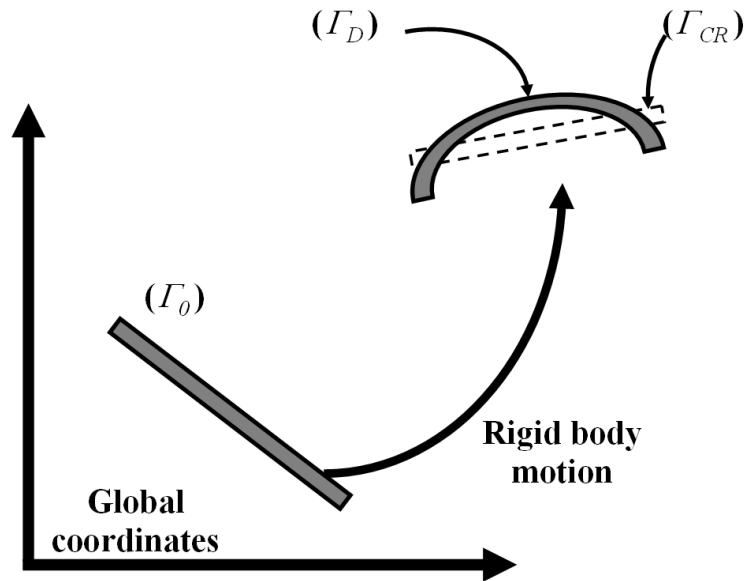


Figure 2.2: CR kinematic description

2.3.5.3 Element Limitations

The Belytschko-Lin-Tsay shell element is very computationally efficient due to its optimized formulation. However, the element has certain limitations, which can be summarized as follows:

- The element is based on the assumption of perfectly flat geometry, and this limits its ability when membrane shear deformation occurs [115]. In problems when significant shear is expected to occur and its effect cannot be ignored, other elements such as the Belytschko-Wong-Chiang element can be used [119].
- The formulation of the element is based on the uncoupling of the membrane and bending effects and thus it is limited to small bending strains.
- The element is not suitable for warped structures. Loads parallel to the local x-y plane will cause bending strains to develop, which are not accounted for

in element formulation. This may subsequently underestimate the structure's bending stiffness.

2.3.6 Material Models

There is a broad library of material models that are available in LS-DYNA, which includes more than 300 material models. These models can be effectively used to describe the behavior of different materials varying from composites, ceramics, fluids, foams, glasses, hydrodynamic materials, metals, plastics, rubber, soil, concrete, rock, adhesives to civil engineering components and biological materials.

2.3.6.1 Material Strain Rate Sensitivity

It is the phenomena in which for some materials the dynamic plastic flow stress (σ_d) is dependent on the strain rate ($\dot{\epsilon}$), known as viscoplasticity [128]. For dynamic impact loading, the static flow stress (σ_0) should be modified to account for the material strain rate sensitivity that can be significant in some materials. Cowper and Symonds [27] proposed a constitutive equation to calculate the dynamic flow stress (σ_d) as a function of static flow stress (σ_0), strain rate ($\dot{\epsilon}$), and two material constants (q and D) to be determined experimentally as:

$$\sigma_d = \sigma_0 \left[1 + \left(\frac{\dot{\epsilon}}{D} \right)^{1/q} \right] \quad (2.21)$$

In LS-DYNA, there are two commonly used material models; the MAT PLASTIC KINEMATIC model (material type 3), and the MAT PIECEWISE LINEAR PLASTICITY model (material type 24) to address the strain rate sensitivity of the material. In the plastic kinematic model, the values of the modulus of elasticity and the tangential modulus are directly used while the piecewise linear plastic model requires

an elaborate description of the stress-strain diagram. Both can be effectively used in elastic-plastic modeling with strain rate sensitivity, and are suitable for crashworthiness analysis.

2.3.7 The Role of Imperfection in Nonlinear FE Analysis

In nonlinear and also in linear FE analysis, many assumptions are made due to the lack of information about some physical parameters or due to the uncertainties about their actual values, such as, the exact value of material yield strength and the exact value of the part's thickness. This may lead to deviation between the results from test experiments and FE models. The sources of deviation can be classified as follows:

1. Deviation due to material: For example, consider that in FE analysis, isotropic materials are assumed to have homogeneous properties, whereas in reality, there are many factors that may lead to non homogeneous material properties, for example, imperfections in the microstructure, voids, ...etc.
2. Deviation due to geometry: For example, consider that in FE analysis, it is assumed that material thickness is uniform along the tube's circumference, whereas this may not be the case in real world due to manufacturing processes' deviations which can lead to non-uniform sizing.
3. Deviation due to load: For example, consider that in FE analysis, a longitudinal axial loading is assumed to be completely perpendicular to the tube's surface which is also assumed to be completely horizontal. And, it is also assumed that the load is perfectly aligned with the tube's axis, whereas in reality, these complete precise conditions can not be guaranteed.
4. Deviation due to measurement: In reality, physically measured quantities are subject to measuring tools tolerances and are also subject to the variation be-

tween different samples. This may cause a difference between measured and actual values.

The aforementioned sources can lead to a large difference between idealized FE simulations and reality, especially in nonlinear FE analysis. The intentional introduction of slight imperfection within the nonlinear FE model helps in accounting for the difference between reality and idealization. One can refer to Ref. [129] for more information on this important subject.

2.4 Applications of the Nonlinear FE Analysis

Due to the rapid development in the computational capabilities, the use of nonlinear FE analysis has been growing steadily in industry, especially in the automotive sector. In vehicle crash design, nonlinear FE analysis has been used to model: simple structural components, vehicle components, full vehicle structures, occupants and pedestrians. However, it should be noted that, despite the major development in current computation capabilities, nonlinear FE analysis remains a highly computationally demanding process, especially for large size models including different parts made of different materials as in crashworthiness simulations. In the following sections, the application of nonlinear FE analysis to simulate the crash in vehicle accident problems are briefly discussed.

2.4.1 Modeling Simple Vehicle Structural Components

Researchers used nonlinear FE extensively to study the response of simple structural components, mainly circular and square tubes used in vehicle structures, under impact. In an early work by Otubushin [130], he used LS-DYNA to model the experimental work of Abramwicz and Jones [131], in which they studied mild steel square

tubes under impact loading. It was shown that the simulation results were in good agreement with those obtained experimentally. Later, Langseth et al. [132] compared the experimental and the numerical results of AA6060 aluminum alloy square tubes under both static and dynamic loadings. They demonstrated that simulation results are in good agreement with experiments. Kormi et al. [133] studied the effect of implementing helical grooves in circular thin walled steel tubes under axial static and dynamic loading, they concluded that a system of tubes can be designed to serve as a crash energy absorber.

2.4.2 Modeling Vehicle Structures

Zheng et al. [134] studied the quasi-static crushing of an S-shaped aluminum front rail and derived a simple analytical solution for the force-deflection response, which compared reasonably well with the numerical results. Tehrani et al. [135] investigated improving the crashworthiness performance of S-frames by incorporating ribs inside. They also used two materials in the S-frame design to improve crashworthiness and to reduce the weight [136]. Hosseinzadeh et al. [137] used LS-DYNA to perform a parametric study on a commercial bumper system, and studied the shape, material, and impact conditions to reduce its weight and to improve its crashworthiness performance. Mao et al. [138] studied rollover accidents using LS-DYNA, they concluded that simple design modifications can improve roof strength and energy absorption capabilities.

2.4.3 Modeling Full Vehicle Structure

Zaouk et al. [139, 140] presented a detailed procedure for modeling a full vehicle as part of a project to assess vehicle safety and to reduce the number of physical tests. They recommended that accurate geometric and material specifications in vehicle

structural components are important to obtain accurate responses using nonlinear FE models. Kwasniewski et al. [141] also used LS-DYNA to study, the crashworthiness of a commercial paratransit bus model consisting of 73600 finite elements and 23 material models, and proposed recommendations for bus body manufactures to improve its safety. Qi et al. [142] used LS-DYNA to simulate a full frontal impact with a rigid wall at low and high impact speeds of a commercial automobile, and then used simulation to improve the design. Zhang et al. [143] used LS-DYNA as a simulation tool to produce input data to train a neural network. Then they used the neural network to reconstruct accidents scenarios and to predict the pre-impact velocity of the vehicle.

2.4.4 Modeling Occupants

Maruthayappan et al. [144] described the development of a FE dummy model to be used in simulating side impacts inside a Ford Taurus passenger car and they validated their model against test data. Arnoux et al. [145] presented the development process of a FE dummy model using RADIOSS which can be used to simulate occupants in vehicle accidents. Shah et al. [146] used a whole human FE model to simulate the response to impact in a car to car accident. They also studied the effect of impact on the thoracic and abdominal organs especially the effect on the blood vessels and the aorta and they compared their findings with autopsy data. Kitagawa et al. [147] used a human FE model to understand the mechanism of whiplash (injury to the cervical spine caused by an abrupt jerking motion) during rear collisions. Kim [148] studied the effect of restraint systems and air bags on brain injuries. He developed a simple model of the head only based on the analysis of a full human body model and concluded that the simplified model can be used effectively as it produced almost identical kinematic responses.

2.4.5 Modeling Pedestrians

Takahashi et al. [149] developed a FE model of the human lower limb using PAM-CRASH to understand the injury mechanisms of ligaments damages and bone fractures in car-pedestrian accidents. After validating their model with data from Post-Mortem Human Subjects (PMHS), they integrated their model with an upper body and finally used their full pedestrian model with FE car model to simulate a full car to pedestrian accidents. Lee et al. [150] used FE to develop a better hood and bumper designs to mitigate the effects of accidents on pedestrians. Yasuki [151] also used FE models of human male, female, and child to simulate the effect of impact on lower limbs and concluded that better designs of frontal structures can be achieved by varying their stiffnesses for less injuries to pedestrians. Kikuchi et al. [62] developed a FE model of the pelvis and lower limb of a pedestrian in a standing position subjected to impact by a Sport Utility Vehicle (SUV) modeled by another FE model and validated their model with published data.

2.5 Simulation of a Square Tube

Vehicle structures are made of simple building blocks in the form of thin wall (usually square) tubes. In accidents, these tubes serve as crash energy absorbing structures. Many researchers studied the response of these structural components under dynamic axial loading [25, 152, 153]. In this section, a nonlinear FE model of a thin wall square tube has been developed and the results are compared with these obtained from published experiments by Abramwicz and Jones [131]. The objective is to validate the nonlinear FE model (developed in LS-DYNA) and conduct a systematic sensitivity analysis on the number and types of elements to be used.

The experimental tests conducted by Abramwicz and Jones [131] included dropping

a 73.6 kg weight with a pre-impact speed of 10.288 m/s over a square tube with a side length of 37.07 mm, a wall thickness of 1.152 mm, and a height of 244.1 mm. From their published work, the time-velocity diagram of a specimen called I21 is used to validate the nonlinear FE model.

2.5.1 Description of the Nonlinear FE model

A geometrical model has been developed with the same dimensions of specimen I21 in Ref. [131]. To match the experimental results, an imperfection has been introduced in the form of a 0.5 mm outward misalignment in the middle of the wall section. Hypermesh [154] is a commercial parametric pre-processor which includes an automatic remesher, and it was used to develop the FE model for LS-DYNA. A view of the FE model is shown in Figure 2.3.

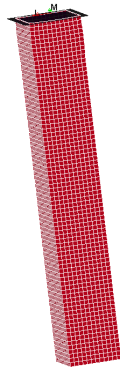


Figure 2.3: View of the FE model of the square tube

The *MAT PLASTIC KINEMATIC*, which is material type 3 in LS-DYNA [114], was used to model the material behavior under impact loading. This material model is suitable for modeling isotropic materials under impact loading and it is computationally efficient. The model is capable of capturing the material hardening effect and strain rate sensitivity by including the Cowper Symonds parameters [27]. The material properties taken from Ref. [131] are: yield strength $\sigma_y = 277.5$ MPa, density

$\rho = 7830 \text{ kg/m}^3$, Poisson's ratio $\nu = 0.3$, modulus of elasticity $E = 210 \text{ GPa}$, and Cowper Symonds parameters: $D = 6884 \text{ s}^{-1}$ and $q = 3.91$.

The impactor mass was modeled by a moving rigid wall using the *RIGIDWALL PLANAR* keyword in LS-DYNA [114]. The wall was given the same mass (73.6 kg) as the impactor in experiments and the same initial velocity 10.288 m/s. To prevent sliding at the proximal ends, the nodes located on the lower tube end were constrained in all directions and the nodes located at the upper tube end were allowed to move only in the longitudinal direction and constrained in other directions. The contact between the tube surfaces was modeled using the *CONTACT AUTOMATIC SINGLE SURFACE* keyword in LS-DYNA, in which the surfaces were given a coefficient of static friction of 0.74 and a coefficient of dynamic friction of 0.57 [155]. The default element type in LS-DYNA, which is the Belytschko-Lin-Tsai (T2) element was used to model the tube. The results of the simulation are presented and discussed in the following section.

2.5.2 Results and Discussion

In their published work, Abramowicz and Jones [131], published the velocity history diagram of the upper end of the tube (specimen I21). The same experimental results in Ref. [131] were also used by Otubushin [130] to validate his nonlinear FE model results using LS-DYNA. Thus, his results are also presented here for comparison. It should be noted that Otubushin used a total of 2124 elements of the Belytschko-Lin-Tsay (T2) shell element. In the following section, mesh sensitivity analysis is conducted to find the optimum number of elements to generate results close to the published velocity history signal in Ref. [131].

2.5.2.1 Mesh Sensitivity Analysis

In this study, the number of elements used to conduct mesh sensitivity analysis are: 384, 1372, 2232, 3888 and 38885. LS-DYNA simulation is conducted with each number of elements and the results of the velocity history signals are compared with those of Refs. [130, 131]. The results are shown in Figure 2.4. It is interesting to note that finer meshes are not necessarily producing accurate results in crash simulations. For example, a coarse mesh (384 elements) resulted in a relatively closer velocity signal to the experimental one. However, in order to verify that 384 elements are enough to model the tested tube, the final deformed shapes when using 384 and 1372 elements are compared with the final deformed shape of the tested tube in Ref. [131]. The final deformed shapes are shown in Figure 2.5, which clearly shows that there is a large difference between the deformed shape when using 384 elements and the deformed shape of the tube in Ref. [131]. On the other hand, using 1372 elements produces a final deformed shape that resembles the one in Ref. [131]. Moreover, using 1372 elements also produces a very close velocity time signal to the tested one in Ref. [131], thus 1372 is the optimum number of elements enough to model the tube.

It is interesting to note that using 1372 elements produces a velocity history that is in a good agreement with that reported in Ref. [131] and it is even in better agreement with experimental results compared with that of Ref. [130]. The number of elements (1372) is 35% less than that used in Ref. [130]. This can be attributed to the fact that in the present work 5 integration points through the thickness have been used, while 3 integration points have been used in Ref. [130]. Thus, to increase the accuracy with the same number of elements, one may use more integration points through the thickness.

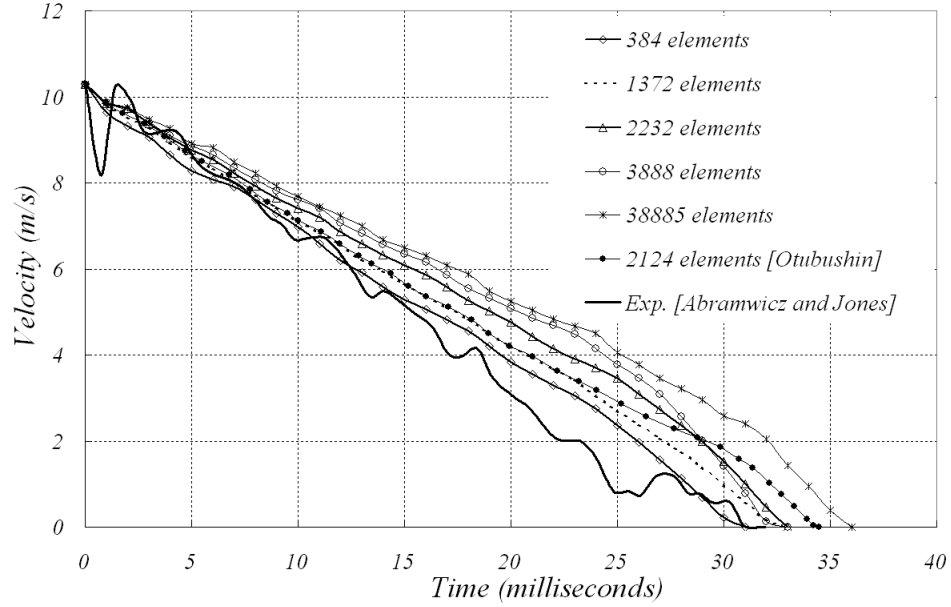


Figure 2.4: Velocity vs time for element T2 using different mesh sizes

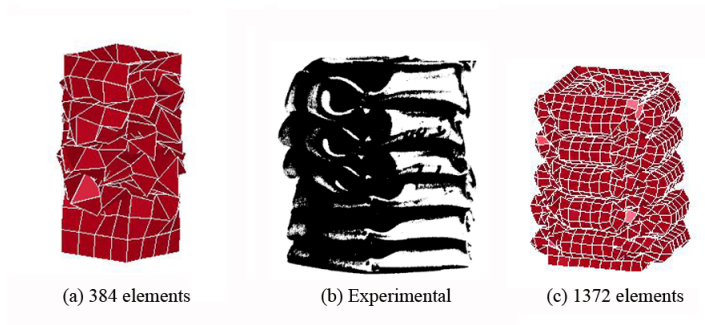


Figure 2.5: Final deformed shapes of the square tube

Figure 2.6 shows a comparison between the deformation-time signals of the upper tube end extracted from numerical simulations using different number of elements. It should be noted that no information regarding deformation versus time is provided in Ref. [131] explicitly. Thus, for the sake of comparison, the velocity versus time is integrated to obtain the deformation-time signal.

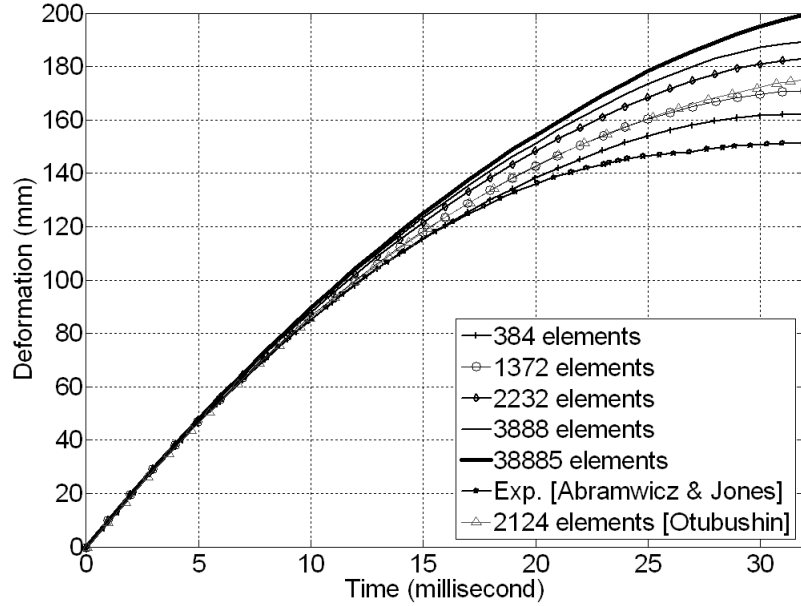


Figure 2.6: Deformation vs time for element T2 using different element sizes

It is obvious that, the final simulated deformation is generally higher than the experimental result. This observation is in accordance with previous findings by Langseth et al. [132], who reported that numerical analysis tends to overpredict the maximum deformation when compared with experimental test data. It is interesting to note that the results seem to deviate from the physical signal as the number of elements increase, which can be attributed to the aspect ratio (ratio between element thickness and length). Increasing the number of elements seems to deteriorate the convergence of the solution. This effect has also been reported by Wu and Saha [156], who mentioned that extreme mesh refinement can even lead to questionable results.

2.5.2.2 The Effect of Using Different Shell Elements

In this study, different shell elements are used to model the tube in order to compare their effect on the results. The final crush deformation (the final distance traveled by the tube end) is calculated for each element type. The values are then compared with the final crush deformation of specimen (I21) (151.16 mm). Figure 2.7 shows

the percentage error between the final crush deformation for each element and the one of specimen (I21). It should be noted that the triangular element (T27) has failed completely to model the tube. It is clear that triangular elements (T3, T4, T17 and T26) have large error values. It can be concluded that the use of triangular elements should be limited in areas where mesh refinement is needed. Finally, element (T25) has a large error value (about 50%). This element as well as other elements with thickness stretch, such as (T26 and T27) are primarily designed for modeling shells when large strains through the thickness are expected as in metal forming applications. Conventional shell elements assume that the thickness remains constant under loading which in turn leads to neglecting through the thickness stresses [157].

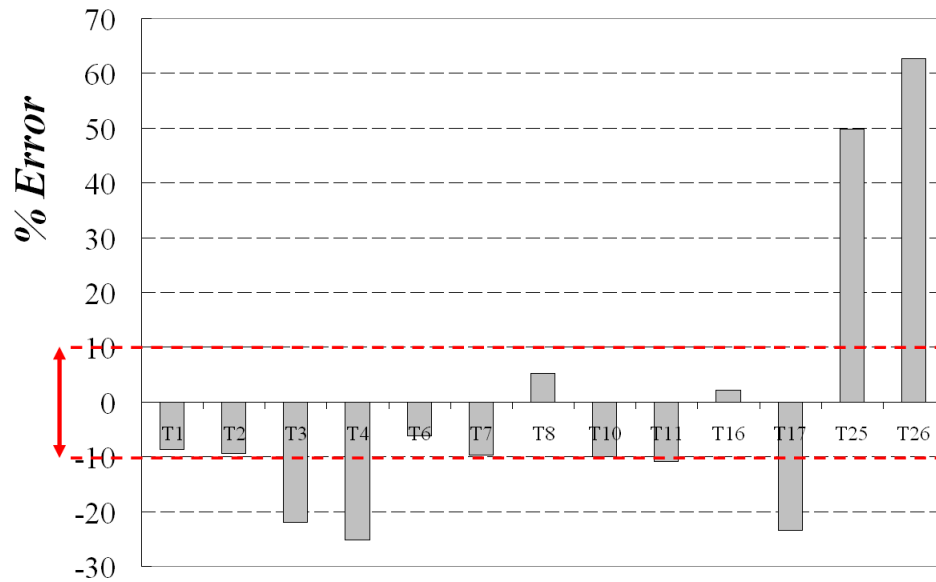


Figure 2.7: Error values between specimen (I21) and simulations for all element types

2.5.2.3 The Computational Time of Different Shell Elements

Figure 2.8 shows the recorded computation time for all element types. It can be noted that element type (T2) is the most computationally efficient element among all element types. Considering this, the element type (T2) offers a fine balance between accuracy and computation efficiency.

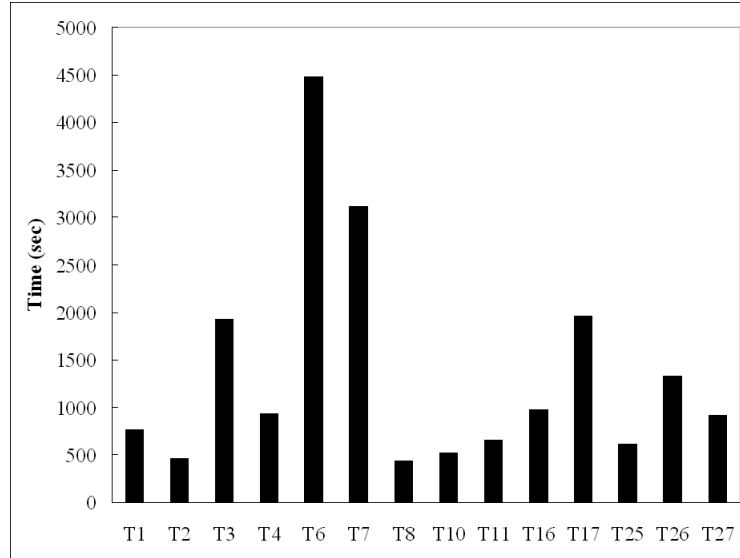


Figure 2.8: Recorded computational time for all element types

2.5.2.4 Snapshots of the Deformation History

Figure 2.9 shows the different stages of deformation and it shows that the tube deforms in a progressive manner into folds. The tube was modeled using the Belytschko-Lin-Tsay (T2) shell element and the number of elements was 1372.

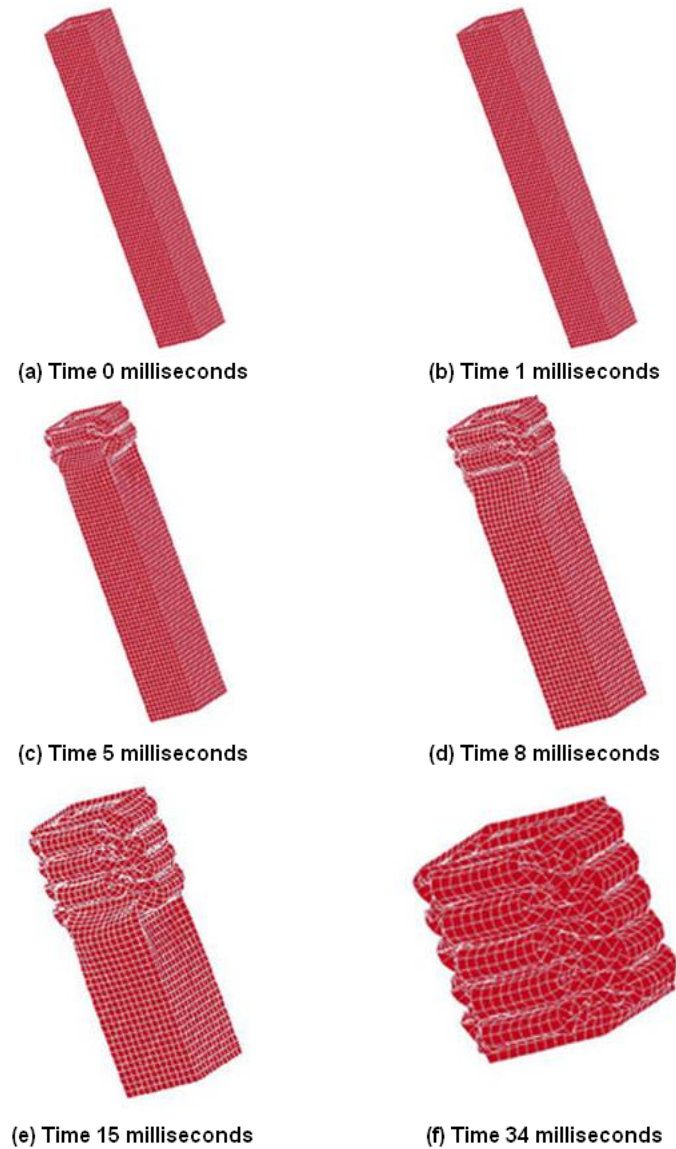


Figure 2.9: Different snap shots of the deformation history

2.5.2.5 The Effect of Imperfection

Figure 2.10 shows a comparison between two final deformed shapes: with and without consideration of imperfection. The imperfection was introduced in the form of a 0.5 mm outward misalignment in the middle of the wall section. Its purpose is account for the imperfection that naturally exists in the experimentally tested tube. It is clear that the two profiles have completely different folding patterns. The final

deformed shape of the tube with imperfection resembles the one for the tube that was tested experimentally in Ref. [131]. This clearly shows the importance of the role of imperfection in nonlinear FE analysis to generate realistic results, which has been previously discussed in section 2.3.7.

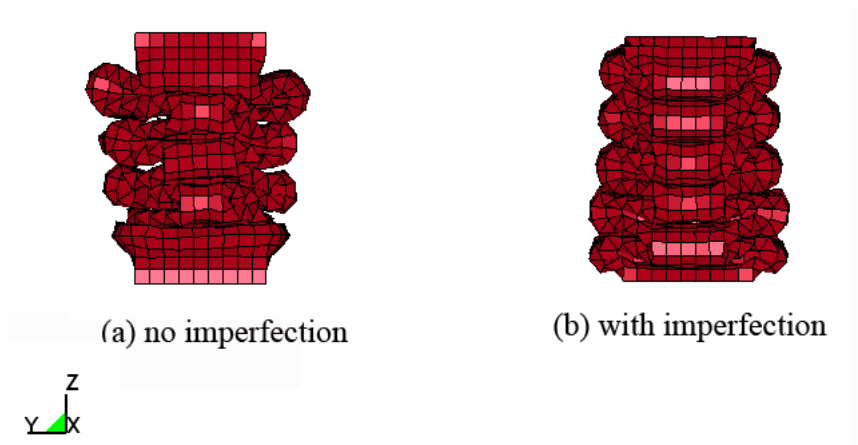


Figure 2.10: Comparison between two deformation profiles

2.5.3 Conclusion

It can be concluded that, the Belytschko-Lin-Tsay (T2) shell element is the most suitable element for modeling thin walled structures in crash simulations. The results clearly showed that the T2 shell element achieves a balance between accuracy and computational cost. Also, it can be concluded that, using a reasonable number of elements can produce accurate results compared to using a very large number of elements. Finally, it can be concluded that, implementing imperfection into the nonlinear FE model is important to acquire realistic results.

Chapter 3

Optimization for Crashworthiness

3.1 Introduction

As previously mentioned in chapter 1, in current competitive environment, applying optimization is inescapable for rapid product development and cutting production costs. However, applying optimization to the field of crashworthiness design is faced with certain challenges due to the complexity of the physical phenomenon of impact and the unavoidable complicated modeling approaches. In crashworthiness design, many responses are highly nonlinear with high frequency noisy characteristics. For instance, Figure 3.1 shows a typical rigid wall force on a 1839 kg pickup truck during a full frontal impact at 56 km/h with a rigid wall barrier.

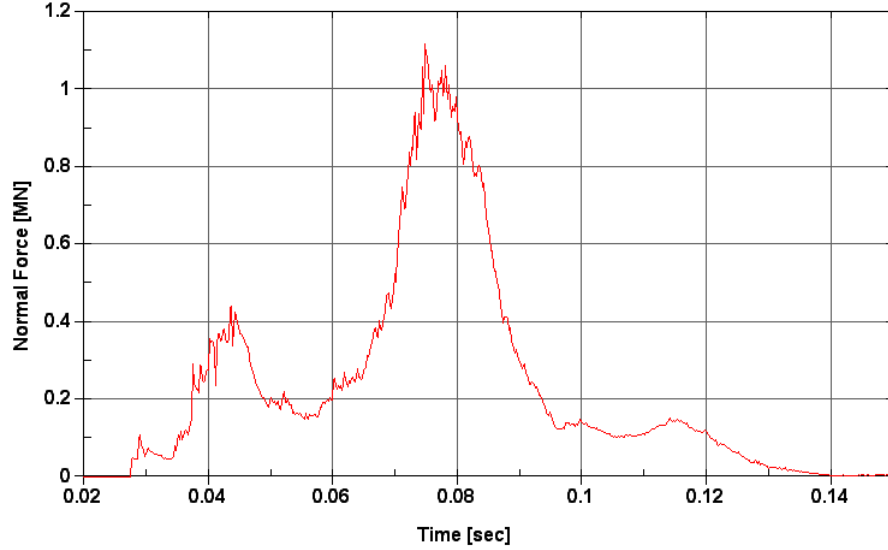


Figure 3.1: Typical reaction force-time history in a frontal impact

It is clear that, the system is highly nonlinear and it includes high frequency noise. If a gradient based algorithm is directly connected with the nonlinear FE analysis, the problem becomes impossible to solve due to the extremely high computational cost. Moreover, gradient based algorithms require gradients of the objective and constraint functions, which cannot be obtained analytically due to the complexity of the problem. Numerical evaluation of the gradients may also fail or generate spurious results due to the noisy nature of the responses. In the case of using nongradient based algorithms such as genetic algorithms, a much larger number of iterations is required compared with gradient based techniques. However, applying optimization directly to a nonlinear FE model is not practical and an alternative method based on approximation techniques should be investigated. In the following section, the meta-model building using approximation techniques is described. Then, meta-models are used to solve two optimization problems: (1) the Rosenbrock function and (2) crash-worthiness improvement of an S-Rail. Next, the proposed methodology is explained in detail and followed with an illustrated example. Finally, a detailed discussion of the results is presented.

3.2 Meta-model Building

Meta-models are *easy to calculate* approximate models of the *difficult to calculate* actual models. The process of building a meta-model is illustrated in the flow chart shown in Figure 3.2. Meta-models are constructed from sampled data either gathered from physical experiments or calculated from computer simulations using nonlinear FE analysis. The data is sampled from the design space of interest. The designer based on his experience specifies the range in which design variables can change. Then, this multi-dimensional design space is discretized to points, where each point represents a combination between variables at different levels. To minimize the number of required data points needed to build the meta-model, Design of Experiments (DOE) is used. DOE is a statistical technique used to maximize the information gain using the minimum number of experiments. In the following section, a brief review of DOE is presented.

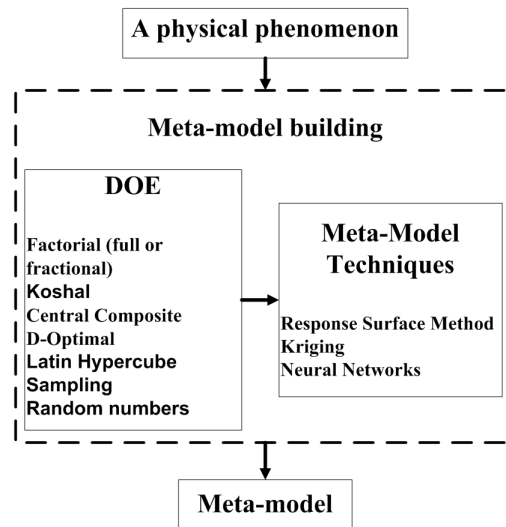


Figure 3.2: The meta-model building process

3.2.1 Design of Experiments (DOE)

DOE is the science of designing experiments with different influencing variables to understand the behavior of one or more responses. DOE was founded by Sir Ronald A. Fisher, who in the early 1920's published his landmark book (The Design of Experiments) [158]. He formulated the basics of the science in his book and studied the effect of different fertilizers and other variables (soil condition and moisture content, ...etc) in different land plots on the final condition of the crop [159]. Now, DOE is widely used in agriculture, industrial design, pharmaceuticals, management, marketing, chemical engineering, life science, ...etc. DOE is basically the statistical tool for minimizing the number of expensive time consuming experiments while maximizing the information gain from these experiments. In a report published by NASA in 1969 [160], it was described in detail how DOE along with mathematical optimization principles were used to develop an improved Cobalt-Nickel alloy. With the advancement of computer hardware and software, researchers realized the usefulness of DOE and started using it as means to minimize the burden of computations without sacrificing accuracy as much as possible. It should be noted that, although there are many different DOE designs for selecting data points from a multi-dimensional design space [161], not all of them are suitable for computer experiments. A brief description of the suitable DOE methods is provided here.

3.2.1.1 Factorial

There are two kinds of factorial design techniques called, full factorial and fractional factorial. In full factorial design, the design is composed of all the combinations of design variables at all levels. For a system with two design variables in which each variable can take a value from one of two values (levels), a full factorial design then has $2^2 = 4$ points. Thus for a design with k variables and l levels, there are l^k

data points. The number of points increases exponentially with the number of design variables. Therefore, it is typically used with small number of design variables.

In a fractional factorial design, a fraction of the full factorial design is considered. The number of design points is l^{k-p} , where p is a number that defines the size of the fraction.

3.2.1.2 Koshal

The Koshal design was suggested by Koshal in 1933 [162] to minimize the number of points in the full factorial design, and it uses the one factor at the time principle.

3.2.1.3 Central Composite

The central composite design uses a 2^k factorial design plus the center point and the face center points. The design then consists of $2^k + 2k + 1$ points.

3.2.1.4 D-optimal

The D-optimal criterion is one of the alphabetic optimality techniques, which are based on minimizing the variance within the estimated response from the meta-model [163].

Assume β as the vector of unknown coefficients in a meta-model of the form $\hat{y} = X\beta$, where \hat{y} is the approximated response and X is the design matrix. The value of the variance in β , $var(\beta)$ is related to $(X^T X)^{-1}$ [164].

An accurate meta-model is a model with minimum value of $var(\beta)$. Minimizing the value of $var(\beta)$ corresponds to maximizing the value of $|X^T X|$. This can be formulated into an optimization problem as:

$$\begin{aligned}
& \textit{Find } X \textit{ that :} \\
& \textit{Maximizes } |X^T X| \tag{3.1}
\end{aligned}$$

X can be continuous, discrete or a combination of both. The genetic algorithm [165] is a natural choice for solving this type of problems [166].

For selecting design points for crashworthiness problems, Redhe et al. [167] suggested using 1.5 times the minimum number of points. It is noted that, the minimum number of points is the same number as unknown coefficients in the model. For example, for a linear model with only two variables in the form of $y = a_0 + a_1 \cdot x_1 + a_2 \cdot x_2$, three points are the minimum for calculating the values of the coefficients a_0 , a_1 and a_2 .

3.2.1.5 Latin Hypercube Sampling

The Latin Hypercube Sampling (LHS) design was proposed by Mckay et al. [168] and was specifically designed for computer simulation experiments. Each design variable is divided at n number of intervals. n values for the first variable are randomly selected based on equal probability. Then, these n values are randomly combined with n randomly selected values for the second design variable. The two n pairs are then combined with n randomly selected values for the third design variable. The process proceeds until all variables are included. LHS allows unbiased estimation of the main effect of all variables in the design space.

3.2.1.6 Random Numbers

In this type of design, the design space is sampled at random. It is usually used to study new systems when no a priori knowledge is available.

3.2.1.7 Remarks on DOE Designs

Both LHS and random numbers designs depend on the quality of the used pseudo-random numbers. *Pseudo-random* are random numbers created using an algorithm, different from the *true-random* numbers generated from a physical process.

The creation of the design matrix for certain type of DOE design can be made automatically with any of the available statistical softwares. However, special care must be taken as some of the DOE techniques are not suitable for meta-modeling of computer based simulations. This originates from the fact that computer simulations are deterministic in nature, i.e., a computer simulation will always give the same results for a fixed input, whereas physical experiments will have a varying output within a certain limit according to the testing conditions. This has been pointed out by Sacks et al. [169] and by Welch et al. [170], who mentioned that not all DOE are ideal for deterministic computer experiments. Sacks et al. [171] also discussed the differences between deterministic and non deterministic based meta-models.

The D-optimal criterion has been proven to be suitable for computer based simulations as it is based on minimizing the variation within the model's estimated output and it has been recommended to produce acceptable results [172, 173]. In his PhD thesis, Roux [174] states that the D-optimal criterion offers a compromise between computational cost and accuracy.

Xu et al. [175] have studied different DOE techniques and they mentioned that the D-optimal criterion is *specially recommended* for situations when there is a priori knowledge available about the design variables and is *necessary* when this information is unavailable.

Roux et al. [176] described other advantages of the D-optimal criterion as: (1) It is suitable for design spaces with irregular shapes, (2) It is flexible in offering any number of design points, and (3) A new design of experiments can be altered to

incorporate design points from an older design.

3.2.2 Meta-Model Techniques

The three basic techniques for building meta-models are: (1) Response Surface Method (RSM), (2) Kriging and (3) Neural networks. A brief description of each technique is provided in the following sections.

3.2.2.1 Response Surface Method (RSM)

RSM is an approximation technique used to construct response functions in the form of polynomial (usually second order) functions. These functions are smooth approximations and are ideal for responses with noisy behaviors. Thus, they can be effectively used in any gradient based or non gradient based optimization algorithm. Giunta et al. [173] demonstrated that RSM is effective at filtering out the numerical noise intrinsic to most computer based simulations. RSM is a global approximator, which offers the designer the opportunity to explore the response within the global design space [177]. A detailed review of RSM can be found in [163].

RSM first appeared in the work of Box and Wilson [178], who in 1951 published an article on the subject of proper model selection for arriving at optimum output responses in experiments. They suggested a linear model to approximate the output responses. Although their work was applied to chemical engineering experiments, they mentioned that it can be applied to other disciplines as well.

Having recognized the potentials of RSM, much work has been done for developing more suitable DOE methods for modeling experiments with large variations [163,179–181]. RSM is basically based on using regression analysis to formulate a polynomial function. For instance, a second order polynomial model can be written as:

$$\hat{y} = X\beta \quad (3.2)$$

where X is the $n \times m$ design matrix, in which n is the number of undertaken experiments and m is the number of unknown model coefficients β . \hat{y} is the approximation of the output response y that can be written as:

$$y = \hat{y} + \epsilon \quad (3.3)$$

where $\epsilon = y - X\beta$ is the error between the true response y and its approximation \hat{y} . As it can be realized, an optimum approximate model is the one with minimum error ϵ . The problem then is to find the values of the unknown coefficients β that will minimize the value of ϵ . This can be easily achieved using the least squares technique.

Let $L = \sum_{i=1}^n \epsilon_i^2$ be the value of the summation of squared error ϵ for all data points. In matrix form L can be represented as $L = \epsilon^T \epsilon$, where ϵ^T is the transpose of ϵ . Substituting $\epsilon = y - X\beta$ into L yields:

$$L = \epsilon^T \epsilon = (y - X\beta)^T (y - X\beta) \quad (3.4)$$

To minimize L , one may simply differentiate L with respect to β and equate it to zero to find β as:

$$\beta = (X^T X)^{-1} X^T y \quad (3.5)$$

It should be noted that $X^T X$ is assumed to be nonsingular.

Model Types

There are four types of regression models. For instance, for a model with five design variables $(x_1, x_2, x_3, x_4, x_5)$, which will be used later in Section 3.5, the four models can be represented as follows:

(1) A linear model (Model 1) that includes only basic variables and does not include any interaction between variables can be described as:

$$\hat{y} = a_0 + a_1x_1 + a_2x_2 + a_3x_3 + a_4x_4 + a_5x_5 \quad (3.6)$$

This type of model, represent a hyper-plane in the 5 dimension design space with no curvature since only first degree variables are included. The constant term represents the initial value of the response.

(2) A linear model with interaction (Model 2) that includes constant, linear, and interaction terms as in the following form:

$$\begin{aligned} \hat{y} = & a_0 + a_1x_1 + a_2x_2 + a_3x_3 + a_4x_4 + a_5x_5 + a_{12}x_1x_2 + a_{13}x_1x_3 \\ & + a_{14}x_1x_4 + a_{15}x_1x_5 + a_{23}x_2x_3 + a_{24}x_2x_4 + a_{25}x_2x_5 \\ & + a_{34}x_3x_4 + a_{35}x_3x_5 + a_{45}x_4x_5 \end{aligned} \quad (3.7)$$

This model allows for the first order interaction between variables and it represents a hyper-plane in the variables space.

(3) A quadratic model (Model 3) that includes constant, linear, interaction, and

squared terms in the following form:

$$\begin{aligned}
 \hat{y} = & a_0 + a_1x_1 + a_2x_2 + a_3x_3 + a_4x_4 + a_5x_5 + a_{12}x_1x_2 + a_{13}x_1x_3 \\
 & + a_{14}x_1x_4 + a_{15}x_1x_5 + a_{23}x_2x_3 + a_{24}x_2x_4 + a_{25}x_2x_5 \\
 & + a_{34}x_3x_4 + a_{35}x_3x_5 + a_{45}x_4x_5 + a_1x_1^2 + a_2x_2^2 + a_3x_3^2 + a_4x_4^2 + a_5x_5^2
 \end{aligned} \tag{3.8}$$

This model is quite flexible in representing wide varieties of models especially when there is no prior knowledge about the type of the model to be used. Thus, it is the default model of choice in RSM application. It represents a hyper plane in the design space with curvature due to the second degree terms.

(4) A pure quadratic model (Model 4) that includes constant, linear, and squared terms described in the following form:

$$\begin{aligned}
 \hat{y} = & a_0 + a_1x_1 + a_2x_2 + a_3x_3 + a_4x_4 + a_5x_5 \\
 & + a_1x_1^2 + a_2x_2^2 + a_3x_3^2 + a_4x_4^2 + a_5x_5^2
 \end{aligned} \tag{3.9}$$

This model represents a hyper-plane with curvature, but it includes no interacting terms.

Meta-model selection is the process in which the designer tries to find the best approximation that fits the data. A prior knowledge about the system being modeled will facilitate this process. This knowledge can include the type of variables that are important to the output response. Also, knowledge about the type and level of interaction between variables, if any exists, will help in formulating the approximate model. However, this information is not always available, and a trial and error process is inevitable. In such a case, different meta-models are evaluated based on their success in approximating the data, the model with the highest accuracy is then selected.

Measuring Accuracy

It is important that the accuracy of the developed meta-model is verified so that it can be used with confidence in the optimization process. The coefficient of determination known as R^2 is typically used to check the model's ability to identify the variation within the output response [182] and is defined as:

$$R^2 = 1 - \frac{SSE}{SST} \quad (3.10)$$

where

$$SSE = \sum_{i=1}^n (y_i - \hat{y}_i)^2 \quad (3.11)$$

and

$$SST = \sum_{i=1}^n (y_i - \bar{y})^2 \quad (3.12)$$

where y_i is the true output response, here calculated from nonlinear FE analysis, \hat{y}_i is the approximate response calculated from RSM, \bar{y} is the average of the true response, and n is the number of design points used to generate the model. R^2 varies between 0 and 1, where values close to 1 mean that the approximate model has high ability to explain the variations within the output response [182].

The value of R^2 will not decrease by adding new variables. This means that R^2 can increase even by adding unnecessary variables. In fact, R^2 can be brought to 1 if a model with $(n - 1)$ of variables is used to fit n points. Therefore, $adjR^2$ is used instead, which adjusts R^2 by dividing both SSE and SST by their associated degrees of freedom as:

$$adjR^2 = 1 - \frac{\frac{SSE}{(n-p)}}{\frac{SST}{(n-1)}} \quad (3.13)$$

where p is the number of design variables. $adjR^2$ will then account for adding unimportant design variables. Since for n points, the value of $\frac{SST}{(n-1)}$ is constant, then $adjR^2$ will increase only when adding new variables results in reducing the value of $\frac{SSE}{(n-p)}$. In fact $adjR^2$ may even decrease when adding new variables decreases the value of $(n-p)$ more than it decreases the value of SSE .

3.2.2.2 Kriging

Kriging, is a statistical technique for building empirical interpolations based on sampled data. It was named after D.G. Krige [183], who is in his Master's thesis applied this technique to estimate the true ore grade from sampled data. The Kriging model can be written as:

$$\hat{y} = f(x) + \kappa(x) \quad (3.14)$$

which is a combination of a polynomial function $f(x)$ which globally approximates the design space, and a stochastic component $\kappa(x)$ which adds deviations.

3.2.2.3 Neural Networks (NN)

Neural Networks (NN) are mathematical models based on principles inspired by brain style computation [184]. NN (or ANN for Artificial NN) can be considered as universal approximators [185], which require a considerable number of training data in order to generate reasonable approximations of the true responses. Thus, they are widely used in applications where large data are available such as in data mining [186–188].

The basic building block of a neural network (NN) is the neuron. A neuron is a processing unit which has some (usually more than one) inputs and only one output as shown in Figure 3.3. First each input x_i is weighted by a factor ω_i and the whole sum of inputs is calculated as $\sum_{i=1}^n \omega_i x_i = a$. Then an activation function (f) is applied to the result (a) to provide the neuron output as $f(a)$.

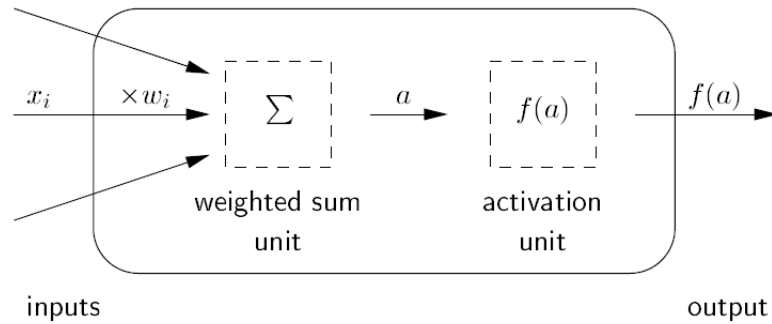


Figure 3.3: A schematic drawing of a neuron

As mentioned before, the function (f) is called the activation function. The most widely used function is the S-shaped or the sigmoid function as shown in Figure 3.4, which can be described as:

$$f(a) = \frac{1}{1 + e^{-a}} \quad (3.15)$$

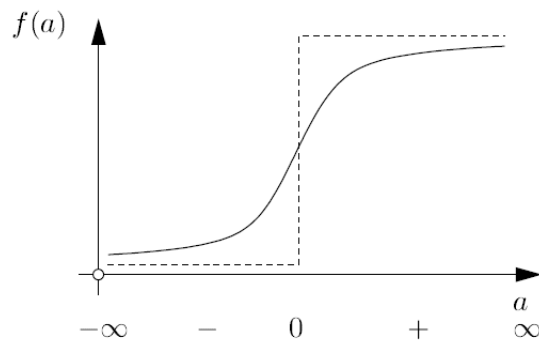


Figure 3.4: The Sigmoid activation function

Generally, neural networks are built by assembling neurons into layers and connecting the outputs of neurons from one layer to the inputs of the neurons in the next layer. Figure 3.5 shows a schematic drawing of a feed forward NN, i.e., with no feed back. Note that there is no processing on layer 0 and its role is basically limited to distributing the inputs to the next layer, so data processing starts at layer 1. The output of one neuron may go to the input of any neuron, including itself. If the outputs of a neuron from one layer are going to the inputs of neurons from previous layers then the network is called recurrent, thus providing feedback.

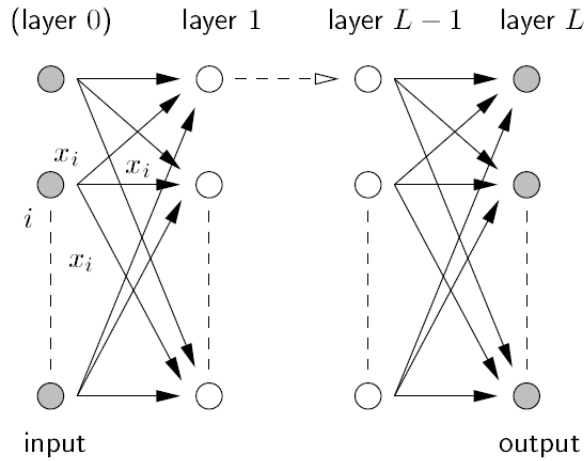


Figure 3.5: A schematic drawing of a NN

The process of adjusting the values of weights ω_i is called the training phase, in which an optimization algorithm adjusts the values of weights ω_i in order to minimize the Mean Squared Error (MSE) between predicted response \hat{y}_i and y_i :

$$MSE = \sum_{i=1}^n \frac{(\hat{y}_i - y_i)^2}{n} \quad (3.16)$$

In the training phase, a data set of sampled data from computer simulations or physical experiments is used and the neural network is presented with a pair of design variables and the associated response or responses. The weights are then adjusted

and the process proceeds until all the training data set is used. Another data set is then used to check the accuracy of the NN.

NN's are widely used in many applications. For example in an early work by El-Gindy et al. [189], the potentials of using NN for modeling vehicle dynamics and control systems has been investigated. Omar et al. [190] used NN to predict the nonlinear dynamic characteristics of the vehicle structure under frontal impact. Hajela and Lee [191] used NN to model crash responses of a rotorcraft and used the models to optimize the subfloor structure of the rotorcraft.

3.2.2.4 Remarks on Meta-Model Techniques

The Kriging technique has been criticized for its complexity and the lack of available software [192]. Moreover, Meckesheimer et al. [193] described some numerical problems with the model fitting. Jin et al. [194] concluded that the Kriging method can be very sensitive for noisy data .

For NN's, if a large number of layers (large number of unknown parameters) is used and if the training is allowed to run long enough, then the MSE could approach to zero value, which is known as *overfitting*. For a noisy data, this means that the model fits the noise within the data instead of interpreting the general trend of the data.

Stander et al. [195] compared between RSM, NN and Kriging for optimization of crashworthiness improvement and concluded that RSM and NN have performed better for this type of application. However, the problem with NN is that model's performance depends heavily on the layer architecture, which is unknown. Furthermore, the size of training data set drastically increases with the addition of a new layer. A well established application of NN technique can achieve good results, however, this is subject to the user's experience. On the other side, RSM has been used successfully with optimization problems and provided good results [196, 197].

It should be noted that *all* the above mentioned techniques suffer from the *Curse of Dimensionality*, which means that as the number of design variables increases, the number of data points needed for meta-model building also increases. This is further amplified depending on the level of complexity of the model being used.

In this current work, RSM is selected as an efficient meta-modeling technique to build the approximate models of the physical system.

3.3 Optimization of a Benchmark Analytic Function

In this section, the potentials of connecting the principles of meta-modeling with mathematical optimization for solving complex nonlinear problems is demonstrated using the Rosenbrock function. The Rosenbrock function was introduced by Rosenbrock in 1960 [198] as a complex nonlinear function and then was adopted as a benchmark problem for testing optimization algorithms. It was first used by De Jong [199] in 1975 to test the performance of a genetic algorithm. The Rosenbrock function is a two dimensional function in the following form:

$$f(x, y) = (1 - x)^2 + 100 \cdot (y - x^2) \quad (3.17)$$

The function has only one global minimum, which lies on a narrow flat valley with a parabolic shape. Although this minimum at (1, 1) can be easily obtained by simple differentiation, it is very difficult to be found numerically due to the high level of nonlinearity. The Rosenbrock function serves as an example of typical crashworthiness responses with high nonlinear behaviors. However, the difference is that in crashworthiness design, the form of the function is unknown and one has to steer for innovative techniques to estimate it using meta-modeling techniques.

Similar to crashworthiness problems, here the objective is to find the minimum value of the Rosenbrock function by building a meta-model which can approximate its behavior. Also, the solution should be found with as minimum number of function calculations as possible to make it comparable with crashworthiness design in which the value of the function is calculated by intensive nonlinear FE simulations.

Meta-modeling techniques such as RSM can be used to find an approximation of the unknown form of the function. Then, the approximate function can be connected with any optimization algorithm to find the optimum solution. The D-optimal DOE criterion is used to find a suitable number of data points. Here, twenty points are used and the Rosenbrock function is calculated at each point. The four meta-models as described in section 3.2.2.1 are used to model the data points. The $adjR^2$ value is then used to evaluate the performance of each model. As listed in Table 3.1, the pure quadratic model (Model 4) has higher $adjR^2$ value compared with other models and thus is selected as a proper approximation (\hat{y}) of the true function (y).

Table 3.1: Values of $adjR^2$ for different response surface models of the Rosenbrock function

Model 1	0.57
Model 2	0.54
Model 3	0.73
Model 4	0.75

Now, a mathematical optimization problem can be formulated as:

Find X^ that :*

Minimizes \hat{y} (3.18)

where, $x_L \leq x \leq x_U$

where $x_L = [-1, -1]$ and $x_U = [1, 1]$. The direct search method [200] in the MATLAB optimization tool box is used to solve the optimization problem stated above. The initial point was assumed to be $x_{in} = [-1, -0.5]$ with a function value $f(x_{in}) = 229$. The optimal solution was found to be at $X^* = [-0.0031, 0.8583]$ after 36 iterations. The value of the Rosenbrock function at the optimum solution (74.5) is 67% times less than the initial value (229). This means that the objective function has been improved significantly. It should be noted that the optimum solution is not the global optimum, however, it was achieved at a compromise between time and accuracy.

3.4 Optimization of a Vehicle S-Rail

The S-Rail is a longitudinal thin walled structure in the shape of the letter S and is used as a supporting structure. The automobile sub systems are supported on lateral cross members which are connected to the S-Rail. The S-Rail and the cross members basically form the chassis frame of the vehicle structure. For more information, one may refer to Ref. [201]. The S-Rail plays an important role as a crush member, especially in frontal crashes. In this section, the principle of using meta-models for improving the crashworthiness of the S-Rail by mathematical optimization is demonstrated. To simplify and to lower the computational requirements, a simple prototype FE model is used.

3.4.1 Problem Statement

It is required to improve the baseline design of an S-Rail for crashworthiness. The objective is to increase the amount of impact energy that this structure can absorb at an impact velocity of 10 m/s (27 km/h). The baseline design as shown in Figure 3.6 consists of three parts. The thickness of each part is considered as a design variable,

thus there are three design variables. The initial design values are assumed to be $[x_1=0.5, x_2=2.5, x_3=2.5]$ mm. With these initial values, the S-Rail weighs 3.1 kg and absorbs a maximum of 251.4 J at the designated impact speed of 27 km/h. Lower and upper bounds of the design variables are assumed to be 0.5 and 2.5, respectively.

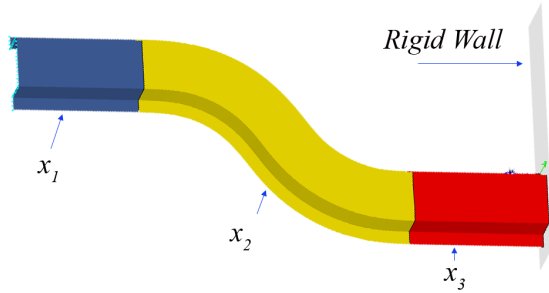


Figure 3.6: View of the S-Rail

3.4.2 Solution Approach and Results

One way of solving this problem is to conduct physical experimental tests at all design space points until a feasible optimum design is reached. However, considering a step size of 0.5 mm for each design variable, yields a total of $(5 [levels])^{3[variables]} = 125$ design points, which is clearly impractical and very expensive to perform. It should be noted that the number increases to 729 if a step size of 0.25 mm is used instead. Even if a DOE technique is used to minimize the number of experiments, the time and cost is still inconceivable. Also, using intuition or even experience to guide the tests does not guarantee that a feasible solution can be reached.

On the other hand, adopting numerical simulation by nonlinear FE modeling is an attractive option. Although, the method has not been matured enough to the point that no physical experiments are required, the method is admissibly reliable to cut down on the number of required tests, and mostly, only a final physical test is needed to validate the simulation results. Nevertheless, due to the complexity of nonlinear

dynamic problems, FE simulation does come with its own cost in terms of computational demands. Consequently, it is also impractical to simulate the 729 designs or even the 125 ones, especially in the current competitive environment, in which the design time window is being narrowed steadily. For these reasons, a meta-model is established with an appropriate number of simulations by a DOE technique and this meta-model is then used in a systematic form to search for a feasible optimum solution.

The FE Model

The FE model has been developed in LS-DYNA to simulate the impact behavior of the S-Rail. For the sake of simplicity and lowering the computational cost, a model at a reduced scale has been constructed. A scale of 0.4 is used to scale down the full model, and scaling laws [11] are used to transform other model parameters, such as component mass and initial kinetic energy, into reduced values. The parameters of both the full scale model and the reduced scale model are presented in Table 3.2. It should be noted that neither material properties nor impact speed can be scaled [11].

Table 3.2: Full scale and prototype model parameters for the S-Rail

Quantity	Full scale	Prototype
Component mass (kg)	46.8	3
Kinetic energy (kJ)	586	3.75

The FE model consists of 5093 shell elements modeled by the Belytschko-Lin-Tsay element (type 2 in LS-DYNA) with an average element length of 6 mm. The MAT PLASTIC KINEMATIC material model (type 24 in LS-DYNA) is used to model the behavior of material under impact. The material properties are presented in Table 3.3.

Table 3.3: Material properties of the S-Rail

Property	value
Density (kg/m^3)	7820
Young's modulus (GPa)	207
Poisson's ratio	0.3
Yield strength (MPa)	200
Tangential modulus (GPa)	0.2

The D-optimal criterion is used to generate data points for building the meta-model. For a design with three variables coupled with a quadratic RSM model, a minimum of 10 points is needed according to $\frac{(n+1) \cdot (n+2)}{2}$ where n is the number of design variables. Redhe et al. [167] have suggested using 1.5 times this number when using the D-optimal criterion. Here, 20 points are used to generate more accurate results. Using design of experiments based on the D-optimal criterion, the design matrix can now be easily established as provided in Table 3.4.

Table 3.4: The design matrix of the response surface model for the S-Rail

ID	x_1	x_2	x_3	ID	x_1	x_2	x_3
1	1	1	1	11	2.3	2.5	0.5
2	2.5	0.5	1.3	12	1.7	1.3	1.7
3	2.5	0.5	0.5	13	2.5	2.5	1.5
4	0.5	2.5	2.3	14	2.5	2.5	2.5
5	1.5	0.5	0.5	15	1.5	0.5	2.5
6	1.9	2.5	2.5	16	2.5	2.3	2.5
7	0.5	0.5	1.3	17	0.5	1.5	2.5
8	0.9	2.5	0.5	18	1.7	2.5	0.5
9	0.5	1.3	2.5	19	2.5	1.1	0.5
10	2.5	0.5	2.5	20	1.5	1.5	1.7

Next, LS-DYNA simulations are performed at each of the design points provided in Table 3.4 and output responses are evaluated. Since the objective is to maximize the amount of Impact Energy (IE) absorbed without increasing the weight (Mass), these two outputs are then collected and used for building the meta-models.

The four models described in section 3.2.2.1 are used to construct the approximate model of the S-Rail. The accuracy of the models is evaluated using the $adjR^2$ and the values are provided in Table 3.5. The results show that the quadratic model (Model 3) has the highest accuracy and thus is used to approximate the output responses. The $adjR^2$ for Mass is one for all model types because Mass is a function of cross section area, which in turn is a function of parts thicknesses. Thus, the variation within Mass can be totally explained by parts thicknesses.

Table 3.5: Values for $adjR^2$ for different RSM models for the S-Rail

	Mass	IE
Model 1	1	0.75
Model 2	1	0.92
Model 3	1	0.97
Model 4	1	0.80

Now, an optimization problem can be formulated based on the design requirements and developed meta-models, which can be used to represent the objective and the constraint functions as follows:

$$\begin{aligned}
 & \textit{Find } X^* \textit{ that :} \\
 & \textit{Maximizes } IE \\
 & \textit{Subjec to: } Mass - Mass_{original} \leq 0 \\
 & \textit{where, } x_L \leq x \leq x_U
 \end{aligned} \tag{3.19}$$

The optimization problem is solved using the Sequential Quadratic Programming (SQP) algorithm [202], which is a powerful gradient based nonlinear mathematical programming technique in MATLAB. After 9 iterations, as shown in Figure 3.7, the algorithm converged to a feasible optimal solution at $X^* = (2 \ 2 \ 2)$.

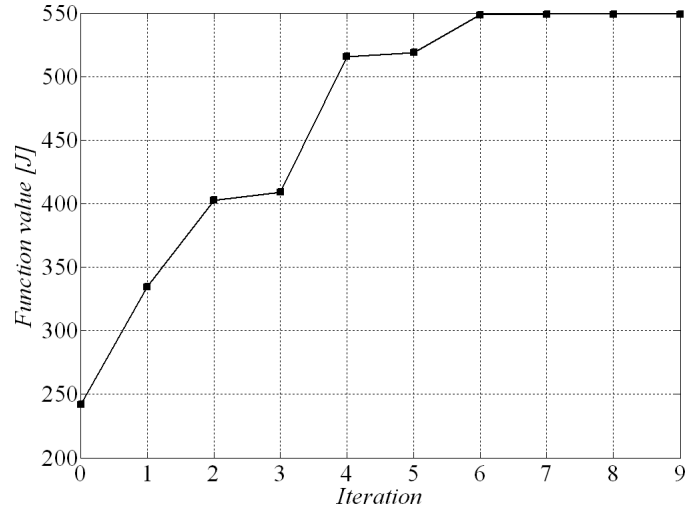


Figure 3.7: Iteration history of the optimization problem of the S-Rail

A full FE analysis of the model at this optimal solution yields a value of 528 J for IE, which is more than double the initial value (251.4 J). Mass is found to be slightly less than 3 kg, Thus the derived optimal design not only has increased IE appreciably, it has reduced mass slightly as well.

Adding Another Constraint to the Problem

While inspecting the time response of the Rigid Wall reaction Force (RWF), a peak value (RWFmax) of 60.34 N is observed which is about 3.4 times the corresponding value in the baseline design. According to the regulations, RWFmax must not exceed 40 N. In fact, the baseline design marked 17.6 N for RWFmax.

Considering this, another meta-model was established to account for RWFmax. Again, in this case, the quadratic model (Model 3), also proved to be more accurate than

other models with a value of 0.95 for the $adjR^2$ parameter.

The optimization problem is redefined to reflect the new design requirement by adding another constraint to the optimization problem as:

$$\begin{aligned}
 & \text{Find } X^* \text{ that :} \\
 & \text{Maximizes } IE \\
 & \text{Subject to: } Mass - Mass_{original} \leq 0 \\
 & \quad \quad \quad RWF_{max} - RWF_{limit} \leq 0 \\
 & \quad \quad \quad \text{where, } x_L \leq x \leq x_U
 \end{aligned} \tag{3.20}$$

After 10 iterations, as shown in Figure 3.8, the algorithm converged to a feasible solution at $X^* = (2.5 \ 2.27 \ 1)$.

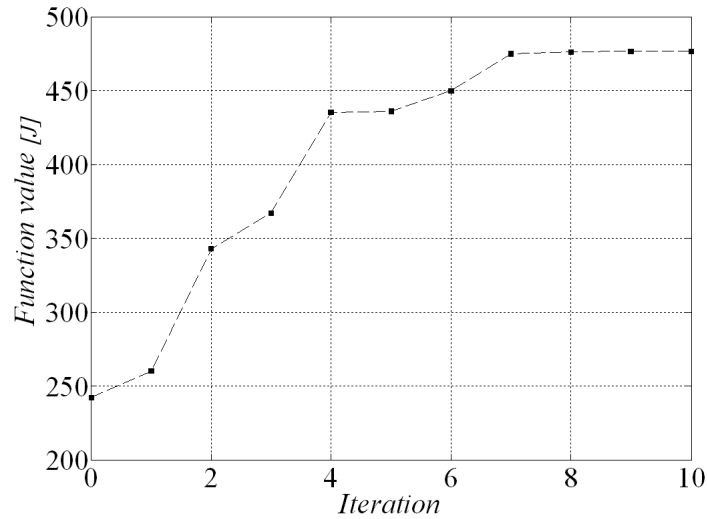


Figure 3.8: Iteration history of the constrained optimization problem of the S-Rail

This design configuration weighs slightly less than 3 kg and after conducting full FE simulation on the optimal solution, it gives a value of 522.75 J for IE and 37 N for RWFmax. The values for Mass, IE, RWFmax for the optimum design without

consideration of RWFmax as a constraint (Design 1) and the optimum design with consideration of RWFmax as a constraint (Design 2) are all normalized with respect to the baseline design and shown in Figure 3.9.

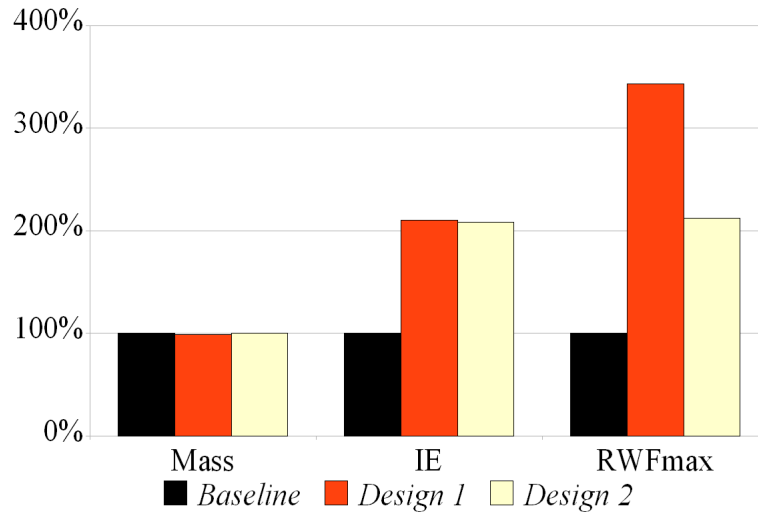


Figure 3.9: Comparison between Design 1, Design 2 and baseline for Mass, IE and RWFmax

Examination of the results reveals that by conducting the design optimization based on RSM on the S-Rail component, one can considerably increase IE of the S-Rail while guarding against maximum allowable rigid wall force. The optimal solutions basically obtained parts' thicknesses for better energy absorption and the two optimal designs improved IE by approximately twofolds while keeping the mass slightly lower than the mass of the baseline design.

3.5 Proposed Methodology

Here, a methodology for enabling an efficient and practical application of optimization for crashworthiness of vehicle structures under impact is proposed. The proposed methodology consists of three main stages. In stage 1, a full nonlinear transient dynamic finite element analysis using LS-DYNA is conducted on the full vehicle model

under frontal impact. The crashworthiness behavior of different major structural parts is examined based on their impact energy absorbed. Then, the main structural part contributing most to the total amount of impact energy absorbed in the whole vehicle structure is identified. This part is then modified to assure its crashworthiness behavior when treated individually under the same impact scenario, is similar to that in the full vehicle model. Crashworthiness design optimization is then conducted on this modified major component. However, as the traditional direct gradient based optimization is not practical for this large size complex problem, in stage 2, a surrogate model of this major component will be developed based on the design of experiment and response surface methodology. The developed surrogate model is the smooth representation of the crash response signals (which have noisy behavior) and can be effectively used in formulating a crashworthiness design optimization problem in stage 3.

Stage 1

In stage 1, as shown in Figure 3.10, the major influential structural components are identified based on analyzing the detailed nonlinear FE model of a full vehicle under frontal impact. Separate nonlinear FE models of these major parts are then created and modified so that their response characteristics once treated individually will match their relative response once integrated in the full model under the same conditions. This step is important as the output of these separate models can be related to that in the full model.

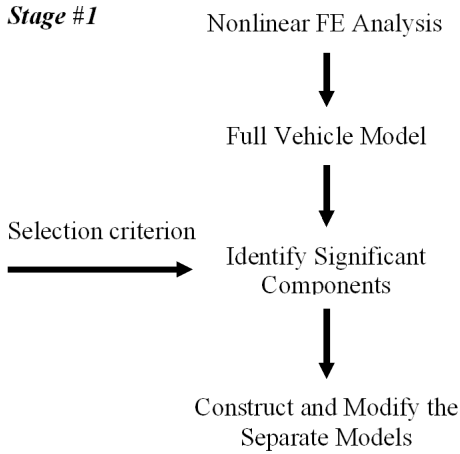


Figure 3.10: A flow diagram of stage 1

Stage 2

In stage 2, the models are parametrized so that simulation can be automated, as shown in Figure 3.11. A suitable approximate model is selected, and design points are determined using DOE. Simulation is then conducted at each point to generate the required output responses. The unknown coefficients are calculated using linear regression analysis and the accuracy of the model is checked. If the accuracy is not satisfactory, another approximate model is then selected, and the process continues until acceptable models are reached.

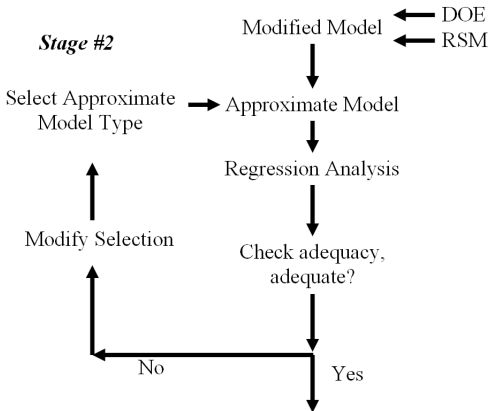


Figure 3.11: A flow diagram of stage 2

Stage 3

In stage 3, an optimization problem is formulated using the approximate models to represent the objective function and the constraints as shown in Figure 3.12. Now, no longer the optimization problem depends on intensive calculations by nonlinear FE simulations, instead easy to calculate RSM polynomials are used. This makes the optimization problem manageable by any available optimization algorithms.

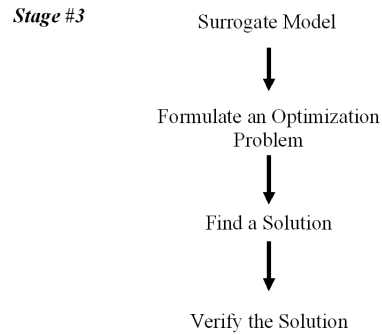


Figure 3.12: A flow diagram of stage 3

3.6 Illustrative Example

To demonstrate the proposed methodology, a full vehicle model of a Chevrolet C2500 pickup from the public domain [203] is used. Using LS-DYNA, a full frontal vehicle impact test is simulated in which the vehicle is impacted to a rigid wall at a velocity of 56 km/h (35 mph) according to the Federal Motor Vehicle Safety Standard FMVSS208 regulations for frontal impact [16]. The FE model of the vehicle is shown in Figure 3.13 and the model parameters are summarized in Table 3.6.

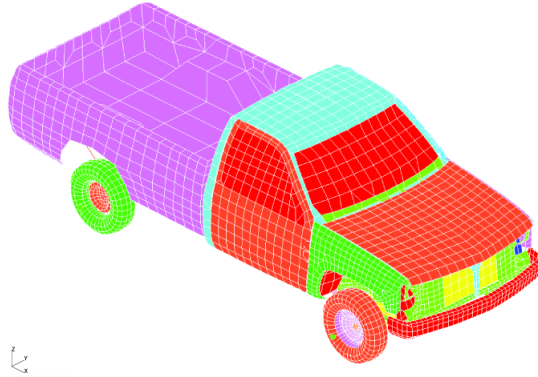


Figure 3.13: View of the Chevrolet C2500 pickup model

Table 3.6: FE model parameters of the vehicle model

Total mass	1839 kg
Pre-impact speed	56 km/h (35 mph)
Total length	235 mm
Number of shell elements	10518
Elements type	Belytschko-Lin-Tsay
Barrier	RIGID WALL PLANAR
Material type	Steel
Material model	MAT PIECEWISE LINEAR PLASTICITY
Contact model	CONTACT AUTOMATIC SINGLE SURFACE

3.6.1 Identification of Major Influencing Components and Construction of Reduced Models (Stage 1)

The Impact Energy absorbed (IE) is chosen as the selection criterion to identify the most influential components. Examination of the simulation output results reveals that the chassis frame as shown in Figure 3.14 is the major IE absorbing structure, which contributes nearly 61% of the total IE in the whole vehicle structure as shown in Figure 3.15.

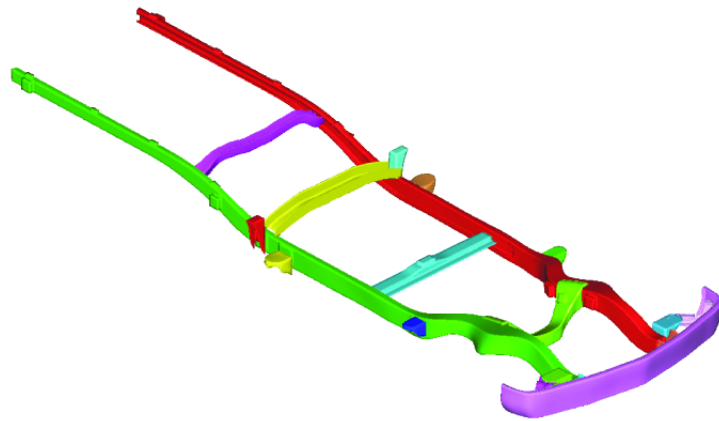


Figure 3.14: View of the chassis frame

Impact Energy Absorbed Analysis

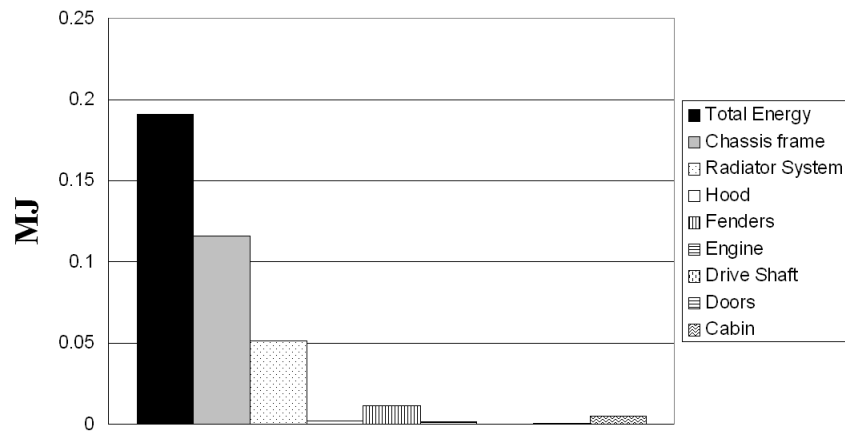


Figure 3.15: Comparison between IE for major structural components

Now, a separate nonlinear FE model of the chassis frame is constructed as shown in Figure 3.16 and then modified by adding lumped mass elements using the (*ELEMENT MASS) card in LS-DYNA [114]. The values of the masses are adjusted so that similar responses between the separate model and the full one can be achieved. The model is also modified by applying similar boundary conditions to those in the full model using the (*BOUNDARY SPC NODE) card [114].

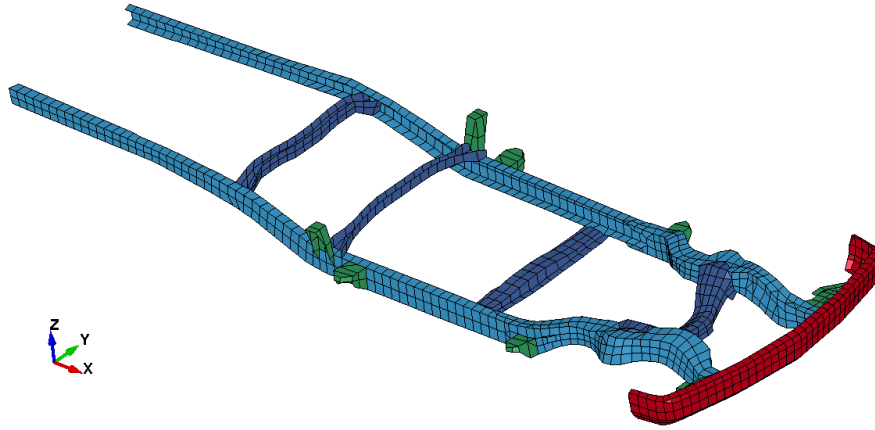


Figure 3.16: View of the FE model of the chassis frame

Now, the chassis frame is analyzed individually at the same conditions for the full vehicle simulation. To check the model accuracy and its ability to represent the part in the full model, output results from both models are compared as shown in Figure 3.17. It can be realized that both responses are in good agreement, where the difference between the final maximum values is approximately 2 %.

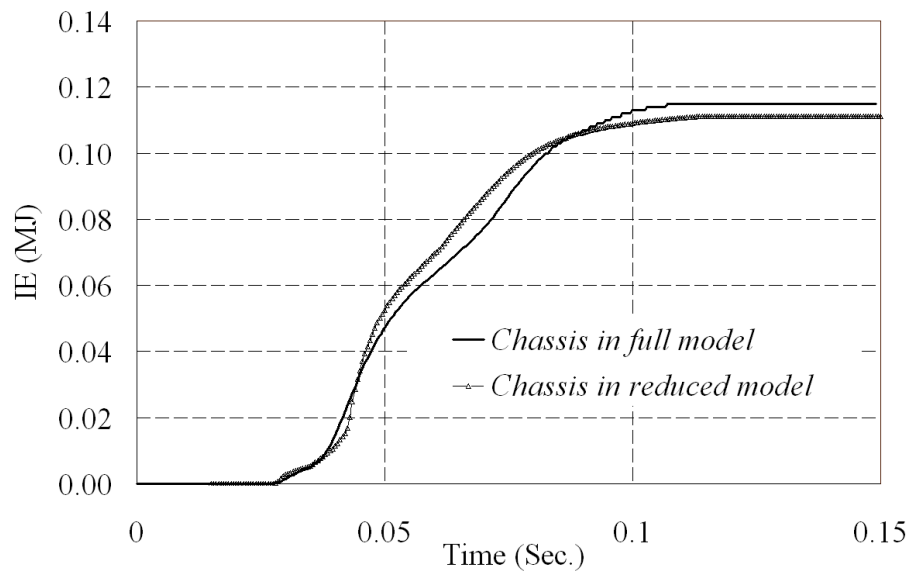


Figure 3.17: Impact energy absorbed by the chassis in full vehicle model and in the reduced model

3.6.2 Model Parametrization and Construction of the Approximate Model (Stage 2)

Thicknesses of different chassis parts are selected as design variables to parametrize the model as shown in Figure 3.18. The variables are x_1 as the bumper thickness, x_2 as the front rail section thickness, x_3 as the middle rail section thickness, x_4 as the rear rail section thickness, and x_5 as the cross rail section thickness.

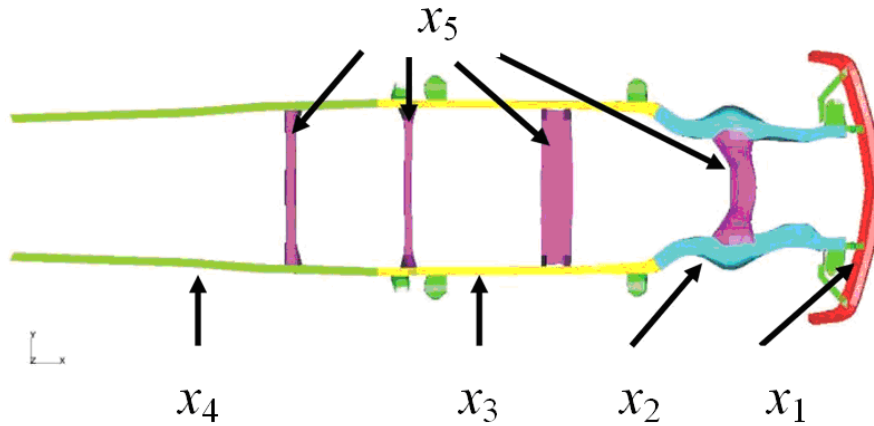


Figure 3.18: Design variables on the chassis frame

To develop the approximate models using RSM, the design space along with the output responses are to be assigned. The design space includes a range between 1 mm and 5 mm for all the five variables, as this presents a reasonable range for actual parts. Also here, two output responses, the chassis Mass (Mass) and the Impact Energy absorbed (IE), which represents the total amount of impact energy absorbed by the structure are selected. These responses are coded inside the nonlinear FE model in LS-DYNA, so that they are generated as results in the output data file. These responses are selected since they represent the most important design output responses, and will be used to formulate the optimization problem in the final stage of the proposed methodology.

The four types of meta-models (linear, interactive, quadratic and pure-quadratic)

mentioned in section 3.2.2.1 are used to construct the approximate RSM models and the accuracy of each model is checked using the $adjR^2$. The model with highest value is then selected.

To locate the design points, the D-optimality criterion is applied. Since the model includes five variables, thus 21 data points are required for the quadratic model (Model 3). In the current research, more design points (40 points) were used to ensure proper modeling representation. The points are given in Table 3.7. After selection of the design points in the design space, nonlinear FE analysis is conducted at each design point using LS-DYNA and the output responses are collected and used in regression analysis by which the unknowns of the RSM models are determined using Eq.(3.5).

Table 3.7: The design matrix of the response surface model for the chassis frame

ID	x_1	x_2	x_3	x_4	x_5	ID	x_1	x_2	x_3	x_4	x_5
1	1.37	1.53	1.24	2.17	1.30	21	3.20	2.70	3.80	5.00	5.00
2	2.93	1.33	1.05	3.91	1.99	22	1.80	3.00	5.00	4.00	5.00
3	2.17	1.51	3.80	1.02	1.05	23	2.00	4.80	3.80	2.20	1.00
4	1.02	1.36	1.42	2.84	4.99	24	1.80	3.00	4.70	5.00	5.00
5	1.00	1.00	4.14	4.14	4.60	25	1.00	3.14	5.00	5.00	5.00
6	2.40	1.00	1.20	1.80	1.00	26	2.90	3.14	3.14	3.14	3.00
7	2.70	1.00	5.00	5.00	5.00	27	2.70	3.14	3.14	3.14	3.60
8	2.50	3.14	3.14	3.14	2.80	28	2.70	3.14	3.14	5.00	3.60
9	3.00	1.00	4.00	4.00	5.00	29	1.80	3.00	5.00	5.00	5.00

continued on next page

ID	x_1	x_2	x_3	x_4	x_5	ID	x_1	x_2	x_3	x_4	x_5
10	2.90	1.00	3.70	3.70	5.00	30	2.90	3.14	3.14	3.14	3.30
11	2.40	1.00	3.40	3.00	5.00	31	2.50	3.14	3.14	3.14	3.00
12	3.20	1.00	3.80	4.00	5.00	32	2.70	3.14	3.14	3.14	3.00
13	3.30	1.50	3.85	4.00	5.00	33	3.20	3.14	3.80	4.00	5.00
14	2.90	2.14	3.14	3.14	3.00	34	1.80	3.14	5.00	5.00	5.00
15	3.20	1.00	3.80	5.00	5.00	35	2.70	3.14	3.80	4.00	5.00
16	3.30	1.00	3.85	4.00	5.00	36	2.70	3.14	5.00	5.00	5.00
17	3.30	1.00	3.85	5.00	5.00	37	2.85	4.74	1.04	2.94	4.00
18	3.30	1.00	4.85	4.00	5.00	38	4.68	3.76	4.10	1.74	4.39
19	3.30	1.00	5.00	5.00	5.00	39	4.80	4.22	3.08	1.52	2.76
20	2.30	1.00	3.90	3.90	5.00	40	4.32	4.72	4.62	4.06	2.84

As mentioned earlier, the different RSM models are used to approximate the output data and each model's adequacy and goodness of fit is quantified based on $adjR^2$ value using Eq. (3.13). The results are listed in Table 3.8. It can be observed that the quadratic model (Model 3) provides the best approximation for all the responses, hence it is selected as the approximate model to be used in the optimization process.

Table 3.8: Comparisons between $adjR^2$ for different RSM models of the chassis frame

	Mass	IE
Model 1	1	0.52
Model 2	1	0.64
Model 3	1	0.85
Model 4	1	0.6

3.6.3 Optimization Problem Formulation (Stage 3)

Once an efficient and accurate approximate model is developed, an optimization problem with the objective of improving the crashworthiness performance can now be formulated using the developed approximate models. Here, IE has been selected as the objective function to be maximized while constraining the Mass not to exceed the mass of the base design. Using the Mass as a constraint will ensure that an improvement in crash performance will not be achieved at the expense of adding more weight to the original design. The optimization problem is formulated as follow:

$$\begin{aligned}
 & \text{Find } X^* \text{ that :} \\
 & \text{Maximizes } IE \\
 & \text{Subjec to: } Mass - Mass_{original} \leq 0 \\
 & \text{where, } x_L \leq x \leq x_U
 \end{aligned} \tag{3.21}$$

The initial design values are $[x_1=2.7, x_2=3.14, x_3=3.14, x_4=3.14, x_5=3.6]$ mm. With these initial values, the total vehicle weight is 1839 kg and it absorbs a maximum of 0.19 MJ at the designated impact speed of 56 km/h. A lower and upper bounds of the design variables are assumed to be 1 and 5 respectively. The optimization prob-

lem is solved using the Sequential Quadratic Programming (SQP) algorithm [202], which is a powerful gradient based nonlinear mathematical programming technique in MATLAB. An optimum solution at $X^* = (1.2 \ 3.6 \ 1.12 \ 1.17 \ 4.6)$ was found after 16 iterations. Different random initial points were used and all converged to the same optimum solution. This solution will be referred to as *Design 1* in the coming discussion. The optimization history is shown in Figure 3.19.

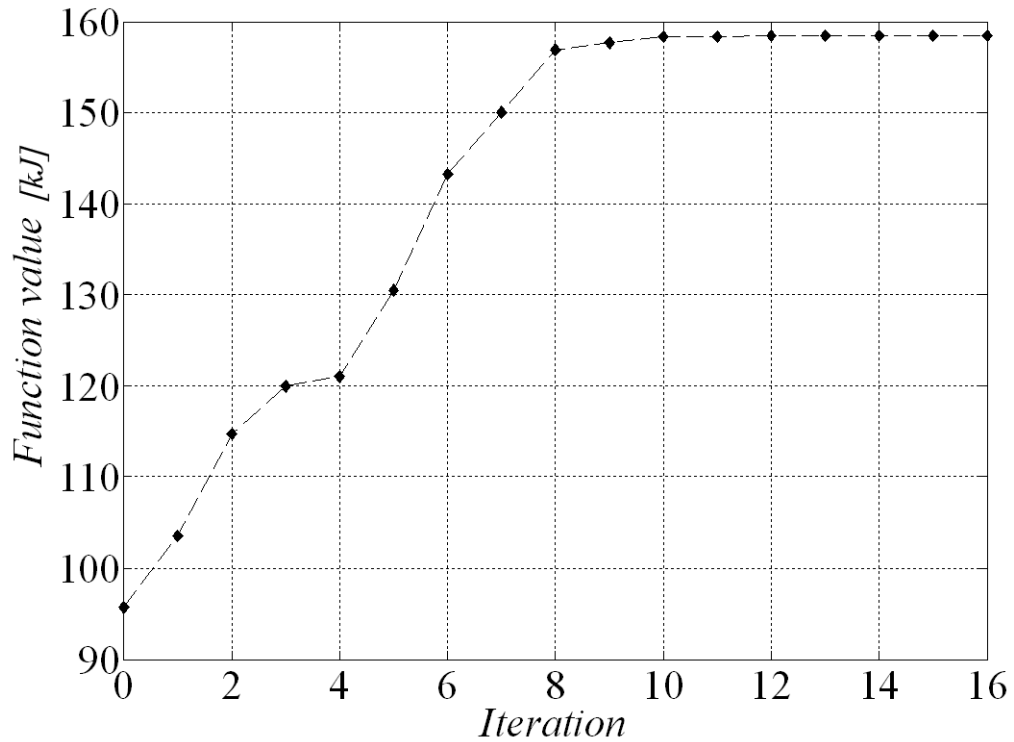


Figure 3.19: Iteration history of the optimization problem of the reduced model

To verify the solution, LS-DYNA simulation is conducted at the optimum solution. The final IE and mass were found to be 0.193 MJ and 1831.7 kg respectively. It can be realized that mass has been reduced while IE has been slightly increased (about 1.6%).

3.6.4 Optimization of the Full Model

In order to compare the developed approximate model of the reduced model with that of the full vehicle model, all previous steps are applied to the full vehicle model, i.e., the full vehicle nonlinear FE model is used instead of the modified one. Again, the four RSM models are used to develop the meta-models. The results are provided in Table 3.9.

Table 3.9: Comparisons between $adjR^2$ for the different RSM models of the full vehicle

	Mass	IE
Model 1	1	0.6
Model 2	1	0.66
Model 3	1	0.72
Model 4	1	0.57

The optimization problem is also formulated with the same objective to increase IE while constraining the Mass. The problem is solved with the SQP algorithm and a solution called (*Design 2*) was achieved after 29 iterations at $X^* = (1\ 5\ 3.26\ 1\ 4.41)$. Different random initial points were used and all converged to the same optimal solution. The optimization history is shown in Figure 3.20. Using the full FE model, mass and IE associated with the optimal point were found to be 1839 kg and 0.196 MJ respectively. Thus mass has remained unchanged and IE has increased by 3.3%.

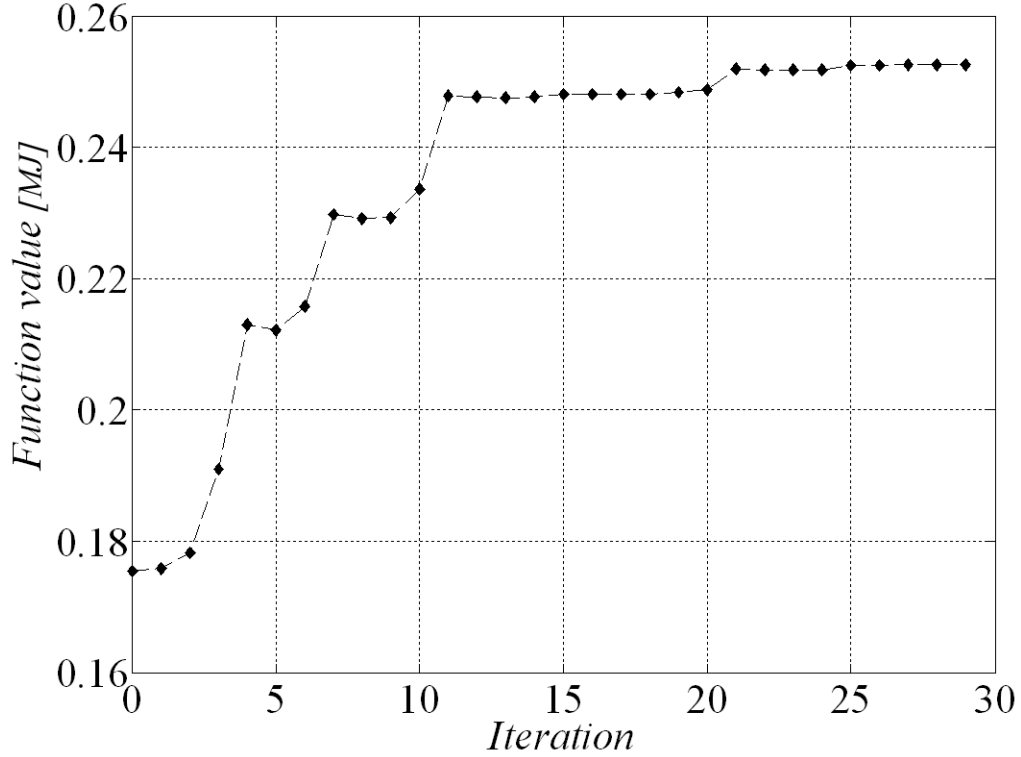


Figure 3.20: Iteration history of the optimization problem of the full model

3.6.5 Discussion

Both solutions increased IE by different degrees. Design 1 increased it by 1.6% and Design 2 increased it by 3.3%. To check how this will affect the occupants within the vehicle, the Head Injury Criterion (HIC) is calculated at a point on the B-pillar, as shown in Figure 3.21. The value of HIC can be calculated as follows [6]:

$$HIC = \left(\frac{1}{t_2 - t_1} \int_{t_1}^{t_2} a \cdot dt \right)^{2.5} \cdot (t_2 - t_1) \quad (3.22)$$

where t_1 and t_2 are any two points in time during the crash where the difference between them is either 15 ms or 36 ms, and a is the translational acceleration. According to federal regulations [16], in frontal impact situations for a 15 ms period, HIC should not exceed 700 and for a 36 ms period, HIC should not exceed 1000.

These values represent the human tolerance to decelerations, above which irrecoverable brain damage can occur. This parameter is based on the work performed by Patrick and Sato [204], who in 1970 used dropped cadavers on flat rigid surfaces to evaluate the required forces to cause fatal injuries in live human bodies. *HIC* provides a numeric value to evaluate the effect of crash on the occupant's brain, for more information one may refer to Ref. [205]. *HIC* has been criticized as it only includes translational acceleration which disregards the effect of other acceleration components such as angular accelerations that may cause other forms of injuries due to the induced shear stresses. With the advancement in computational capabilities, the trend now is to use detailed FE models to simulate brain injuries and to capture more details [206]. Despite these deficiencies, *HIC* is still used in regulations and is used here to evaluate the effect of the new designs on the occupant.

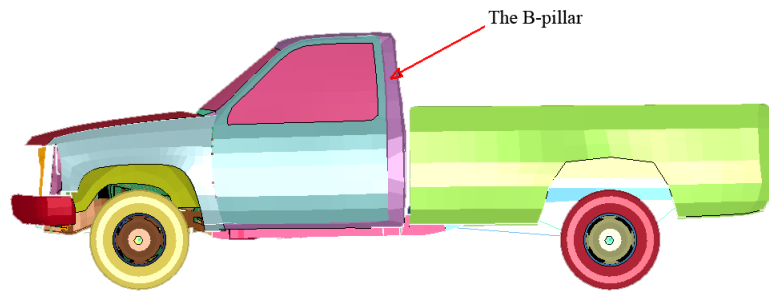


Figure 3.21: Location of B-pillar

Here, the calculated values for *HIC* based on a 36 ms period for the baseline design, Design 1 and Design 2 are found to be 1025, 883 and 1039, respectively. Thus, Design 1 reduced the value of *HIC* by 14% while Design 2 increased *HIC* by 1.4%. To find the cause of this difference, the design variables in Design 1 and Design 2 are normalized with respect to the baseline design and plotted in Figure 3.22. As it can be observed from Figure 3.22, the thickness of the frontal part of the longitudinal rail (x_2) in design 2 is 1.6 times the value of the thickness in the baseline design. This

caused this part to stiffen, thus raising the value of the deceleration and ultimately leading to the observed increase in the value of HIC .

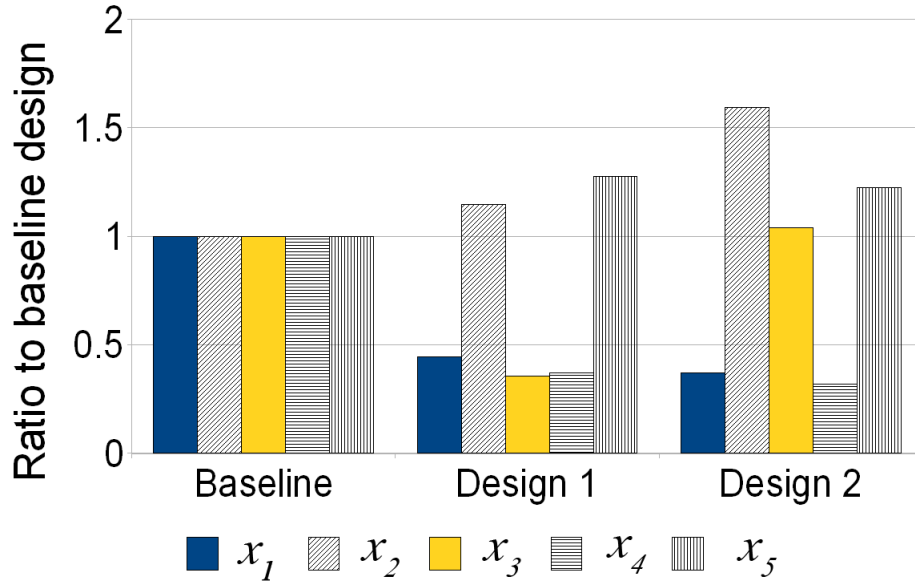


Figure 3.22: Comparison between design variables

The variation of the output response IE versus Mass normalized with respect to the baseline design is plotted in Figure 3.23, which is divided into four regions as:

1. A desirable region in the upper left corner, in which Mass decreases and IE increases. This region includes designs which surpass the baseline design in both aspects. It is also very hard to achieve since as shown in Figure 3.23, IE tends to increase when Mass increases.
2. An undesirable region in the lower right corner, in which Mass increases and IE decreases. This region designates a region which is not desirable as the design points represent heavier designs than the baseline design and yet, they absorb less energy. This implies a bad combination between design variables.
3. Region 1 in the lower left corner, in which both Mass and IE decrease. This region refers to the region at which mass was reduced at the expense of IE. For

example, designs from this region can be selected if a reduction in weight is required at the expense of sacrificing IE.

4. Region 2 in the upper right corner, in which both Mass and IE increase. This refers to a situation at which IE is increased by adding more weight. Designs in this region can be selected where weight saving is of less concern than increasing IE. For example, as in armoured vehicles, they are heavy, however they provide more safety protection than lighter vehicles.

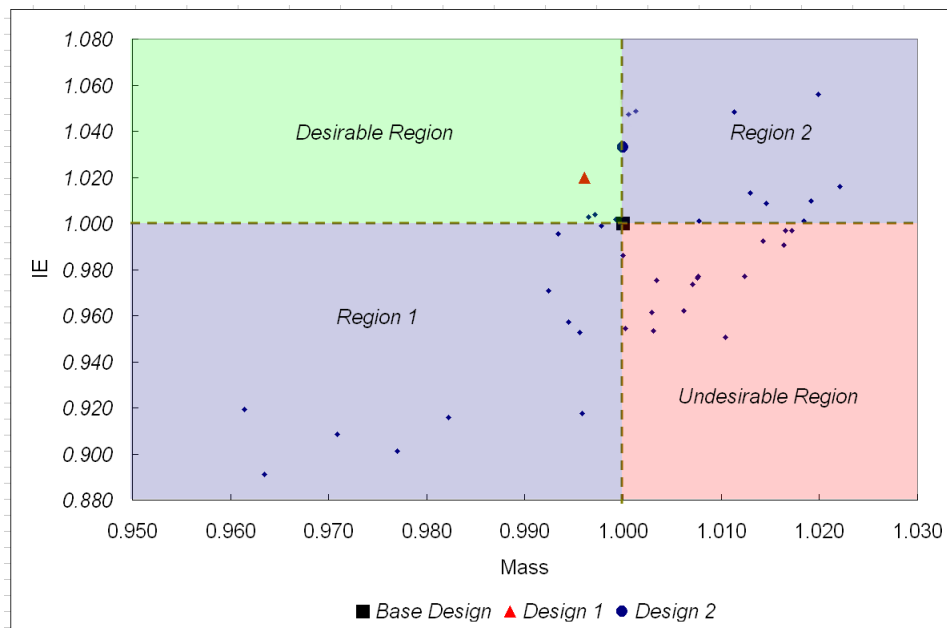


Figure 3.23: Normalized IE versus Mass for the full vehicle

The designer can use polynomial RSM functions to visualize the design space. For example, Figure 3.24 shows a response variation with variables x_1 and x_2 .

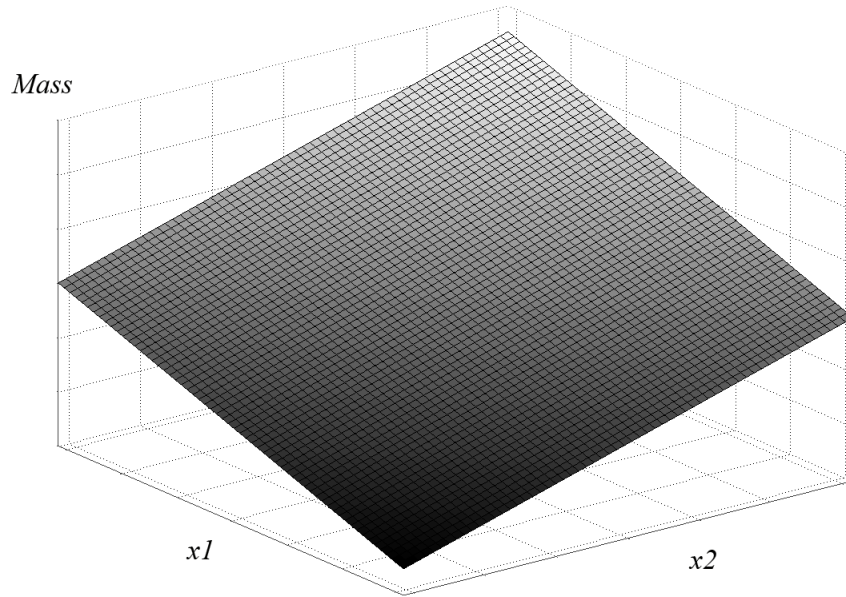


Figure 3.24: View of the mass response surfaces

3.6.6 Remarks

Remark 1 An argument may be made that the amount of weight reduced by applying the proposed methodology is 7 kg only. This may seem as a small value compared with the required amount of work. However, this small amount of weight reduction can lead to large savings in mass production. Another benefit of weight reduction is to improve fuel economy. Reducing weight by 10% decreases fuel consumption by 6-8 % [207]. Consequently, reducing fuel consumption will reduce carbon emissions.

Remark 2 Another argument may be made that advancements in hardware capabilities are increasing rapidly. Kurzweil [208] mentions that the rate of change in computer speed is exponential. However, on the other hand, FE models are also becoming more complicated. FE model developers continue to add more details to their models to capture more realistic output responses. Haug [209] mentions that, no matter how much computer power provided to the designers, they will use it to

its full extent in a very short time.

Figure 3.25 shows the number of elements used to model a mid-size vehicle in frontal impact over 20 years. As it can be realized, the trend follows an exponential rate.

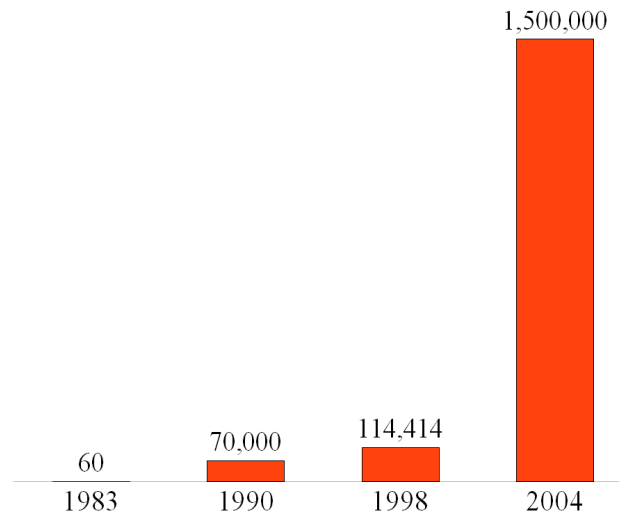


Figure 3.25: The number of elements for modeling a full vehicle over 20 years [210]

Furthermore, Figure 3.25 shows only the trend of increase for vehicle structure models without including FE models of occupants. Human FE models are very complex, a model of the brain alone can include up to 300,000 elements [74]. Combining human models with vehicle structure models will result in extremely complex models. This will raise the computational cost substantially.

In addition, optimization requires several iterations to reach an optimum solution. Using a reduced model at lower computational cost compared with the full vehicle model enables the practical application of optimization for crashworthiness improvement. In this work, using a PC with Intel Pentium D 2.66 GHz processor, the reduced model was simulated in 13 minutes compared to approximately 6 hours for the full vehicle model. For the purpose of this work, simulations were conducted on the University's distributed parallel computing Linux workstation (HP-MPI AMD64), on which 64 processors were used.

Based on the aforementioned remarks, the proposed methodology significantly reduces the amount of time required to find an optimum solution. This also reduces the total development time of the entire vehicle design. As shown in Figure 3.26, crashworthiness is one of many design objectives. Considering that crashworthiness is the first analysis to be completed in modern vehicle design [5], the impact of the methodology on the entire design cycle can be appreciated.

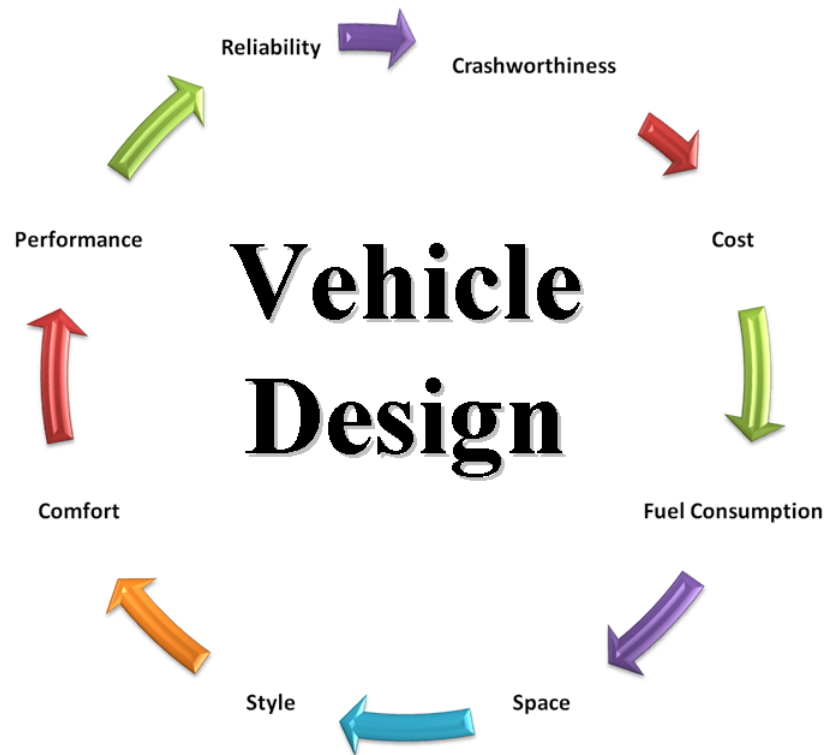


Figure 3.26: Different automobile objectives

Remark 3 The resulting polynomial functions of the different output responses can be considered as closed form approximate solutions. The polynomial functions can be easily shared within other disciplines. Experts from other disciplines can easily use the polynomial functions to predict the crashworthiness behavior in their calculations without running a sophisticated nonlinear FE software as LS-DYNA.

Remark 4 The methodology can also be applied to other vehicle parts. This work focused on the chassis frame as an important structural part to vehicle safety. A complete implementation of the methodology to all vehicle structural parts will further improve the crashworthiness performance.

3.7 Summary

In this chapter, a new methodology for enabling the practical implementation of numerical optimization has been proposed. The methodology has been applied to a case study of a pickup truck. The methodology successfully improved the crashworthiness performance of the pickup truck at a practical computational cost. It is suggested that extending the application of the methodology to other structural parts will further improve the crashworthiness performance of the entire vehicle.

Chapter 4

Vehicle Design Improvement using the Pareto Front

4.1 Introduction

Knowing the form of the relationship between two important engineering quantities can facilitate the design process to a great extent. The two most important engineering quantities in vehicle crashworthiness design as discussed in chapter 3 are: weight and absorbed impact energy. Thus, knowing the relationship between the maximum amount of impact energy absorbed in a structure and its minimum weight is very important. The designer can use this relationship to quickly check any design and find if it absorbs the maximum amount of impact energy for its current weight or not. In this way, the designer can judge the crashworthiness performance of any design with minimum effort and obtain the values of the design variables that can achieve maximum impact energy with minimum weight. Unfortunately, in reality, the relationship between minimum weight and maximum impact energy is unknown. In this chapter, the Pareto front technique is used to find this relationship and the optimum values of the design variables.

4.2 The Pareto Front

The Pareto front is named after Vilfredo Pareto (1848-1923), who in 1906 published the 'Manuale di Economia Politica' (Manual of Political Economy), in which he introduced the principles of non dominance in economics. The book captured the attention of researchers in mathematics and engineering after it was translated to English in 1971 [211]. Later, the principles of non dominance became the basis of multiobjective optimization and are now known as the Pareto front [212].

Here, the principle of the Pareto Front (PF) is explained through an example without any loss of generality. Let us consider a design as shown in Figure 4.1 with two conflicting objective functions: F is to be maximized and G is to be minimized [213]. The term conflicting means that, there is no single solution that will maximize F and minimize G at the same time.

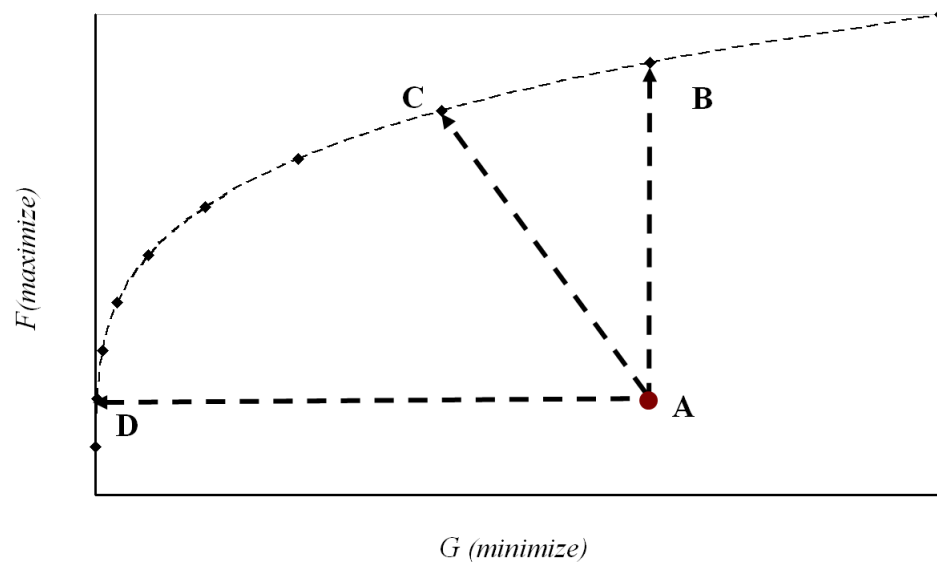


Figure 4.1: A representative drawing of the Pareto Front

First, let us compare point A with point B. Although, A and B have the same values for G , B has a higher value for F than A. In this case, B is said to dominate A. In a similar way, by comparing point A with point D, one can realize that A and D

have the same values for F but D has a smaller value for G than A. In this case, D is said to dominate A. Now, let us compare point A with point C. In this case, C is superior in both objectives; it has larger F and smaller G values than A. In this case, C is also said to dominate A. Finally, considering points B, C and D, it is clear that no single point is better in both objectives than the others, thus they are called non-dominated points. Each non-dominated point is optimum, which means that no improvement in one function can be achieved without deteriorating the other function. The set of non-dominated points is called the Pareto front (PF). The PF can then be considered as the set that includes all optimum solutions while trading off between the different objectives. For example, in the present work, the PF will include all possible maximum absorbed impact energy values and their associated minimum weight values. The process of finding the Pareto front is explained in the following section.

4.3 Finding the Pareto Front

The Pareto front is the solution of a multiobjective optimization problem, which can be written as follows:

$$\begin{aligned}
 & \textit{Find } X^* \textit{ that :} \\
 & \textit{Minimizes } \Pi(X) \tag{4.1} \\
 & \textit{where, } X_L \leq X \leq X_U
 \end{aligned}$$

where X is the vector of design variables and X^* is the vector of optimum values. X_L and X_U are the lower and upper bounds on the design variables, and $\Pi(X)$ is the vector that includes all design objectives, which can be written as:

$$\Pi(X) = [F_1(X) \dots F_n(X)] \quad (4.2)$$

The solution of a multiobjective optimization problem does not include one solution only. Instead, it includes several solutions and each one is optimum. This means that, for a given optimum solution, one cannot find another one that outperforms the first optimum solution in all objectives. Instead, all the optimum solutions are trade-offs between the design objectives. There are two approaches for solving multiobjective optimization problems. A brief review of these approaches is presented here:

i Transforming the Problem into a Single Objective Problem

The objective functions are all combined into a single weighted function as follows:

$$\begin{aligned} & \text{Find } X^* \text{ that :} \\ & \text{Minimizes } W(X) \quad (4.3) \\ & \text{where, } X_L \leq X \leq X_U \end{aligned}$$

where $W(X)$ is a function combining different objective functions. A popular approach to obtain this single objective function is through linearly summing weighted functions. This can be expressed as $(W(X) = \sum_{i=1}^n \frac{\lambda_i \cdot F_i(X)}{\bar{F}_i})$, where λ_i is a weighing factor such that $\sum_{i=1}^n \lambda_i = 1$, F_i is the i^{th} objective function and \bar{F}_i is a normalizing factor for F_i . One can refer to Ref. [214] for a description of other approaches to transform multiobjective functions into a single objective function. After establishing the optimization problem in Eq.(4.3), the multiobjective optimization problem can be solved using different weighing factors. The different solutions obtained will

then constitute the Pareto front. This approach is simple and easy to implement, however, it has two problems that can be summarized as:

(1) The approach will work only with functions in a completely convex region and fails to find a solution in a non-convex region [213].

(2) The selection of the normalizing factor is subjective. It is not clear which value to use for normalization of F_i . \bar{F}_i can be the average, the maximum, or the difference between maximum and minimum. The selection of which normalizing factor to use causes the so called inductive bias, which is favoring one hypothesis over the others. For more discussion on the subject, one can refer to Ref. [215].

ii The Pareto Approach

The Pareto approach alleviates the previously mentioned drawbacks. It uses a multi-objective optimization algorithm for solving the multiobjective optimization problem. As Freitas [216] mentioned, it makes more sense to develop an algorithm to solve the problem instead of adapting the problem itself to the available algorithms. Currently, the genetic algorithm is widely used for solving multiobjective optimization problems [217]. The first algorithm was developed by Schaffer [218], and over the years its performance has been improved significantly due to the works of many researchers [219–222]. The genetic algorithm is a nature inspired search algorithm that is based on the evolutionary principles [223]. The genetic algorithm searches for the non-dominated points by populating many solutions. A schematic drawing of the genetic algorithm is shown in Figure 4.2 and the algorithm can be summarized as follows [213]:

1. The algorithm is initiated by generating random designs.
2. Each design is represented by a vector of bit strings with fixed length.

3. Designs are allowed to mate to produce new designs, which is called crossover and mutation.
4. The values of the objective functions are evaluated and recorded for each design.
5. The designs are sorted according to the recorded values of the objective functions.
6. The algorithm stops if a convergence criterion is reached, otherwise it continues to step 3.
7. The final solution is a set of optimum (non-dominated) designs.

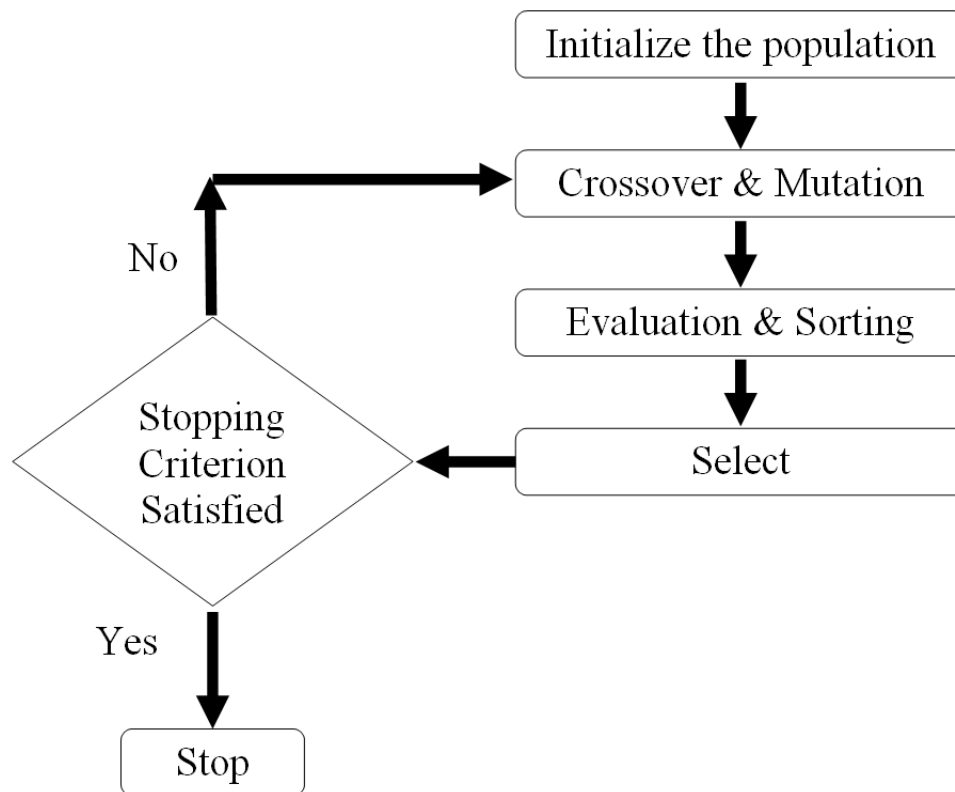


Figure 4.2: A scheme of a typical genetic algorithm

4.4 Proposed Methodology

The methodology developed in this work uses the genetic algorithm in order to find the Pareto front. However, the genetic algorithm requires an exceptionally large number of function evaluations. Hence, approximate models are used with the genetic algorithm instead of the computationally expensive nonlinear FE models. Then, the relation between minimum weight and maximum impact energy absorbed is derived from the Pareto front. The methodology is explained in a flow chart as shown in Figure 4.3 and applied to two crashworthiness design problems: (1) A thin walled tube under axial impact loading and (2) A chassis frame using the response surface model that has been developed in chapter 3.

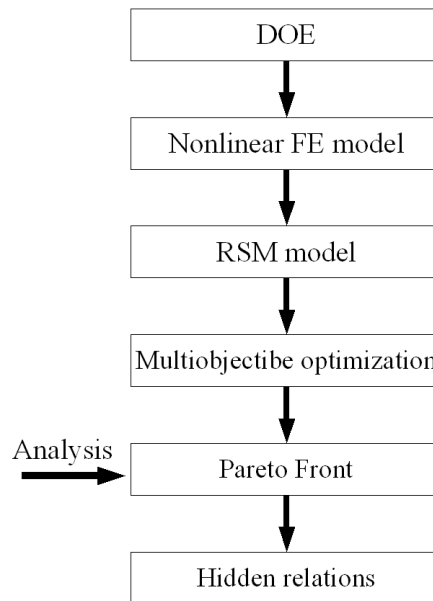


Figure 4.3: A schematic drawing of the methodology

4.5 Design Improvement of a Thin Walled Tube Using the Pareto Front

To simply demonstrate the approach, the Pareto front is constructed to find the relationship between maximum impact energy and minimum weight of a thin walled tube under axial impact. As shown in Figure 4.4, the tube is divided into three parts. Parts thicknesses are assumed to be the design variables. The model parameters are provided in Table 4.1. The tube is modeled using a nonlinear FE model and LS-DYNA is used for simulations.

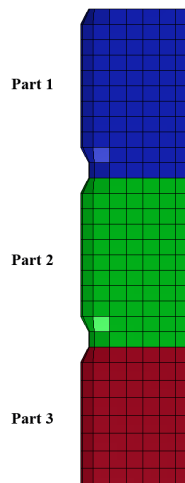


Figure 4.4: View of the thin walled tube model

Table 4.1: Parameters of the nonlinear FE model of the thin walled tube

Dropped mass	80 kg
Pre-impact speed	10 m/s
Total length	235 mm
Number of elements	391
Elements type	Belytschko-Lin-Tsay
Material	Steel
Material model	MAT PIECEWISE LINEAR PLASTICITY
Contact model	CONTACT AUTOMATIC SINGLE SURFACE
Design variables	Parts thicknesses (x1, x2, x3)
Design range	$X_L [1, 1, 1] : X_U [3, 3, 3]$

The nonlinear FE model is relatively simple and it takes a short time to analyze (about 1 minute). To demonstrate the usefulness of the methodology, the model has been simulated at 100 different design points. The values for mass and impact energy absorbed are recorded at each point and plotted in Figure 4.5. As it can be seen, a strong positive relation between Mass and IE exists. Now, the problem is to find the exact correct form of the relationship between minimum Mass and maximum IE as represented by the dotted line in Figure 4.5. Considering point A that is located far away from the Pareto front, it is obvious that the design at this point is far from being optimal.

For large size and complex structures such as automobile structures, simulation using nonlinear FE analysis is computationally expensive and thus it is not possible to conduct 100 simulations to find the relative position of a design. To overcome this problem, the response surface method combined with design of experiments as discussed in chapter 3 may be employed to create simple approximate models instead of the computationally expensive nonlinear FE models.

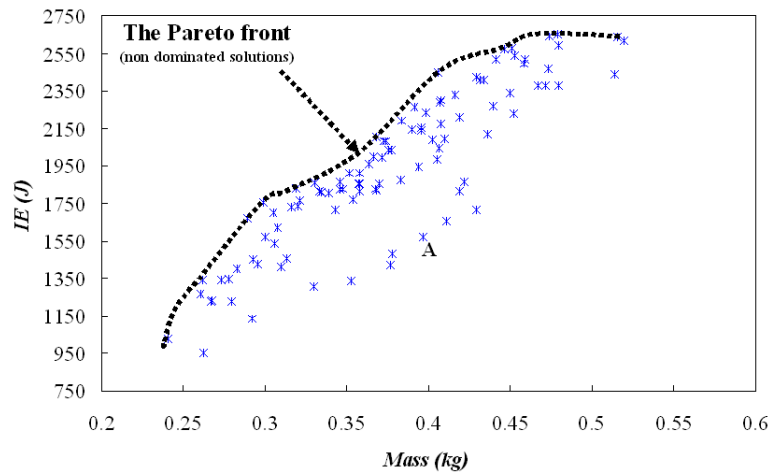


Figure 4.5: IE vs Mass for the thin walled tube

Here, to create the response surface models for Mass and IE, the D-Optimality criterion is used to generate 30 design points as provided in Table 4.2. LS-DYNA is then

used to simulate the nonlinear FE model of the thin walled tube at each point. The values of Mass and IE are evaluated after each FE analysis and used with each of the four RSM model types (linear, interaction, quadratic and pure quadratic) discussed before in chapter 3. The value of the $adjR^2$ is calculated for each model type and the the results are provided in Table 4.3. It is clear that the quadratic model has the largest $adjR^2$ value compared with other model types, hence it is the most accurate model and is used here to model Mass and IE.

Table 4.2: The design matrix of the response surface model for thin-walled tube

ID	x_1	x_2	x_3	ID	x_1	x_2	x_3
1	2.00	2.00	2.00	16	1.35	2.18	2.05
2	2.46	1.89	1.52	17	1.77	2.22	2.40
3	2.92	2.17	2.11	18	1.84	2.56	2.78
4	2.35	2.49	1.67	19	1.90	1.72	2.86
5	2.81	2.20	2.07	20	1.11	1.15	1.87
6	2.14	2.81	2.16	21	2.71	2.78	2.70
7	1.65	1.38	1.87	22	2.70	1.66	2.19
8	1.74	2.75	2.99	23	1.95	1.85	2.97
9	2.66	2.34	2.33	24	2.81	1.50	1.53
10	1.69	1.77	2.78	25	2.08	2.89	1.49
11	1.49	2.88	1.25	26	2.94	2.38	2.35
12	1.62	1.65	2.67	27	2.93	2.16	2.20
13	2.42	1.12	2.06	28	2.91	2.20	1.82
14	1.46	2.77	1.95	29	2.97	1.47	2.65
15	2.55	1.67	2.53	30	1.79	1.51	1.39

Table 4.3: Values for $adjR^2$ for different RSM models for the thin walled tube

	Mass	IE
Linear	1	0.87
Interaction	1	0.88
Quadratic	1	0.94
Pure quadratic	1	0.9

Next, a multiobjective optimization problem is formulated in which Mass and IE are represented by the quadratic RSM model. The optimization problem can be described as:

$$\begin{aligned}
 & \text{Find } X^* \text{ that :} \\
 & \text{Minimizes } Mass(X) \quad \text{and} \\
 & \text{Maximizes } IE(X) \\
 & \text{where, } X_L \leq X \leq X_U
 \end{aligned} \tag{4.4}$$

The problem is solved using the GA in MATLAB's optimization tool box. The genetic algorithm was able to locate the Pareto front after 12121 function evaluations. It should be noted that in case the genetic algorithm has been directly applied to the nonlinear FE model, running such a large number of nonlinear FE simulations would have been impractical. Having found the Pareto front, the process of finding the relationship between minimum weight and maximum absorbed impact energy can be simply made using curve fitting. The Pareto front and the fitted function are shown in Figure 4.6 and the relationships between minimum Mass and maximum IE can be written as follows:

$$IE [J] = 10^4 \cdot (-0.7896 \cdot Mass^2 + 1.3937 \cdot Mass - 0.2019) \tag{4.5}$$

$$Mass [kg] = (1.2158 \cdot 10^{-8} \cdot IE^2 + 7.5838 \cdot 10^{-5} \cdot IE + 0.1638) \quad (4.6)$$

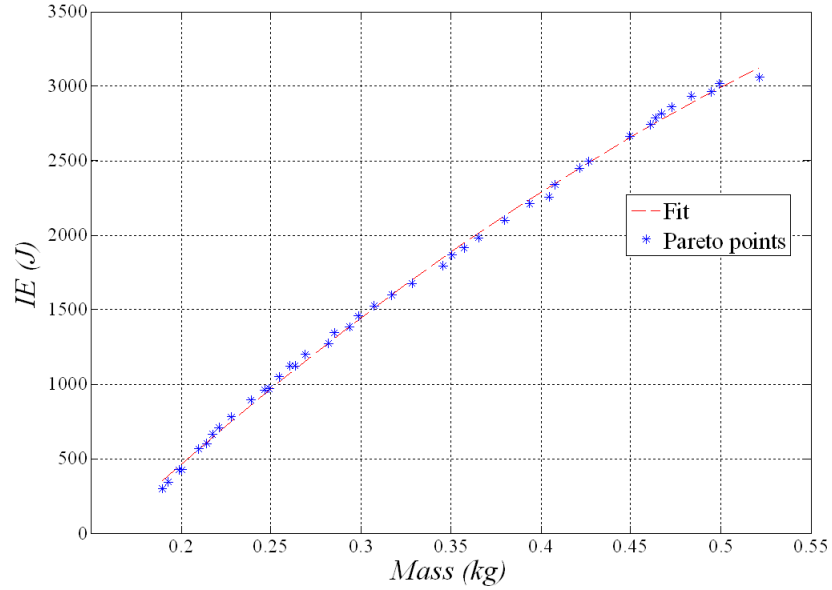


Figure 4.6: The PF and the fit for IE vs Mass for the thin walled tube

The weight of the design at point A is 0.4 kg and its associated IE is 1570 J. Now, using Eq.(4.5), the maximum value that this design should achieve is 2292 J, which is 46% more than the design actually absorbs. Also, according to Eq.(4.6), the design can absorb the same amount of IE (1570 J) with only 0.3 kg, which is 21% lighter than the original design at point A. Thus, it is clear that the design at point A is far from being optimum and the designer can use the Pareto front data in Table 4.4 to improve the design. The designer can improve the design at point A using two approaches: (1) Maintain the mass and maximize IE or (2) Maintain IE and minimize the mass. The two approaches are describes next.

Table 4.4: Values for Mass, IE and their associated design variables for the PF of the thin walled tube

ID	x_1	x_2	x_3	Mass (kg)	IE (J)	ID	x_1	x_2	x_3	Mass (kg)	IE (J)
1	1	1	1	0.189	289.48	22	2.31	1.34	1.54	0.32	1623.58
2	1	1.01	1	0.191	293.48	23	2.46	1.29	1.54	0.325	1666
3	1.01	1.01	1.03	0.192	331	24	2.2	1.75	1.65	0.349	1850
4	1.01	1	1.09	0.195	390	25	2.3	1.86	1.56	0.356	1902
5	1.03	1.02	1.13	0.2	450	26	2.43	1.89	1.64	0.37	2017
6	1.1	1.01	1.15	0.205	509	27	1.95	2.37	1.64	0.375	2057
7	1.14	1.05	1.16	0.211	563	28	2.06	2.37	1.62	0.38	2099
8	1.22	1.03	1.19	0.215	630	29	2.52	2.19	1.78	0.405	2292
9	1.01	1.02	1.44	0.219	697	30	2.76	2.35	1.69	0.422	2433
10	1.22	1.14	1.21	0.224	699	31	2.53	2.37	1.93	0.427	2448
11	1.36	1.02	1.28	0.228	783	32	2.21	2.83	1.81	0.432	2532
12	1.43	1.02	1.49	0.246	987	33	2.37	2.85	1.68	0.434	2556
13	1.38	1.12	1.56	0.255	1055	34	2.37	2.88	1.77	0.441	2616
14	1.56	1.07	1.5	0.258	1092	35	2.3	2.89	1.84	0.443	2623
15	1.88	1.09	1.32	0.264	1133	36	2.87	2.65	1.76	0.453	2677
16	1.39	1.57	1.43	0.277	1194	37	2.69	2.65	1.98	0.458	2691
17	1.59	1.27	1.61	0.28	1273	38	2.9	2.86	1.69	0.464	2777
18	2.12	1.12	1.45	0.289	1369	39	2.9	2.86	1.69	0.464	2778
19	2.11	1.03	1.61	0.292	1422	40	2.77	2.94	1.83	0.472	2844
20	1.99	1.03	1.85	0.302	1483	41	2.81	2.97	2.01	0.488	2937
21	2.35	1.14	1.58	0.311	1571	42	3	3	2.32	0.521	3060

i Maintaining Mass and Maximizing IE

From Table 4.4, the nearest value to the weight of the design at point A is 0.405 kg at point (29), at which the predicted value for maximum IE is 2292 J. The design variables at point A are (1.69, 1.77, 2.78), where the design variables at point (29) are (2.52, 2.19, 1.78). To verify the value of IE, the design variables at point (29) are used to simulate the tube using LS-DYNA. The value of IE from the simulation is found to be 2248 J, which means that IE has been increased by 43% while maintaining the same weight of the tube.

ii Minimizing Mass and Maintaining IE

From Table 4.4, the nearest value to the energy absorbed in the design at point A is 1571 J at point (21), at which the predicted value for minimum mass is 0.311 kg. Thus, the design at point (21) is about 21% lighter than the original design at point A. To verify the value of IE, the design variables at point (21) (2.35, 1.14, 1.58) are used to simulate the tube using LS-DYNA. The value of IE from the simulation is found to be 1943 J, which is even 24% more than the value of IE in the original design at point A. Using this approach, IE has been increased by 24% and mass has been reduced by 22%.

4.5.1 The Anti Pareto Front (APF)

As important as it is to find the Pareto front of the best possible designs, it may also be important to find the Pareto front of the worst possible designs, which is called here the Anti Pareto Front (APF). Finding the APF can be made by simply reversing the objectives in the multiobjective optimization problem. This means that instead of searching for the designs with minimum weight and maximum impact energy, one

searches for designs with maximum weight and minimum impact energy. The new multiobjective optimization problem can be written as:

$$\begin{aligned}
 & \text{Find } X^* \text{ that :} \\
 & \text{Maximizes } \text{Mass}(X) \quad \text{and} \\
 & \text{Minimizes } \text{IE}(X) \\
 & \text{where, } X_L \leq X \leq X_U
 \end{aligned} \tag{4.7}$$

Again, the genetic algorithm is used to solve the multiobjective optimization problem stated in Eq.(4.7) and the APF is found after 7501 function evaluations. The Pareto front and the anti Pareto front can be plotted on the same figure where the area between them constitutes the design space as shown in Figure 4.7. The designer can use Figure 4.7 to visually check how far a design is from being a best or a worst design as demonstrated using point A. It is clear that point A is very close to the APF curve, which means it is far from being optimum.

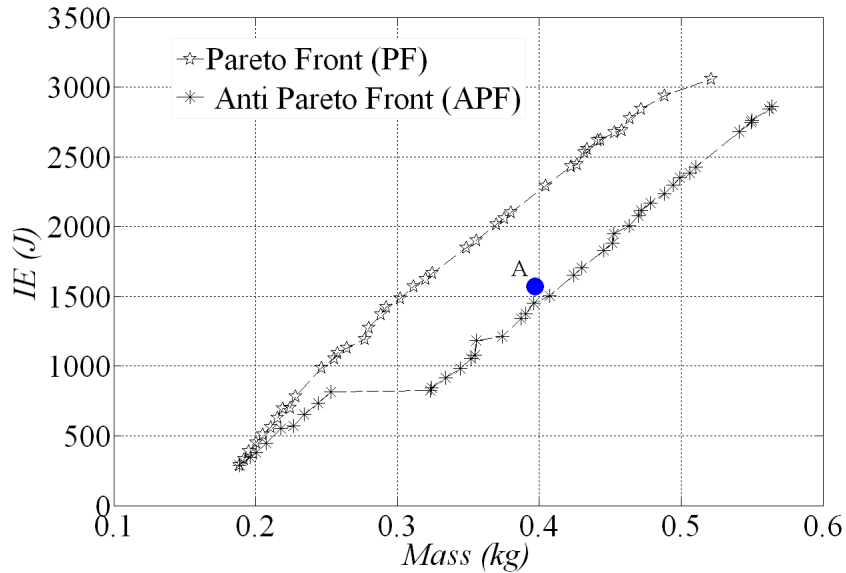


Figure 4.7: The PF and the APF for the thin walled tube

4.6 Design Improvement of a Vehicle Chassis Frame Using the Pareto Front

In chapter 3, the chassis frame has been identified as the major influencing structural part to the crashworthiness performance of the whole vehicle. Then, a reliable RSM model has been developed to model the chassis frame's weight (Mass) and its impact energy absorbed (IE). In this section, the same RSM model of the chassis frame is employed to improve the crashworthiness performance of the chassis and the whole vehicle. A multiobjective optimization problem is formulated using the previously developed RSM model of the chassis frame. Then, the solution of the multiobjective optimization problem is used to create the Pareto front. Table 4.5 provides the associated values of the Pareto front and Figure 4.8 shows the Pareto front and its fitted curve. The derived relationships between minimum weight and maximum energy absorbed in the chassis frame can be written as:

$$IE [MJ] = 10^{-3} \cdot (-0.0013 \cdot Mass^2 + 0.4781 \cdot Mass + 74.1417) \quad (4.8)$$

$$Mass [kg] = 10^5 \cdot (1.8236 \cdot IE^2 - 0.3423 \cdot IE + 0.0166) \quad (4.9)$$

Table 4.5: Values for Mass, IE and associated design variables for the PF of the chassis frame

ID	x_1	x_2	x_3	x_4	x_5	Mass (kg)	IE (kJ)
1	1.05	1.00	1.00	1.00	1.03	52.5	95.19
2	1.44	1.03	1.01	1.01	1.09	55.8	96.27

continued on next page

ID	x_1	x_2	x_3	x_4	x_5	Mass (kg)	IE (kJ)
3	1.50	1.04	1.13	1.04	1.07	57.1	96.72
4	1.51	1.17	1.20	1.08	1.08	59.4	97.41
5	2.17	1.23	1.08	1.07	1.07	63.0	98.00
6	3.17	1.02	1.23	1.00	1.06	67.3	100.80
7	3.56	1.09	1.07	1.20	1.04	70.5	102.06
8	3.07	1.57	1.10	1.10	1.08	72.2	102.21
9	3.31	1.72	1.09	1.01	1.04	74.1	103.03
10	3.20	1.80	1.11	1.18	1.14	76.5	103.29
11	3.75	1.75	1.32	1.02	1.11	79.5	104.46
12	4.62	1.87	1.11	1.21	1.10	85.6	106.70
13	4.62	1.88	1.10	1.25	1.14	86.4	106.77
14	3.90	2.59	1.32	1.22	1.14	90.6	107.23
15	4.65	2.78	1.04	1.14	1.07	93.7	108.66
16	3.87	3.14	1.39	1.46	1.33	100.0	108.84
17	4.93	2.98	1.73	1.29	1.17	104.7	110.61
18	4.87	3.66	1.13	1.61	1.09	108.3	111.48
19	4.90	4.25	1.31	1.06	1.10	111.7	111.98
20	4.94	3.91	1.46	1.39	1.39	114.6	112.13

continued on next page

ID	x_1	x_2	x_3	x_4	x_5	Mass (kg)	IE (kJ)
21	4.94	4.18	1.31	1.63	1.22	116.6	112.65
22	4.93	3.96	1.56	1.76	1.55	120.0	112.71
23	4.65	4.75	1.81	1.56	1.10	122.9	113.38
24	4.79	4.79	1.81	1.77	1.28	127.2	113.85
25	4.91	4.93	1.81	2.00	1.13	129.8	114.26
26	4.92	4.91	1.59	1.87	1.88	133.4	114.38
27	4.98	4.97	1.77	2.02	1.80	136.2	114.72
28	4.97	4.98	1.83	2.05	2.73	145.2	115.52
29	4.80	4.75	1.16	2.14	3.98	148.0	115.84
30	4.93	4.43	1.61	2.37	3.96	150.7	115.94
31	3.32	4.98	1.26	2.45	4.88	152.3	116.88
32	4.07	4.99	1.32	2.30	4.88	156.3	117.42
33	4.32	4.99	1.26	2.43	4.95	158.8	117.81
34	4.88	4.86	1.64	2.21	4.87	161.6	117.99
35	4.41	4.99	1.68	2.57	4.97	163.9	118.41
36	4.79	5.00	1.42	2.87	4.97	166.6	118.70
37	4.97	5.00	1.86	2.78	4.93	170.0	118.98
38	4.97	5.00	2.01	2.99	5.00	173.3	119.23

continued on next page

ID	x_1	x_2	x_3	x_4	x_5	Mass (kg)	IE (kJ)
39	4.97	5.00	2.56	2.85	5.00	176.6	119.28
40	4.97	5.00	2.56	2.98	5.00	177.6	119.29

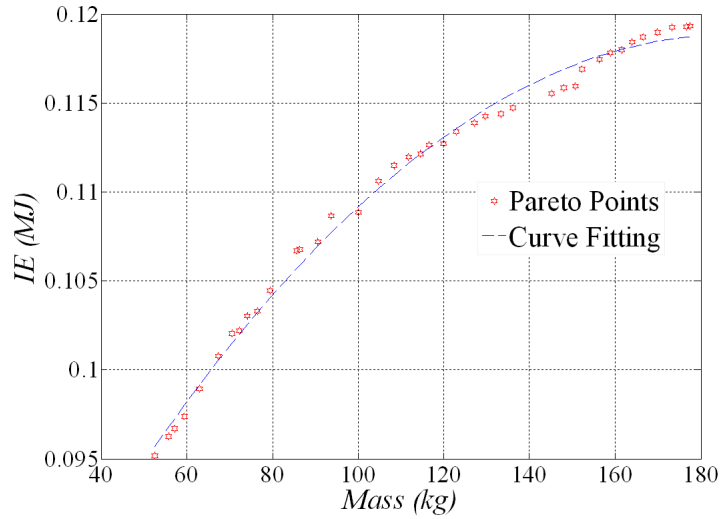


Figure 4.8: The PF of the chassis frame

The Pareto and the anti Pareto fronts are also shown in Figure 4.9, on which a suggested design is represented at point A. Using Figure 4.9, the designer can clearly conclude that the design at point A is one of the worst possible designs since it lies directly on the APF. The weight of the chassis frame at point A is 151 kg and the amount of absorbed impact energy is 0.099 MJ. Also, the total amount of impact energy absorbed in the whole vehicle structure is 0.165 MJ. Similar to the thin walled tube example, the designer can use the data provided in Table 4.5 to improve the design at point A following one of the two approaches explained below.

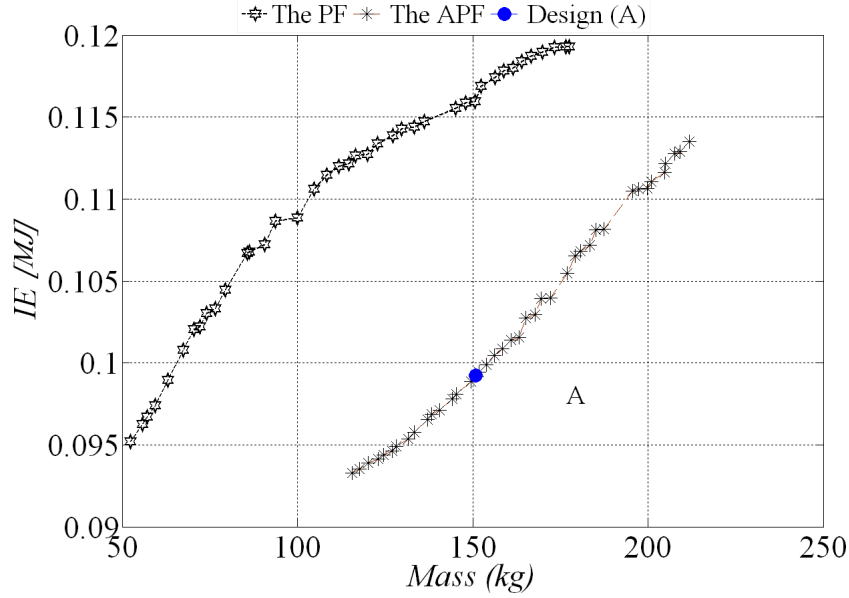


Figure 4.9: The PF and the APF of the chassis frame

i Maintaining Mass and Maximizing IE

Using the data in Table 4.5, the designer can pick the nearest value to the weight at point A, which occurs at point (30). The design at point (30) absorbs 0.116 MJ, which is 17 % higher than that at point A. The design variables are (1, 1, 5, 4, 2.5) at point A and (4.93, 4.43, 1.61, 2.37, 3.96) at point (30). To verify the improvement in the whole vehicle design, LS-DYNA simulation is conducted at the design variables at point (30). The simulation results show that the amount of impact energy absorbed in the whole vehicle structure is 0.192 MJ. This means that the total amount of impact energy absorbed in the whole vehicle structure for the same weight has been improved by 16%.

ii Minimizing Mass and Maintaining IE

The nearest value for IE of the design at point A occurs at point (6) in Table 4.5. The design at point (6) absorbs almost the same amount of impact energy as the

design at point A. However, the design at point (6) is 56% lighter than the original design at point A. To verify the improvement in the whole vehicle design, LS-DYNA simulation is conducted at the design variables at point (6), which are (3.17, 1.02, 1.23, 1, 1.06). The results show that the total amount of impact energy absorbed in the whole vehicle structure is 0.17 MJ, which is even slightly (3%) higher than the 0.165 MJ of the original design at point A. Considering this, not only the total vehicle weight has been reduced (5%) but also the amount of impact energy absorbed in the whole vehicle structure has been increased by 3%.

Finally, the values of IE and Mass obtained from the two approaches are normalized with respect to the initial design at point A. The results are shown in Figure 4.10.

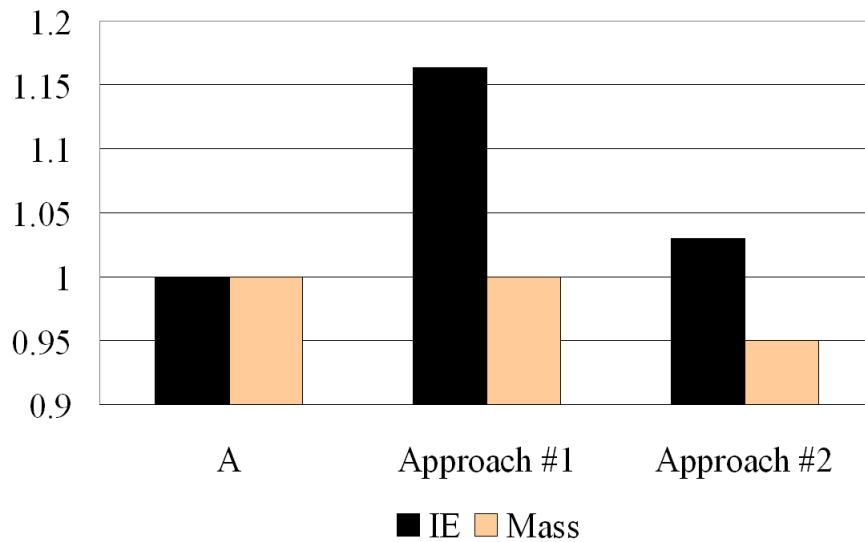


Figure 4.10: Comparison between IE and Mass for the two approaches

4.7 Summary

A new methodology for vehicle structure design has been introduced. The methodology has been applied to the design of a thin walled tube under axial loading and to the design of a chassis frame. The results showed that the methodology enabled

the designer to verify the goodness of any suggested design. Moreover, one may use the approach to find the optimum design variables required to improve the original suggested design. Ultimately, this facilitates the whole vehicle design process.

Chapter 5

Magnesium for Crashworthiness Improvement

5.1 Introduction

In this chapter, the crashworthiness performance of magnesium alloys is studied using nonlinear FE analysis. A new concept to improve vehicle crashworthiness is also introduced. The new concept is formed on the basis that, a conventional vehicle structure is made of one material only (usually steel). And as previously discussed, a conventional method to improve the design is to find best feasible values for parts thicknesses for optimum performance. However, the design can be improved further by combining more than one material, which adds another dimension to the design space as shown in Figure 5.1. Considering this, there are more design alternatives added to the design space, thus allowing more freedom to the designer. The designer can then vary both thickness and material type to find more suitable solutions to improve performance.

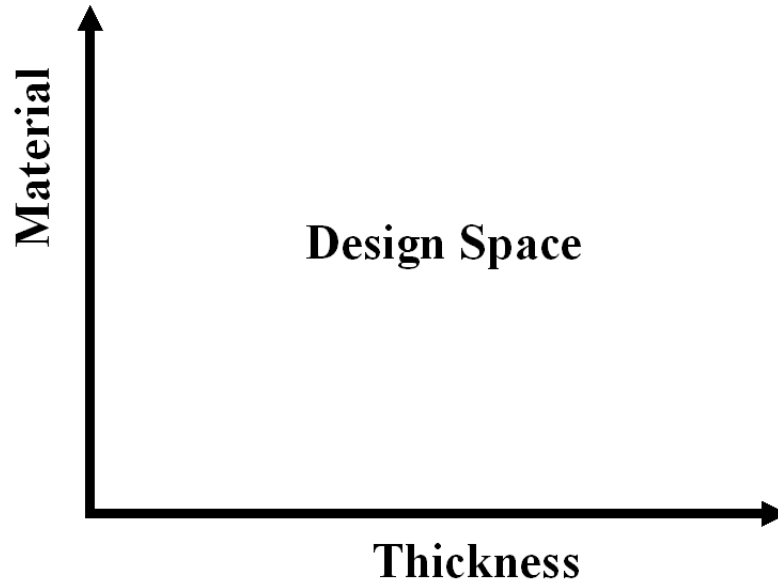


Figure 5.1: The design space after using the proposed concept

Recently, magnesium has been recognized as a strong candidate for automobile manufacturing due to its attractive low density (78% lighter than steel). Thus, using magnesium to replace steel in automobile structures will reduce their weight. Consequently, fuel economy will improve, and carbon emissions will decrease. Another important advantage of magnesium is that, it is strain rate sensitive [102], which means that its strength increases as the load rate increases. This also means that, magnesium can absorb more energy under dynamic loads compared to static loads. Thus, making structural parts of magnesium may improve vehicle crashworthiness performance.

The objective here is to investigate the potentials of magnesium for reducing vehicle weight and at the same time improving safety as much as possible. Moreover, it is required to investigate the effect of using combinations of steel and magnesium on weight and the amount of impact energy absorbed. Finally, direct optimization using the genetic algorithm is conducted to find optimum steel/magnesium combination and optimum parts thicknesses for increasing the amount of impact energy

absorbed without increasing weight. The approach has been demonstrated through two illustrative examples: (1) A thin walled tube under axial impact and (2) Vehicle structure design using the modified nonlinear FE model of the chassis frame that has been developed in chapter 3.

5.2 Design Optimization of a Thin Walled Tube

A thin walled tube is divided into three parts as shown in Figure 5.2. A base design is assumed to be an all steel tube with a constant wall thickness of 2 mm. First, it is required to investigate the effect of using magnesium instead of steel on the crashworthiness performance of the tube under axial impact loading. A nonlinear FE model is created according to the model parameters in Table 5.1.

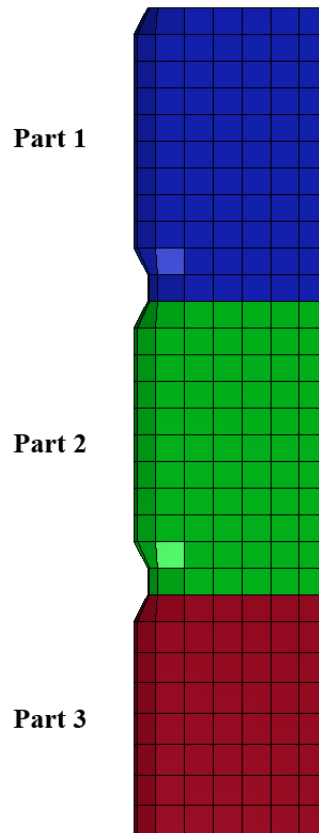


Figure 5.2: View of the nonlinear FE model of the thin walled tube

Table 5.1: Model parameters of the nonlinear FE model of the thin walled tube

Dropped mass	100 kg
Pre-impact speed	10 m/s
Total length	235 mm
Number of elements	391
Elements type	Belytschko-Lin-Tsay
Contact model	CONTACT AUTOMATIC SINGLE SURFACE
Design variables	Parts thicknesses (x1, x2, x3)
Design range	$X_L [1, 1, 1] : X_U [3, 3, 3]$
Steel	
Material model	MAT PIECEWISE LINEAR PLASTICITY
Density (kg/m^3)	7820
Young's modulus (GPa)	207
Poisson's ratio	0.3
Yield strength (MPa)	200
Magnesium	
Material model	MAT PLASTIC KINEMATIC
Density (kg/m^3)	1770
Young's modulus (GPa)	45
Poisson's ratio	0.35
Yield strength (MPa)	165
Cowper-Symonds Parameters (D & q)	1000, 3 taken from Ref. [224]

Let us establish two different designs of the tube made of magnesium: (1) Maintaining the same thickness as the base design, which is referred to as (ST) and (2) Maintaining the same weight as the base design, which is referred to as (SW). A nonlinear FE model is created for each design and simulated using LS-DYNA. The values of the total weight and the total absorbed impact energy are then evaluated. The results are

provided in Table 5.2, which also includes the percentage of increase (+) or reduction (-) with respect to the base design.

Table 5.2: Comparison between Mass and IE of the base, ST, and SW designs for thin walled tube

Design	Mass (kg)	%	IE (kJ)	%
Base	0.38	0	2.15	0
ST	0.09	-78	1.35	-37
SW	0.38	0	4.93	129

As shown in Table 5.2, the (ST) design yields 78% reduction in weight but at a reduction in IE by 37%, and the (SW) design yields a 129% increase in IE. However, when considering the final deformed shapes as shown in Figure 5.3, it is clear that the SW design did not fully deform. This means that the full tube length has not been fully used. This may mean that the reaction force (RWF) can be high compared to other designs since the impact energy was absorbed in a smaller deformed length. To verify this, RWF has been evaluated for all three configurations at each instant of time. The maximum value is evaluated for each configuration and the results are shown in Figure 5.4. As it can be realized, the SW design has a peak RWF value that is 5 times the value of peak of the base design, while the highest RWF value for the ST design is only one half of it.

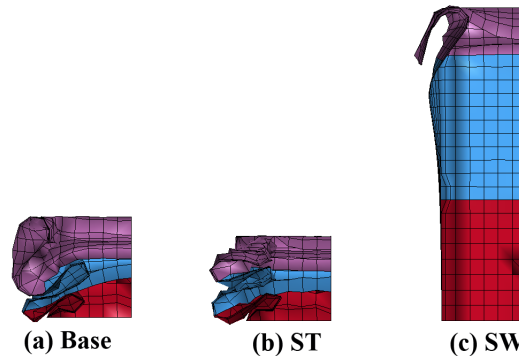


Figure 5.3: Final deformed shapes of the base, ST and SW designs of thin walled tube

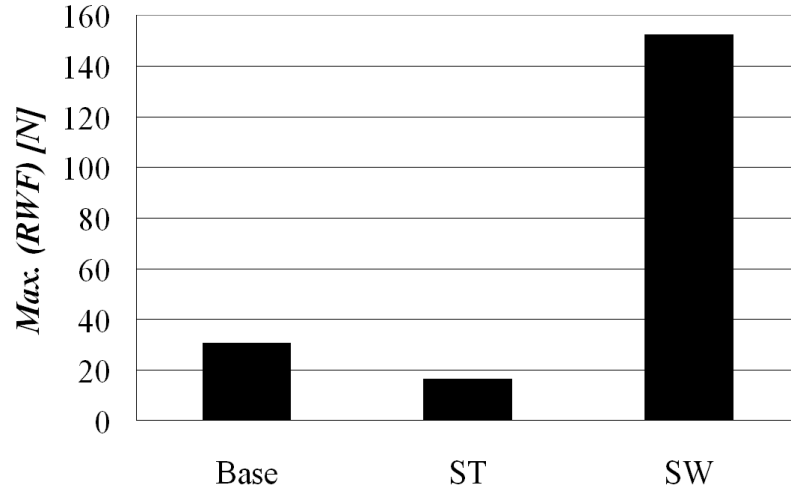


Figure 5.4: Comparison between max (RWF) for the three configurations of thin walled tube

5.2.1 Material Variation of a Thin Walled Tube

In this section, the effect of combining steel and magnesium into the same structure is investigated. The thickness is held constant for all parts at 2 mm. Having three parts and two materials, the number of all combinations is $2^3 = 8$. LS-DYNA simulation is conducted at each material combination and the value of the total energy absorbed is recorded and provided in Table 5.3.

The symbols M_1 , M_2 and M_3 refer to the type of the material for each part. For example, M_1 refers to the material type used in part1. Figure 5.5 shows the values of IE and Mass normalized with respect to the base design for each configuration. It is clear that, although the value of IE has not been increased, there has been reduction in weight at various degrees. For example, changing the material of the third part from steel to magnesium (second design in Table 5.3) yields a 29% reduction in weight with only 3% loss in IE. Considering this, magnesium can be effectively used in crashworthiness design optimization.

Table 5.3: Results for material variation for thin walled tube

ID	Variables			Responses	
	M_1	M_2	M_3	Mass (kg)	IE (kJ)
1	Steel	Steel	Steel	0.38	2.15
2	Steel	Steel	Mg	0.27	2.10
3	Mg	Steel	Steel	0.29	1.98
4	Mg	Steel	Mg	0.19	1.65
5	Steel	Mg	Steel	0.27	1.63
6	Steel	Mg	Mg	0.17	1.80
7	Mg	Mg	Steel	0.19	1.30
8	Mg	Mg	Mg	0.09	1.35

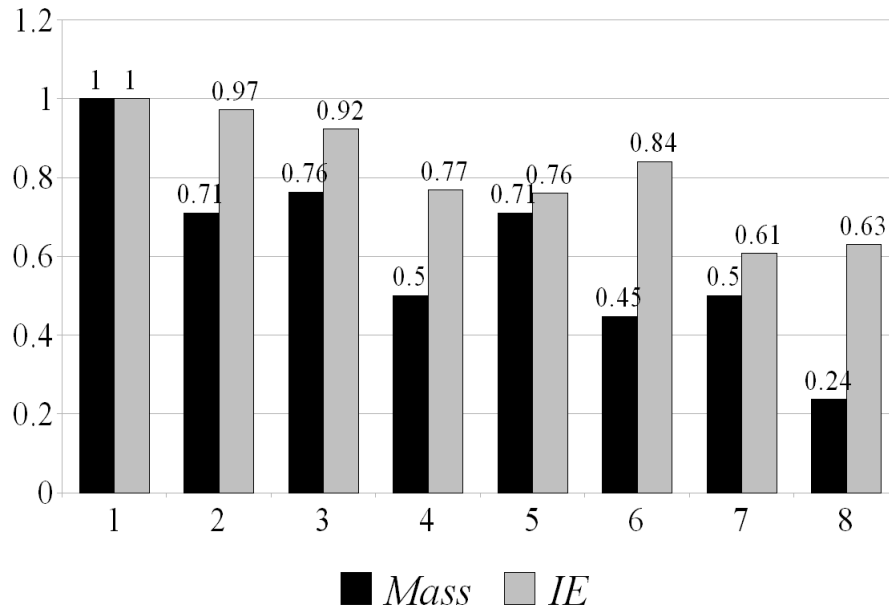


Figure 5.5: Comparison between Mass and IE for the different material combinations of the thin walled tube

5.2.2 Thickness and Material Optimization of a Thin Walled Tube

An optimization problem can be formulated to find the optimum material type and thickness combination. In chapter 3, approximation techniques have been explained and used to alleviate the high computational cost of simulating nonlinear FE models. However, there are two challenges with implementing this approach to the current problem:

1. To create an approximate model to represent all material combinations, an exceptionally large number of data points will then be required. This is due to the fact that, for each case of material combination, data points are required to represent the variation of parts thicknesses. Moreover, the number of data points will increase rapidly if a new variable is added.
2. There are two physically different types of variables: continuous (thickness) and discrete (material type), which constitutes a combinatorial problem. Combinatorial optimization problems are very difficult to solve and time consuming [225]. Formal gradient based algorithms depend on derivatives calculation which can not be applied with discrete variables. Moreover, most of the algorithms deal with linear combinatorial optimization problem [226], where this problem is highly nonlinear.

Considering the aforementioned challenges with using approximation techniques, it is inescapable that direct optimization will be used. The genetic algorithm, which has been described in chapter 4, can be directly combined with the nonlinear FE model. However, the genetic algorithm requires a tremendous number of iterations in order converge to a solution. This will largely increase the computational cost even for the current simple tube model. Therefore, the number of iterations is limited to 100,

which is 10 populations with 10 generations.

The results of the 100 simulations are normalized with respect to the base design and plotted in Figure 5.6. The intersection point between the bolded horizontal and vertical lines represents the base design. The figure is divided into four regions, where region 1 represents the favorable designs with larger IE and smaller Mass values, and on the other hand region 3 represents the unfavorable designs with smaller IE and larger Mass values. Finally, regions 2 and 4 are trade-off designs between Mass and IE. For example, both IE and Mass increase in region 2 and decrease in region 4. There are 8 different designs in region 1, among which the value of IE has been increased by maximum of 20% and the value of Mass has been decreased by maximum of approximately 40%. In region 2, the largest increase in IE is 52%, with only 8% increase in Mass. This design will be called the (TM) design. In the next section, conventional thickness optimization is conducted.

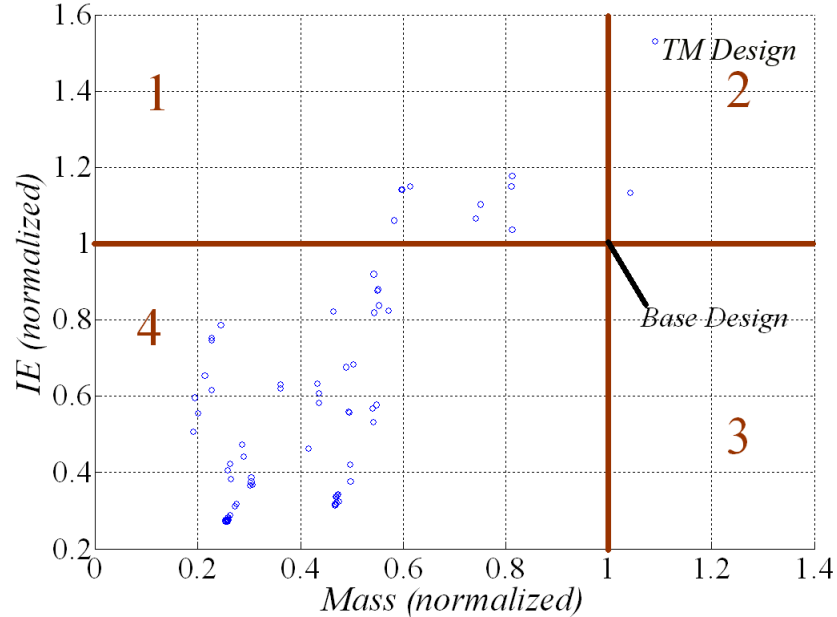


Figure 5.6: Normalized IE versus normalized Mass for the genetic algorithm results for the thin walled tube

5.2.3 Thickness Optimization of a Thin Walled Tube

The D-Optimality criterion is used to generate 15 points as provided in Table 5.4 and nonlinear FE analysis has been conducted at each point. The results of IE and mass are recorded and used to fit each of the four different RSM models (linear, interaction, quadratic and pure quadratic). The value of the $adjR^2$ is calculated for each model type and provided in Table 5.5. Again, the results show that the quadratic model is the most accurate and is used here to model both IE and mass in the optimization problem.

Table 5.4: Design matrix of the RSM model for the thin walled tube

ID	T_1	T_2	T_3
1	2.00	2.00	2.00
2	1.74	1.79	2.13
3	2.19	2.35	2.07
4	2.60	2.40	2.09
5	2.45	1.41	1.03
6	1.54	2.97	2.11
7	2.90	2.92	2.04
8	2.50	1.80	1.09
9	1.23	1.75	1.50
10	2.35	2.96	2.23
11	1.93	1.12	2.35
12	1.39	2.59	1.48
13	2.93	1.29	2.30
14	2.51	1.94	1.92
15	2.12	1.03	1.50

Table 5.5: The $adjR^2$ values for the different RSM models for thin walled tube

	Mass	IE
Linear	1	0.82
Interaction	1	0.85
Quadratic	1	0.91
Pure quadratic	1	0.88

The optimization problem is formulated to search for the optimum thickness values that maximize IE while maintaining the same weight as the base design and the problem can be written as:

$$\begin{aligned}
 & \text{Find } X^* \text{ that :} \\
 & \text{Maximizes } IE \\
 & \text{Subject to: } Mass - Mass_{original} \leq 0 \tag{5.1} \\
 & \text{where, } x_L \leq x \leq x_U
 \end{aligned}$$

Using the SQP algorithm, starting from the base design at $X = (2 \ 2 \ 2)$, an optimum solution was found after 15 iterations at $X^* = (3 \ 1.36 \ 1.8)$ and the iteration history is shown in Figure 5.7. The design at the optimum solution, which will be called the (T) design, absorbs 2.75 kJ, which is about 28% larger than that of the base design (2.15 kJ).

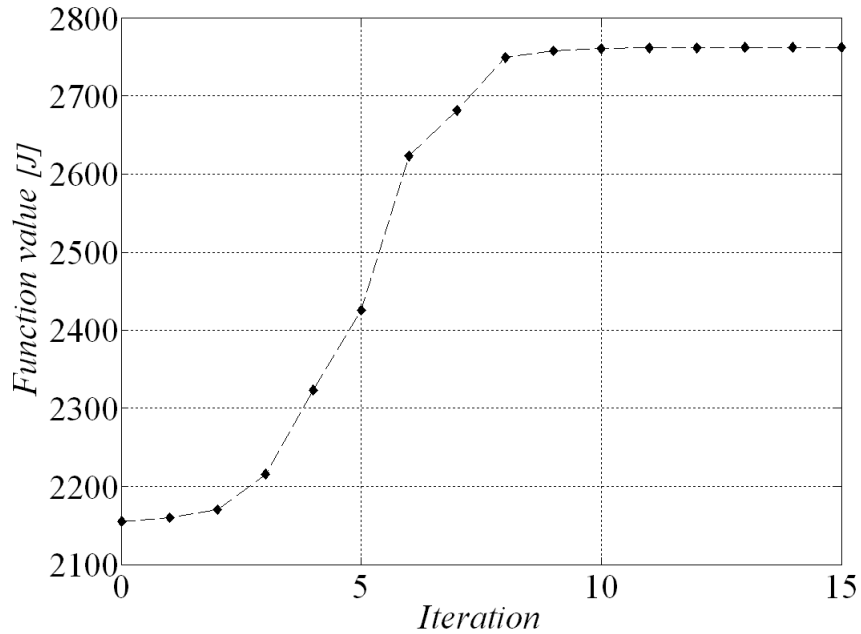


Figure 5.7: Iteration history of the thickness optimization problem for thin walled tube

5.2.4 Comparing the Solutions of a Thin Walled Tube

The Specific Energy Absorbed (SEA) is usually used to compare different designs. SEA is defined as the ratio between the amount of impact energy absorbed and weight. Here, SEA is calculated for the (base, T and TM) designs. The values are shown in Figure 5.8. It is clear that the TM design has the highest SEA value. This proves that using the proposed approach improves the design to a larger extent than using the conventional thickness optimization approach.

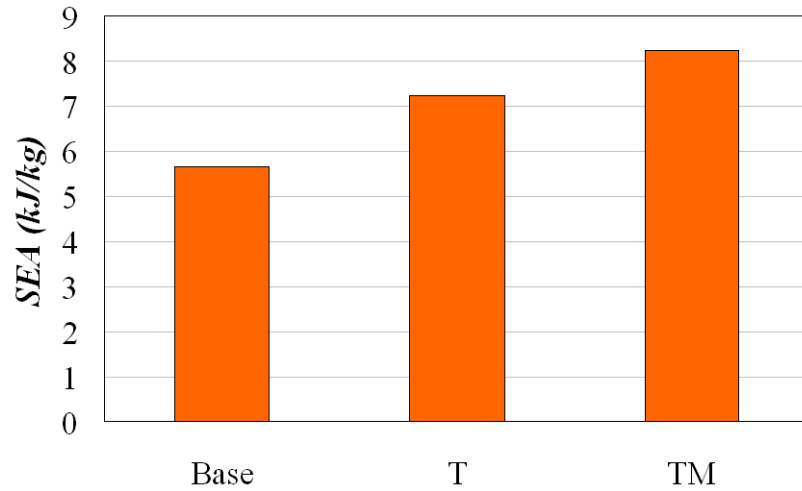


Figure 5.8: Comparison between SEA for the base, T and TM designs for thin walled tube

5.3 Design Optimization of a Vehicle Chassis Frame

In this section, the concept of combining steel and magnesium for crashworthiness improvement is applied to the modified nonlinear FE model that has been developed in chapter 3. The results are then used to improve the crashworthiness performance of the whole vehicle structure. For the sake of clarity, a view of the chassis frame showing the different parts is again shown in Figure 5.9.

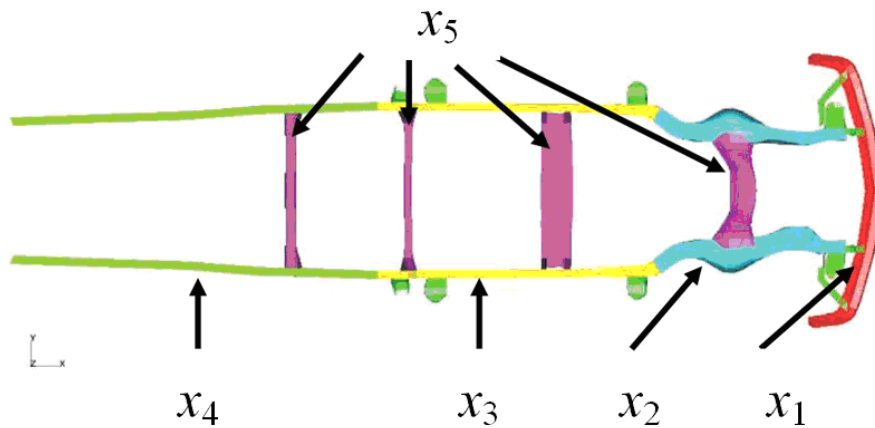


Figure 5.9: Design variables on the chassis frame

5.3.1 Material Variation of a Vehicle Chassis Frame

First, all possible combinations between steel and magnesium while maintaining parts thicknesses as the base design (first design in Table 5.6) are simulated using LS-DYNA. The impact energy absorbed in the chassis frame and its associated mass are evaluated. The results are provided in Table 5.6. The results are normalized with respect to the base design which is made of steel only, and are shown in Figure 5.10.

Table 5.6: Results for material variation for the chassis frame

Point No.	Variables					Responses	
	M_1	M_2	M_3	M_4	M_5	Mass (kg)	IE (MJ)
1	Steel	Steel	Steel	Steel	Steel	140.0	0.1160
2	Mg	Steel	Steel	Steel	Steel	127.3	0.1058
3	Steel	Mg	Steel	Steel	Steel	115.3	0.0778
4	Mg	Mg	Steel	Steel	Steel	102.5	0.0770
5	Steel	Steel	Mg	Steel	Steel	120.8	0.1078
6	Mg	Steel	Mg	Steel	Steel	108.1	0.0985
7	Steel	Mg	Mg	Steel	Steel	96.1	0.0747
8	Mg	Mg	Mg	Steel	Steel	83.3	0.0749
9	Steel	Steel	Steel	Mg	Steel	121.4	0.1133
10	Mg	Steel	Steel	Mg	Steel	108.6	0.1055

continued on next page

Point No.	Variables					Responses	
	M_1	M_2	M_3	M_4	M_5	Mass (kg)	IE (MJ)
11	Steel	Mg	Steel	Mg	Steel	96.6	0.0792
12	Mg	Mg	Steel	Mg	Steel	83.9	0.0778
13	Steel	Steel	Mg	Mg	Steel	102.2	0.1092
14	Mg	Steel	Mg	Mg	Steel	89.4	0.1004
15	Steel	Mg	Mg	Mg	Steel	77.4	0.0762
16	Mg	Mg	Mg	Mg	Steel	64.7	0.0728
17	Steel	Steel	Steel	Steel	Mg	115.5	0.1096
18	Mg	Steel	Steel	Steel	Mg	102.8	0.0969
19	Steel	Mg	Steel	Steel	Mg	90.8	0.0767
20	Mg	Mg	Steel	Steel	Mg	78.0	0.0750
21	Steel	Steel	Mg	Steel	Mg	96.3	0.1100
22	Mg	Steel	Mg	Steel	Mg	83.6	0.0932
23	Steel	Mg	Mg	Steel	Mg	71.6	0.0716
24	Mg	Mg	Mg	Steel	Mg	58.9	0.0675
25	Steel	Steel	Steel	Mg	Mg	96.9	0.1089
26	Mg	Steel	Steel	Mg	Mg	84.1	0.0983
27	Steel	Mg	Steel	Mg	Mg	72.2	0.0776

continued on next page

Variables						Responses	
Point No.	M_1	M_2	M_3	M_4	M_5	Mass (kg)	IE (MJ)
28	Mg	Mg	Steel	Mg	Mg	59.4	0.0734
29	Steel	Steel	Mg	Mg	Mg	77.7	0.1046
30	Mg	Steel	Mg	Mg	Mg	65.0	0.0954
31	Steel	Mg	Mg	Mg	Mg	53.0	0.0721
32	Mg	Mg	Mg	Mg	Mg	40.2	0.0684

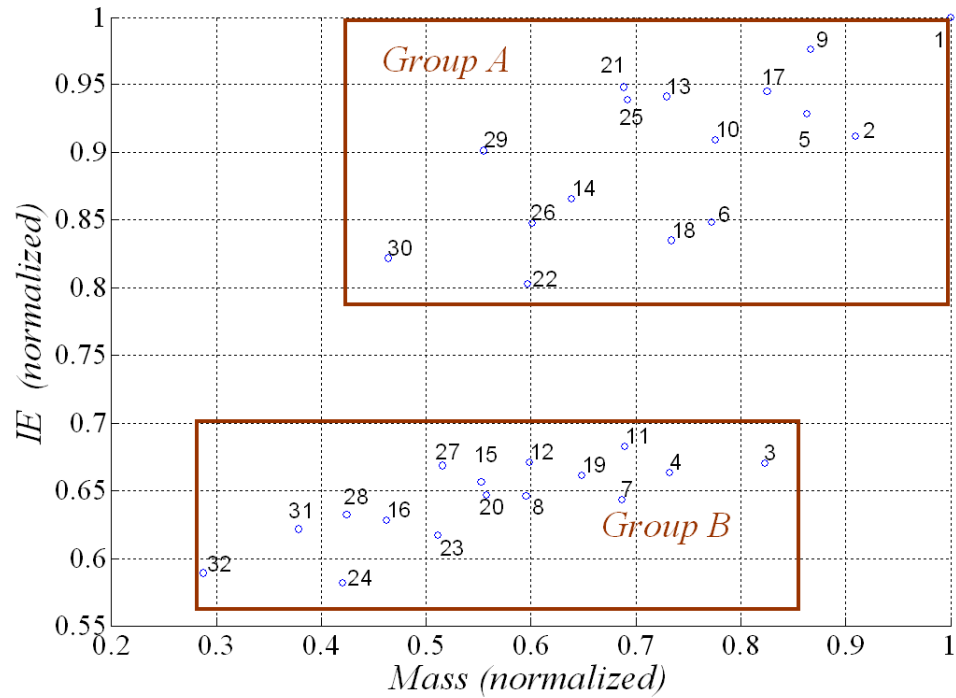


Figure 5.10: Normalized IE versus normalized Mass for material variation for the chassis frame

There are some interesting observations in Figure 5.10, which can be summarized as:

- i. Maintaining the thickness and replacing steel with magnesium will decrease IE. In fact, a chassis frame that is all made of magnesium (point 32) will absorb the least amount of IE.
- ii. The amount of IE at point 9 is 98% of the one at point 1, which is all made of steel. However, it offers a 13% weight reduction, which was achieved by changing the material of part 4 from steel to magnesium.
- iii. The 32 points can be divided to two groups, A and B according to the value of IE as shown in Figure 5.10. In group A, the second part of the chassis frame (front part of the longitudinal rails) is made of steel, while in group B, it is made of magnesium.
- iv. Points 5 and 9, have almost the same weight, however, there is 5% difference in the value of IE. Both designs have one component made of magnesium. The difference is that, this component is part 3 at point 5 while it is part 4 at point 9.
- v. Points 7, 8 and 20 have almost the same values for IE, however, they have different values for mass. This means that IE can be obtained with lower mass at point (20) than at point (7) or (8).

5.3.2 Thickness and Material Optimization of a Vehicle Chassis Frame

Considering the aforementioned observations, it can be concluded that the design can be improved further by allowing both material type and thickness to vary. To find best material combination and thickness values that can improve the crashworthiness performance, the nonlinear FE model of the chassis is combined with the genetic algorithm. The algorithm is limited to 100 iterations and the process is repeated in

the same way as has been done in the previous section. It should be noted that, the computational cost of running 100 simulations is manageable since the reduced modified model has been used. The upper bound on the thickness values is increased from 5 mm to 10 mm since magnesium is lighter than steel. Thus thicker magnesium components can then be used. LS-DYNA simulation is conducted at each point and the values of IE and mass are evaluated, then normalized with respect to the base design. The results are shown in Figure 5.11.

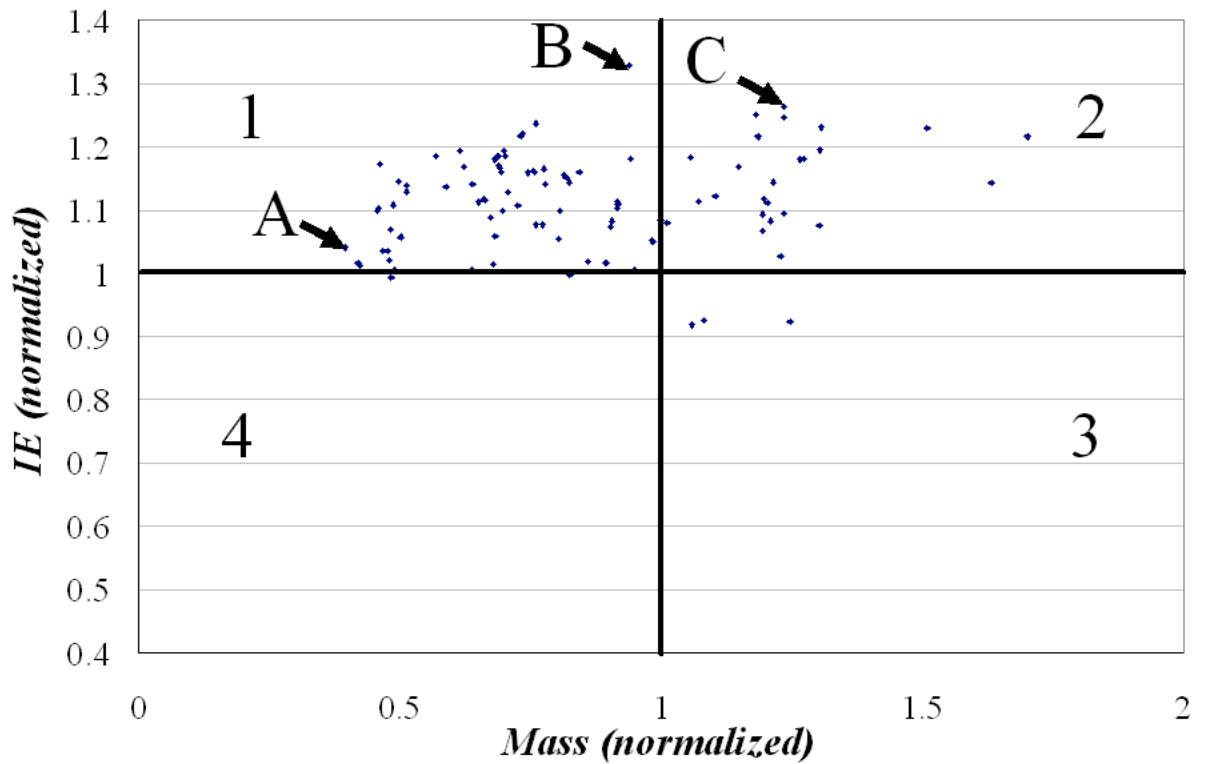


Figure 5.11: Normalized IE versus normalized Mass for the genetic algorithm results for the chassis frame

Figure 5.11 is divided into four regions in the same way as has been done in the previous example. There are three interesting designs named A, B and C as shown in Figure 5.11. Point (A) represents the maximum reduction (60%) in the chassis mass with a slight increase in the value of IE (4%), point (B) represents the largest increase (33%) in the value of IE in the whole design space and point (C) represents

the largest increase (26%) in the value of IE in region 2.

To investigate how these designs will affect the crashworthiness performance of the whole vehicle, LS-DYNA simulation is conducted at each point. The values of IE and Mass are evaluated for each design. The percentage difference between IE for each design and that of the base design (ΔIE) is calculated. The difference between the mass of each design and that of the base design ($\Delta Mass$) is also calculated. The results are provided in Table 5.7, which also includes the associated design variables for each design.

Table 5.7: ΔIE and $\Delta Mass$ and associated design variables for designs A, B and C for the chassis frame

	M_1	M_2	M_3	M_4	M_5	T_1	T_2	T_3	T_4	T_5	$\Delta Mass$	ΔIE
						mm	mm	mm	mm	mm	kg	%
Base	Steel	Steel	Steel	Steel	Steel	2.7	3.1	3.1	3.1	3.6	0	0
A	Mg	Mg	Mg	Mg	Mg	2.11	9.3	8.5	1.6	4.0	-80	-2.2
B	Steel	Mg	Mg	Mg	Mg	9.46	9.2	8.4	9.5	9.5	-8.4	3.0
C	Steel	Mg	Mg	Steel	Steel	6.61	8.5	7.1	1.9	9.8	32.2	7.4

The results show that a maximum reduction in weight (80 kg) has been accomplished at point A with 2.2% reduction in IE. The mass at point B has been reduced by 8.4 kg while IE has been increased by 3%. The largest increase in IE (7.4%) is at point point C but with an additional mass of 32.2 kg. It can be concluded that point A represents the best trade off between IE and mass, where 80 kg were reduced at only 2.2% loss in IE. Point C can be used when increasing IE is required even at the expense of weight increase. It is interesting to note that point B achieved almost the same increase in IE as that of Design 2 in chapter 3 (3.3%), that was obtained using conventional thickness based optimization. However, point B reduced 8.4 kg of mass compared to zero weight reduction for Design 2. Finally, it can be concluded that

through thickness and material optimization, more and better design alternatives can be obtained compared to using thickness optimization alone.

5.4 Summary

A new design approach has been proposed to improve vehicle crashworthiness. The approach adds an extra dimension to the design space through including material type (magnesium) as a variable in the design process. The approach has been applied to two examples and encouraging results have been obtained.

Chapter 6

Investigation of Imperfection in Crush Elements

6.1 Introduction

In this chapter, an important add-on energy absorber system in the form of thin walled columns, known as crush element will be investigated. The objective here is to demonstrate the effect of imperfection on the reaction force and the amount of energy absorbed in these crush elements.

An energy absorber system converts kinetic energy into plastic deformation. Thin walled columns have been identified as very efficient energy absorbing systems [227]. A well designed energy absorber system must satisfy the following two requirements: (1) It must absorb as much Impact Energy as possible by plastically deforming in a controllable manner. Thus, the remaining kinetic energy can be handled by the restraint system. (2) It must maintain the reaction forces transmitted to the occupants within the human tolerable limits.

The system is typically attached to the frontal vehicle structure to absorb impact

energy and minimize the reaction forces on the occupants. Some researchers studied the design of energy absorber systems. For example, Sharpe et al. [228] describe the development process of an energy absorber system attached to a mid-size sedan. They used aluminum extrusions to absorb impact energy in frontal impact. Simulations and prototype testing proved that this system is effective in improving the safety of vehicles under frontal impact. Also, Motzawa and Kamei [229] suggested changing the cross section of a thin walled tube used in an energy absorber system to control the deformation modes for improved performance.

The deformation modes of thin wall tubes under impact loading have been studied by many researchers [230–233]. They concluded that the most efficient (and the most difficult to acquire) mode of deformation is the progressive buckling mode, in which the tube deforms progressively into multiple folds in an accordion-like style. Crush initiators are intentionally embedded stress concentrators used to trigger and maintain this mode of deformation. The most widely used type of triggers is to chamfer the end of the tube [234]. Crush initiators not only help in minimizing occupants injuries, but they also indirectly help in reducing the weight of other vehicle structures behind the rails. This can be explained as, reducing initial peak force values will subsequently cause these structures to endure lower load values than they would have if crush initiators have not been included and hence, their weight can be reduced [235]. Furthermore, since air bag triggering sensors are usually located on the longitudinal rails, large forces may accidentally trigger them and cause injuries. Therefore, crush initiators are very important in vehicle design for crashworthiness.

Figure 6.1 represents a typical load curve in progressive buckling of a thin wall tube under impact loading [235]. As the tube is loaded, the stress at the tube cross section increases uniformly until it reaches point 'A', which marks the elastic buckling load. If the buckled region is to be represented by plate like segments, then the stress at the centers of those segments will remain constant while the stresses around their

corners start to increase. The corners then plastically deform forming the first fold at point 'B', which marks the crippling load. The crippling load is the maximum load carrying capacity of the tube. After point 'B', the load decreases until point 'C' after which, the load starts to increase again and the second fold is formed at point 'D'. The process then continues and folds are formed in the same manner until the end of the tube is reached or until the kinetic energy of the dropped weight is fully absorbed [235]. Point 'B' is of significant importance as it marks the maximum load that the tube can withstand before it starts to form its first fold.

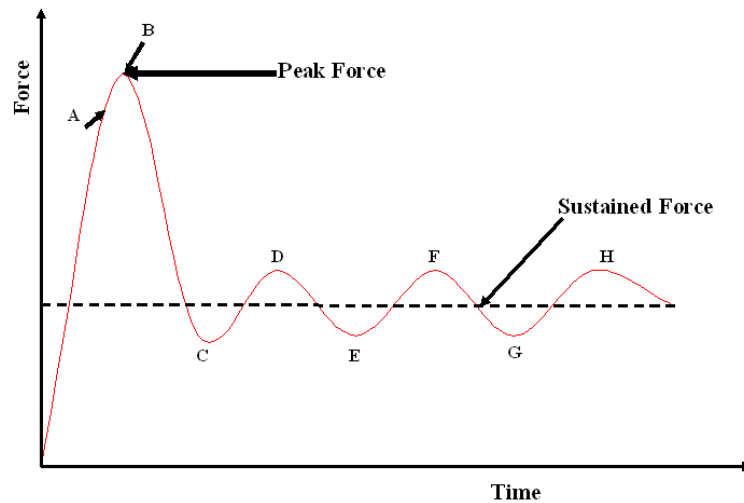


Figure 6.1: A typical load curve [235]

The objective of crush initiators is to decrease the value of the peak force and to maintain a steady force along the allowable deformed distance. Thus, a sufficient amount of impact energy is absorbed in the plastic deformation process. The amount of absorbed impact energy is computed by calculating the area under the load displacement curve. It can also be calculated by multiplying the average crashing force by the total distance traveled by the end of the tube.

6.2 Methodology

Here, the same square tube that was modeled in chapter 2 is used as a typical energy absorber system. Crush initiators are introduced in the form of sine wave imperfection along the walls of the tube. The imperfection can be represented as:

$$P(z) = \text{ampl} \cdot \text{Sin}\left(\frac{2\pi \cdot z}{wvl}\right) \quad (6.1)$$

where, P is the imperfection function, ampl is the amplitude value, wvl is the wave length of the harmonic wave and z is the value of the distance along the z direction at which the tube wall is perturbed. ampl and wvl are the two design variables considered in this study. Lower and upper bounds of the design variables are assumed to be 0 and 2 mm respectively. The imperfection function P is coded in LS-DYNA. Different imperfection configurations are introduced by applying the imperfection to different locations on tube's wall sides. They can be grouped as:

Group A: This group includes perturbing one corner (1C) as shown in Figure 6.2 or four corners (4C) of the tube as shown in Figure 6.3.

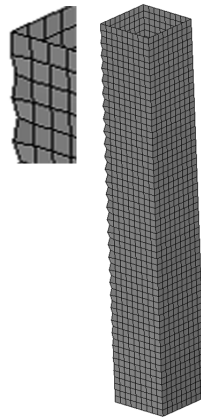


Figure 6.2: A view of the 1-C class model

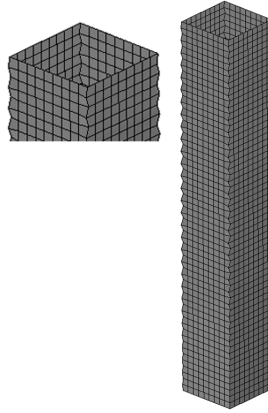


Figure 6.3: A view of the 4-C class model

Group B In this group, two opposite sides of the tube are perturbed as shown in Figure 6.4. This includes perturbing two opposite sides with the same *ampl* and *wvl* values (2S_S), or perturbing them with different *ampl* and *wvl* values (2S_D).

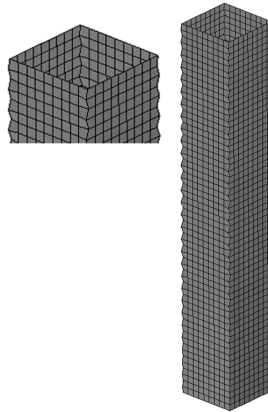


Figure 6.4: A view of the 2-S class model

Group C In this group, four sides of the tube are perturbed as shown in Figure 6.5. The group contains different configurations as follows:

- (1) The four sides are perturbed with the same (*ampl* and *wvl*) values (4S_AS).
- (2) Each pair of two opposite sides is perturbed with the same (*ampl* and *wvl*) values, but each pair has a different value (4S_2S).

(3) Each side of the four sides is perturbed with different (*ampl* and *wvl*) values (4S_AD).

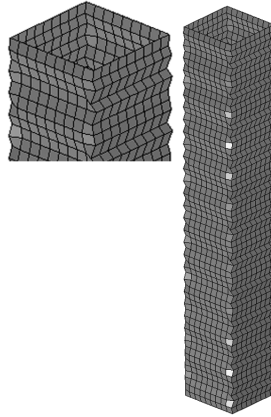


Figure 6.5: A view of the 4-S class model

The baseline design of the tube with no imperfection is modeled with LS-DYNA under a dropped weight of 73.6 kg at 10.3 m/s pre-impact speed. The peak reaction force and the amount of impact energy absorbed (IE_b) were found to be 35 kN and 3.8 kJ, respectively. Figure 6.6 shows the load variation at the base of the tube versus time.

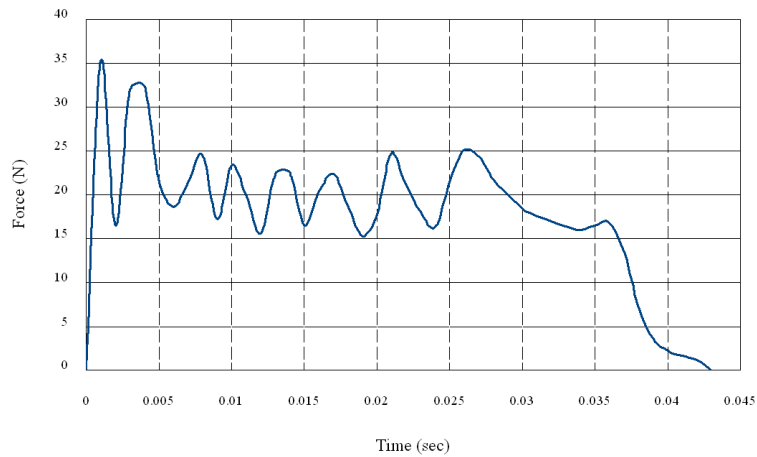


Figure 6.6: Load vs time of the baseline design

The objective here is to compare the effect of the aforementioned imperfection configurations on the amount of impact energy absorbed IE and peak reaction force RWF.

An optimum imperfection configuration should minimize RWF without decreasing IE below the initial value of the baseline design (IE_b). The problem then is to find the optimum set of the design variables ($ampl$ and wvl). The optimization problem can be formulated as:

$$\begin{aligned}
 & \textit{Find } X^* \textit{ that :} \\
 & \textit{Minimizes } RWF \\
 & \textit{Subjec to: } IE - IE_b \leq 0 \tag{6.2} \\
 & \textit{where, } x_L \leq x \leq x_U
 \end{aligned}$$

where X^* is the optimum design vector, x is the vector of the design variables and x_L and x_U are the lower and upper bounds on the design space. Since the nonlinear FE model is relatively simple, hence the analysis model is directly combined with an optimization algorithm based on the Genetic Algorithm (GA) to find the optimal solution. The reasons for selecting GA as the optimization algorithm are:

1. It does not require computation of the derivatives as in gradient based algorithms. This is important since numerical methods can give spurious results due to the round off errors and the complexity of the nonlinear FE models.
2. It has the ability to resolve itself from being trapped into a local minima region.

Although, the nonlinear FE model of the tube is relatively simple, the main drawback of GA is that it requires an extremely large number of computations. Thus, the settings of the GA is limited to a population size of 10 and 3 generations (iterations). It should be noted that an overview of the GA has been presented in chapter 4.

6.3 Results and Discussion

The GA runs 30 FE analysis for each configuration. The values of impact energy absorbed (IE) and peak reaction force (RWF) are evaluated at each analysis. The results are then analyzed and the design with minimum RWF is selected. The values of minimum RWF, associated IE and design variables for all configurations as well as the base design are provided in Table 6.1. For the sake of clarity, the values of IE and RWF are normalized with respect to the base design. The results are shown in Figure 6.7. It is clear that all configurations succeeded in reducing RWF and at the same time, slightly increased IE. It is interesting to note that the 4C configuration has the maximum reduction in RWF (22%) and the maximum increase in IE (2.3%).

Table 6.1: Values for IE, RWF and design variables for the different configurations

	<i>ampl</i> mm	<i>wvl</i> mm	<i>IE</i> kJ	<i>RWF</i> kN
Base	0	0	3.831	35.213
1C	1.78	1.19	3.856	29.1
4C	1.12	0.54	3.919	27.612
2S_S	1.23	0.11	3.877	28.134
2S_D	(0.54, 0.91)	(0.17, 0.05)	3.871	29.996
4S_AS	1.09	0.6	3.874	28.688
4S_2S	(0.21, 1.07)	(0.17, 1.06)	3.903	29.465
4S_AD	(1.04, 1.44, 1.22, 1.09)	(0.74, 0.92, 0.25, 1.46)	3.875	28.744

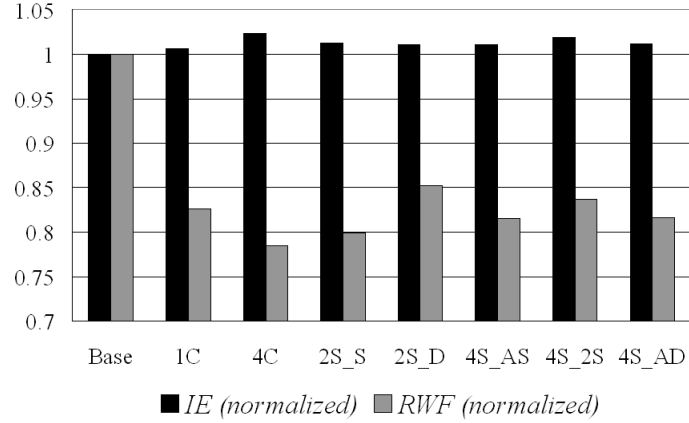


Figure 6.7: A comparison between *RWF* and *IE* for all configurations

From the foregoing results, it is clear that introducing the proper values of imperfection to energy absorber systems, improves their performance by reducing the peak reaction force and consequently reducing the transmitted loads to other vehicle structural parts. However, it is important to note that, the amount of introduced imperfection should be selected properly. In this work, the GA was employed to find optimum values of the design variables *ampl* and *wvl*. To prove the need for an optimization algorithm, the design of the (1C) configuration is manually changed and the results are analyzed in the following section.

6.3.1 Manual Design of the (1C) Configuration

The (1C) configuration is the simplest of all configurations. It introduces imperfection to only one corner of the tube. Three design points are selected from the design space which is bounded between 0 and 2 mm. The first design point is selected at [*ampl* = 0.01, *wvl* = 0.01] and will be referred as Extreme_1. The second design point is selected at [*ampl* = 0.5, *wvl* = 0.5] and will be referred as Mid_Case. Finally, the third design point is selected at [*ampl* = 2, *wvl* = 2] and will be referred as Extreme_2. Nonlinear FE analysis is conducted at each of the three points to evaluate the value

of RWF and IE. The values are normalized with respect to the base design and the results are shown in Figure 6.8. The three designs slightly increased the value of IE (about 1%). However, none has succeeded in reducing the value of RWF. On the other hand, the Extreme_2 design increased RWF by 67%. This proves that an ad-hoc approach to the problem is not practical and it is necessary to conduct formal optimization to find the optimal solution.

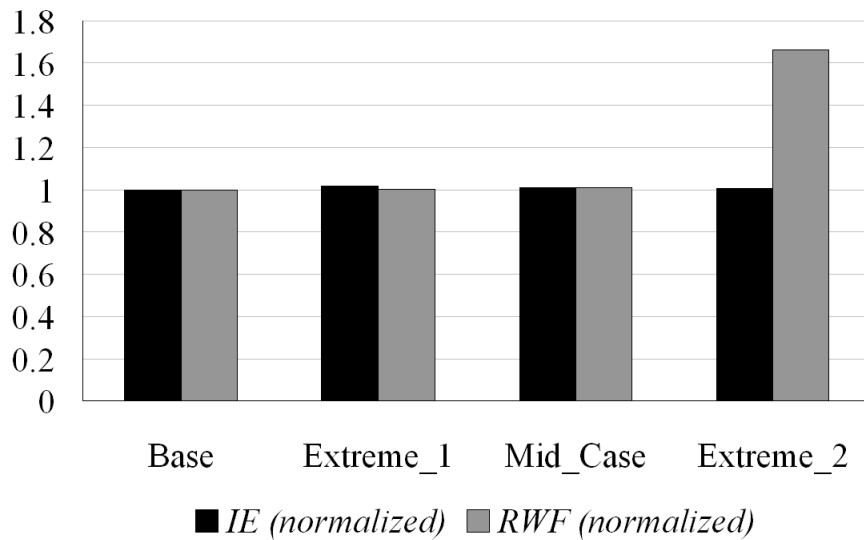


Figure 6.8: A comparison between *RWF* and *IE* for different design cases

6.3.2 The Deformation States

Studying the deformation states of each configuration can be helpful in understanding the effect of each configuration on the crash performance of the energy absorber system. There are two important deformation states: (1) The state at which the first fold starts to form and (2) The final state at the end of the deformation process. The two states for each configuration are shown in Figure 6.9.

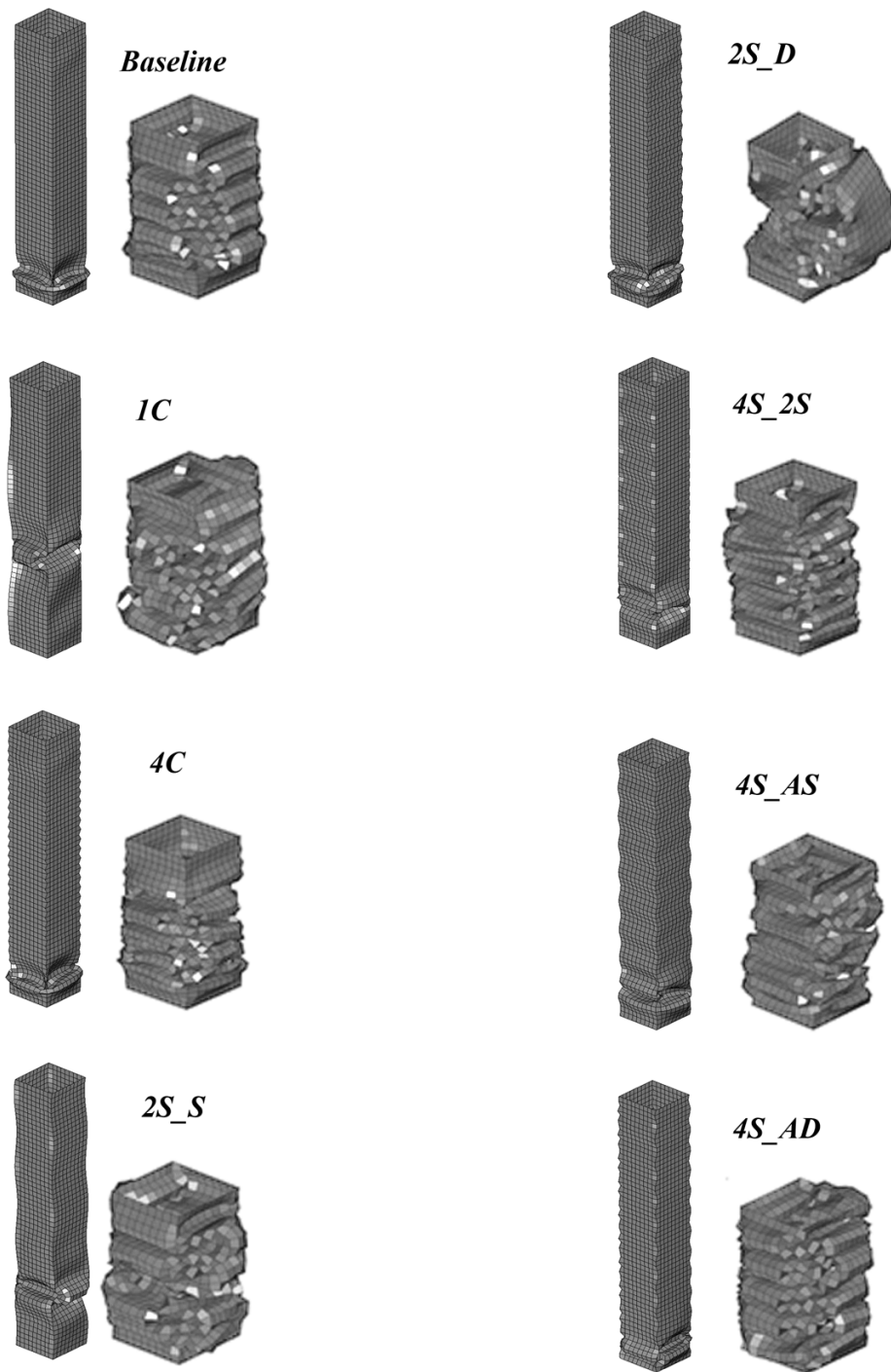


Figure 6.9: States of deformation for all configurations

The observations from Figure 6.9 can be summarized as:

1. The final form of the deformed folds is different between every configuration.

2. The place at which the first fold started to form is near the bottom of the tube for all configurations. Only in the (1C) configuration, the first fold started to form near the middle of the tube.
3. The final deformed state for all the configurations show the effect of the progressive buckling mode. Only the (2S_D) shows that the tube has gone through a global bending mode during the deformation process. Figure 6.10 shows the deformed state of the (2S_D) configuration at the time when global bending started to occur at 0.025 sec, and the final deformed state at 0.043 sec. The global bending mode is an undesirable mode that can significantly reduce the crashworthiness performance of a structure. To evaluate this effect, the reaction force versus time during the whole deformation process of the (2S_D) configuration is shown in Figure 6.11. It is clear that the value of the reaction force rapidly decreases at the moment of occurrence of the global bending mode. Consequently, this also reduces IE, since it is represented by the area under the RWF curve.

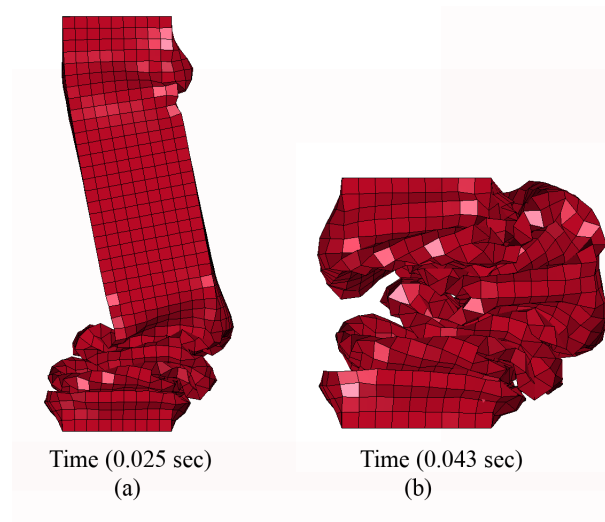


Figure 6.10: Two deformed states of the (2S_D) configuration: (a) Start of the global bending mode (b) Final deformed state

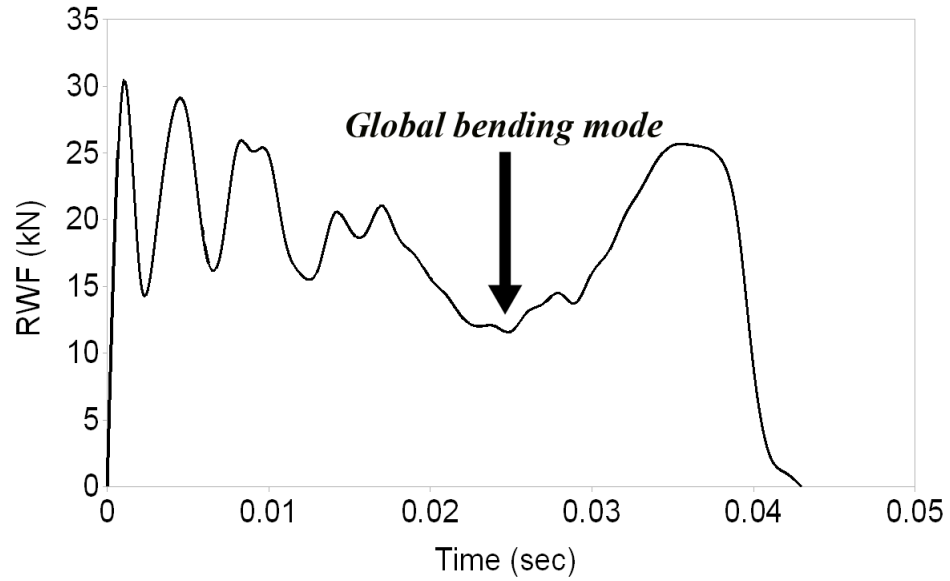


Figure 6.11: The reaction force history for the (2S.D) configuration

6.4 Summary

In this chapter, the effect of imperfection on the crash performance of crash energy absorbers has been investigated. The optimum imperfection values have been found using design optimization algorithm in which nonlinear FE analysis was combined with the genetic algorithm. The results showed that introducing proper imperfection into energy absorbers may significantly improve their performance by reducing the values of peak reaction forces.

Chapter 7

Summary, Contributions, and Future Work

7.1 Summary and Conclusions

The complicated nature of the physical crash processes of complex vehicle structures makes the design optimization process for crashworthiness a very challenging mission. Although, approximation techniques such as the response surface method, have been used successfully for design optimization of vehicle structures for crashworthiness. However, it is still difficult and impractical to apply approximation techniques to full vehicle structures due to the very expensive computational cost. Moreover, applying approximation techniques becomes computationally demanding when the number of design variables increases, which is known as the curse of dimensionality. Considering this, new methods are required to enable the designer to practically and accurately conduct design optimization of vehicle structures for crashworthiness. In this research, a practical and efficient methodology for design optimization of vehicle structures for crashworthiness has been developed. The developed methodology was successfully used to improve the crashworthiness performance of a pickup truck model, and the

results were achieved at a very manageable computational cost. It should be noted that the present study has been limited to the load case of full frontal impact with a rigid wall barrier at a speed of 56 km/hr. Also, the maximum amount of impact energy absorbed has been considered as the design metric. However, the basic principles on which the methodology has been based can be applied to other load cases using other design metrics, such as when studying side impact considering intrusion as the design metric.

Also, the problem of evaluating the goodness of a design quickly and easily has been examined. A new methodology was proposed to derive the relation between maximum impact energy absorbed and minimum structural weight. The methodology is based on the Pareto front principle and multiobjective optimization. It can be concluded that the proposed methodology can enable the designer to evaluate any design quickly and optimize its performance using optimum design variables. It should be noted that both the Pareto and Anti-Pareto fronts represent an envelope over the design space. Hence, only designs that fall within the design space can be examined. In case a design that lies outside this design space, both the Pareto and Anti-Pareto fronts must be created again based on the new limits.

Furthermore, the crashworthiness behavior of a pickup truck structure made of magnesium has been studied. A new approach has been proposed to improve the crashworthiness performance of vehicle structures using thickness and material optimization. The approach included material type as a design variable in addition to parts thicknesses. It can be concluded that magnesium can improve vehicle crashworthiness performance and by applying the proposed approach, design alternatives better than through formal thickness optimization only can be found.

Finally, the effect of imperfections on the performance of crush elements has been studied. Different configurations have been proposed and the optimum imperfection values were found through direct optimization using the genetic algorithm. It has been

shown that the effect of imperfection has slight effect on the amount of impact energy absorbed. Adding imperfection to tubes will increase manufacturing costs. However, these costs will be traded off with increased occupant protection. Besides, the costs will decrease with mass production. It can be concluded that the crashworthiness performance of crush elements can be significantly improved by introducing the proper values of imperfection.

7.2 Contributions

The major contributions of this research can be summarized as follows:

1. Developing an effective and practical methodology for design optimization of vehicle structures for crashworthiness improvement.
2. Developing a new approach to enable the designer to quickly and efficiently evaluate the optimality of a current design.
3. Deriving the relationship between minimum structural weight and maximum absorbed impact energy and the associated design variables using the Pareto front principle and multiobjective optimization.
4. Introducing the Anti-Pareto front terminology for the first time in vehicle crashworthiness design.
5. Developing a new approach in which material type is included as a design variable.
6. Studying vehicle structural components made of magnesium under impact loads.
7. Developing a systematic approach for studying the role of imperfection in designing efficient crush elements.

7.3 Future Work

This thesis includes a fundamental and systematic study of the design optimization of vehicle structures for crashworthiness improvement. However, there are other interesting aspects, which are identified for future work that can be summarized as:

Applying the methodology to other vehicle types:

In this research, the methodology has been applied to a pickup truck. The methodology can then be applied to other vehicle types such as a sedan. This can reveal differences in application between different vehicle types.

Including the effect of uncertainty:

In this research, deterministic optimization was used, which means that values of design variables and model parameters were assumed to be exact. In reality, values are uncertain, for example, material properties can be given with a certain statistical distribution. Optimization under uncertainty will then be more realistic, yet more challenging.

Including more design variables:

In this research, parts thicknesses were used as design variables (size optimization). Nevertheless, different design variables such as shape parameters can also be used (topology optimization).

Including more design objectives:

In this research, weight and the amount of impact energy absorbed, the two most important design objectives, were considered. However, the methodology can be

expanded by including other design objectives, such as noise and vibration.

Finding strain rate sensitivity parameters of magnesium:

Although, material properties are very important for accurate modeling, very few research has been published on the behavior of thin-walled structures made of magnesium. It is suggested that more experimental research should be devoted to deriving the important strain rate sensitivity parameters of different magnesium alloys.

References

- [1] World Health Organization, “The global burden of disease, http://www.who.int/healthinfo/global_burden_disease/2004_report_update/en/,” accessed on May 2009.
- [2] Transport Canada, “Canadian motor vehicle traffic collision statistics: 2006, <http://www.tc.gc.ca/roadsafety/tp/tp3322/2006/page1.htm>,” accessed on May 2009.
- [3] Transport Canada, *Analysis and Estimation of the Social Cost of Motor Vehicle Collisions in Ontario*, Ministry of Transportation, 2007.
- [4] Transport Canada, *Transport Canada Road Safety’s Traffic Accident Information Database TRAIID.*, Ministry of Transportation, 2008.
- [5] T. Khalil and P. Du Bois, *Finite element analytical techniques and applications to structural design*, Vehicle crashworthiness and occupant protection, Michigan: American Iron and Steel Institute, 2004.
- [6] U. Seiffert and L. Wech, *Automotive safety handbook*, SAE International, Warrendale, Pa., 2007.
- [7] S. Natori and Q. Yu, “An Application of CAP (Computer-Aided Principle) to Structural Design for Vehicle Crash Safety,” *SAE Technical paper 2007-01-0882*, 2007.

- [8] P. N. Koch, T. W. Simpson, J. K. Allen, and F. Mistree, “Statistical approximations for multidisciplinary design optimization: The problem of size,” *Journal of Aircraft* **36**(1), pp. 275–286, 1999.
- [9] C. J. Chen, J. Magadi, and M. Usman, “Up-front Design of the Air Cleaner Bracket Using Topology Optimization,” pp. 23–27, 1997.
- [10] C. J. Chen and M. Usman, “Design optimisation for automotive applications,” *International Journal of Vehicle Design* **25**(1), pp. 126–141, 2001.
- [11] N. Jones, *Structural Impact*, Cambridge University Press, 1997.
- [12] J. McQuaid and N. Jones, “A re-examination of Andrews research on impact resistance of railway axles,” *International Journal of Impact Engineering* **22**(7), pp. 727–738, 1999.
- [13] N. Jones, “Several phenomena in structural impact and structural crashworthiness,” *European Journal of Mechanics/A Solids* **22**(5), pp. 693–707, 2003.
- [14] R. A. Galganski, “Crashworthiness design of HSGGT vehicles,” in *Proc. IEEE/ASME Joint Railroad Conference*, pp. 121–130, 1993.
- [15] J. A. Newman, “Head injury criteria in automotive crash testing,” in *Stapp Car Crash Conference. Twenty-fourth. Proceedings. Warrendale, Society of Automotive Engineers*, pp. 701–747, 1980.
- [16] “Federal motor vehicle safety standards and regulations, <http://www.nhtsa.dot.gov/cars/rules/import/fmvss/index.html>,” accessed on May 2009.
- [17] “Canadian motor vehicle safety regulations , <http://www.tc.gc.ca/acts-regulations/regulations/crc-c1038/menu.htm>,” accessed on May 2009.
- [18] “European regulations related to crash testing, <http://www.crash-network.com/regulations/ece-regulations/ece-regulations.html>,” accessed on May 2009.

- [19] M. Richter, D. Otte, T. Pohlemann, C. Krettek, and M. Blauth, “Whiplash-type neck distortion in restrained car drivers: frequency, causes and long-term results,” *European Spine Journal* **9**(2), pp. 109–117, 2000.
- [20] M. El-Gindy and L. Ilosvai, “Experimental investigation into vehicle response during steering and braking manoeuvres,” *International Journal of Vehicle Design* **2**(4), pp. 463–469, 1981.
- [21] M. El-Gindy and X. Tong, “Stability and braking performance analysis of bus/pony-trailer combination vehicles,” *International Journal of Heavy Vehicle Systems* **8**(3), pp. 285–300, 2001.
- [22] W. Abramowicz and N. Jones, “Transition from initial global bending to progressive buckling of tubes loaded statically and dynamically,” *International Journal of Impact Engineering* **19**(5-6), pp. 415–437, 1997.
- [23] J. M. Alexander, “An approximate analysis of the collapse of thin cylindrical shells under axial loading,” *Q J Mechanics Appl Math* **13**(1), pp. 10–15, 1960.
- [24] T. Wierzbicki and T. Akerstrom, “Dynamic crushing of strain rate sensitive box columns,” *SAE Technical Paper 770592*, 1977.
- [25] W. Johnson, P. D. Soden, and S. T. S. Al-Hassani, “Inextensional collapse of thin-walled tubes under axial compression,” *The Journal of Strain Analysis for Engineering Design* **12**(4), pp. 317–330, 1977.
- [26] T. Wierzbicki and W. Abramowicz, “On the crushing mechanics of thin-walled structures,” *Journal of Applied Mechanics* **50**, pp. 727–739, 1983.
- [27] G. R. Cowper and P. S. Symonds, *Strain-hardening and strain-rate effects in the impact loading of cantilever beams*, Brown University Division of Applied Mathematics, 1957.
- [28] W. Abramowicz and N. Jones, “Dynamic progressive buckling of circular and square tubes,” *International Journal of Impact Engineering* **4**(4), pp. 243–270, 1986.

- [29] C. L. Magee and P. H. Thornton, "Design considerations in energy absorption by structural collapse," *SAE Technical Paper 780434* , 1978.
- [30] H. F. Mahmood and A. Paluszny, "Design of thin wall columns for crash energy management - their strength and mode of collapse," *SAE Technical Paper 811302* , 1981.
- [31] H. F. Mahmood and A. Paluszny, "Stability of Plate-Type Box Columns under Crush Loading," *Computational Methods in Ground Transportation Vehicles: Presented at the Winter Annual Meeting of the American Society of Mechanical Engineers, Phoenix, Arizona* , 1982.
- [32] "National Highway Traffic Safety Administration (NHTSA) | U.S. department of transportation, <http://www.nhtsa.gov/>," accessed on May 2009.
- [33] M. M. Kamal, "Analysis and Simulation of Vehicle to Barrier Impact," *SAE Technical Paper 700414* , 1970.
- [34] H. F. Mahmood and B. B. Fileta, "Design of Vehicle Structures for Crash Energy Management," *American Iron and Steel Institute, Southfield, MI* , 2004.
- [35] J. E. Greene, "Computer simulation of car-to-car collisions," *SAE Technical Paper 770015* , 1977.
- [36] C. L. Magee, "Design for crash energy management - present and future developments," in *The Seventh International Conference on Vehicle Structural Mechanics*, pp. 2-4, 1988.
- [37] G. G. Lim and A. Paluszny, "Side impact research," *SAE Technical Paper 885055* , 1989.
- [38] C. L. Magee, "Design for crash energy management, present and future developments," in *Seventh International Conference on Vehicle structural mechanics*, (Detroit, Michigan, USA), 1988.

- [39] H. F. Mohamed and B. B. Fileta, *Design of vehicle structures for crash energy management*, pp. 11–110. Vehicle Crashworthiness and Occupant Protection, American Iron and Steel Institute, 2004.
- [40] B. Deshpande, T. J. Gunasekar, R. Morris, S. Parida, M. Rashidy, and S. Summers, “Methodology development for simulating full frontal and offset frontal impacts using full vehicle MADYMO models,” *ASME Applied Mechanics Division Publications AMD* **237**, pp. 19–38, 1999.
- [41] R. T. Shea and J. Kral, “Madymo simulations of occupant and vehicle kinematics in offset and oblique barrier tests,” *ASME Conference Proceedings* , pp. 419–426, 2005.
- [42] R. Winter, M. Mantus, and P. A.B., “Finite element crash analysis of a rear engine automobile,” in *4th International Conference on Vehicle Structural Mechanics*, pp. 55– 61, 1981.
- [43] A. B. Pifko and R. Winter, “Theory and Application Of Finite Element Analysis to Structural Crash Simulation,” in *Computational Methods in Nonlinear Structural and Solid Mechanics: Papers Presented at the Symposium on Computational Methods in Nonlinear Structural and Solid Mechanic*, pp. 277–285, 1981.
- [44] E. Haug, F. Arnaudea, J. Du Bois, and A. Rouvay, “Static and dynamic finite element analysis of structural crashworthiness in automotive and aerospace industries,” *Structural Crashworthiness* , pp. 175–217, 1983.
- [45] J. Argyris, H. Balmer, J. St. Doltsinis, and A. Kurz, “Computer simulation of crash phenomena,” *International journal for numerical methods in engineering* **22**(3), pp. 497–519, 1986.
- [46] E. Haug, T. Scharnhorst, and P. Du Bois, “FEM-Crash, Berechnung eines Fahrzeugfrontalaufpralls,” *VDI Berichte* **613**, pp. 479–505, 1986.

- [47] J. Hallquist, *A Procedure for the Solution of Finite Deformation Contact-Impact Problems by the Finite Element Method*, University of California, Lawrence Livermore National Laboratory, 1976.
- [48] E. Haug, “Engineering safety analysis via destructive numerical experiments,” *Engineering Transactions* **29**(1), pp. 39–49, 1981.
- [49] “PAM-CRASH, <http://www.esi-group.com/products/crash-impact-safety/pam-crash>,” accessed on May 2009.
- [50] “RADIOSS, <http://www.altairhyperworks.com/default.aspx>,” accessed on May 2009.
- [51] “LS-DYNA , <http://www.lstc.com/lsdyna.htm>,” accessed on May 2009.
- [52] “ABAQUS , http://www.simulia.com/products/abaqus_fea.html,” accessed on May 2009.
- [53] C. D. Kan, D. Marzougui, G. T. Bahouth, and N. E. Bedewi, “Crashworthiness Evaluation Using Integrated Vehicle and Occupant Finite Element Models,” *International Journal of Crashworthiness* **6**(3), pp. 387–398, 2001.
- [54] H. Zhang, “Evaluation of frontal occupant protection system responses to crash pulse variations,” *International Journal of Crashworthiness* **11**(3), pp. 243–250, 2006.
- [55] J. Wu, *Crashworthiness simulation of roadside safety structures with development of material model and 3-D fracture procedure*. PhD thesis, University of Cincinnati, 2000.
- [56] H. A. Whitworth, R. Bendidi, D. Marzougui, and R. Reiss, “Finite element modeling of the crash performance of roadside barriers,” *International Journal of Crashworthiness* **9**, pp. 35–43, 2004.

- [57] A. O. Atahan and M. ASCE, “Finite-Element Crash Test Simulation of New York Portable Concrete Barrier with I-Shaped Connector,” *Journal of Structural Engineering* **132**, pp. 430–440, 2006.
- [58] J. Yang, “Pedestrian head protection from car impacts,” *International Journal of Vehicle Design* **32**, pp. 16–27, 2003.
- [59] C. Y. Kam, J. R. Kerrigan, M. Meissner, C. Drinkwater, D. Murphy, J. Bolton, C. Arregui, R. Kendall, J. Ivarsson, J. Crandall, B. Deng, J. Wang, C. Kerkeling, and W. Hahn, “Design of a full-scale impact system for analysis of vehicle pedestrian collisions,” *SAE Technical Paper 2005-01-1875* , 2005.
- [60] D. Longhitano, B. Henary, K. Bhalla, J. Ivarsson, and J. Crandall, “Influence of vehicle body type on pedestrian injury distribution,” *SAE Technical Paper 2005-01-1876* , 2005.
- [61] T. Yasuki, “Mechanism analysis of pedestrian knee-bending angle by SUV type vehicles using human FE model,” *International Journal of Crashworthiness* **12**(6), pp. 645–651, 2007.
- [62] Y. Kikuchi, Y. Takahashi, and F. Mori, “Full-scale validation of a human fe model for the pelvis and lower limb of a pedestrian,” *SAE Technical Paper 2008-01-1243* , 2008.
- [63] N. Rebelo, J. Nagtegaal, L. Taylor, and R. Passmann, “Comparison of implicit and explicit finite element methods in the simulation of metal forming processes,” *Numerical Methods in Industrial Forming Processes* , pp. 99–108, 1992.
- [64] D. Yang, D. Jung, I. Song, D. Yoo, and J. Lee, “Comparative investigation into implicit, explicit, and iterative implicit/explicit schemes for the simulation of sheet-metal forming processes,” *Journal of Materials Processing Technology(Switzerland)* **50**(1), pp. 39–53, 1995.

- [65] H. Naceur, S. Ben-Elechi, J. Batoz, and C. Knopf-Lenoir, “Response surface methodology for the rapid design of aluminum sheet metal forming parameters,” *Materials and Design* **29**(4), pp. 781–790, 2008.
- [66] H. Nagarajan, M. McCoy, C. S. Koshy, and H. M. Lankarani, “Design, fabrication and testing of a component hic tester for aircraft applications,” *International Journal of Crashworthiness* **10**(5), pp. 515–524, 2005.
- [67] H. Kim and B. P. D. Kirby, “Investigation of External Airbags for Rotorcraft Crashworthiness,” *Journal of Aircraft* **43**(3), pp. 809–816, 2006.
- [68] S. Heimbs, D. Vogt, R. Hartnack, J. Schlattmann, and M. Maier, “Numerical simulation of aircraft interior components under crash loads,” *International Journal of Crashworthiness* **13**(5), pp. 511–521, 2008.
- [69] A. Wittek, K. Miller, J. Laporte, R. Kikinis, and S. K. Warfield, “Computing reaction forces on surgical tools for robotic neurosurgery and surgical simulation,” in *Proc. of Australasian Conference on Robotics and Automation ACRA, Canberra, Australia*, pp. 1–8, 2004.
- [70] R. Sakai, M. Itoman, and K. Mabuchi, “Assessments of different kinds of stems by experiments and FEM analysis: Appropriate stress distribution on a hip prosthesis,” *Clinical Biomechanics* **21**(8), pp. 826–833, 2006.
- [71] J. Wismans, *Design tools: Human body modeling*, pp. 227–268. Vehicle crashworthiness and occupant protection, Michigan: American Iron and Steel Institute, 2004.
- [72] R. R. McHenry, “Analysis of the Dynamics of Automobile Passenger-Restraint Systems,” in *Stapp Car Crash and Field Demonstration Conference*, pp. 207–248, 1963.
- [73] R. Happee, A. Janssen, E. Fraterman, J. Monster, and R. Happee, “Application of MADYMO Occupant Models in LS-DYNA/MADYMO Coupling,” in *4th European LS-DYNA Users Conference*, pp. 3–10, 2003.

- [74] S. Figgins, “Biomechanics and the Cyberhuman,” *IEEE Computer Graphics and Applications*, pp. 14–20, 2002.
- [75] M. Iwamoto, Y. Kisanuki, I. Watanabe, K. Furusu, K. Miki, and J. Hasegawa, “Development of a Finite Element Model of the Total Human Model for Safety (THUMS) and Application to Injury Reconstruction,” in *Proceedings of the 2002 IRCOBI International Conference The BRIDGE*, pp. 31–42, 2002.
- [76] J. P. C. Kleijnen, *Statistical Tools for Simulation Practitioners*, Marcel Dekker Inc, 1987.
- [77] L. A. Schmit and A. Farshlf, “Some Approximation Concepts for Structural Synthesis,” *AIAA Journal* **12**(5), pp. 692–699, 1974.
- [78] J. F. M. Barthelemy and R. Haftka, “Approximation concepts for optimum structural design: a review,” *Structural and Multidisciplinary Optimization* **5**(3), pp. 129–144, 1993.
- [79] A. Schoofs, M. Klink, and D. van Campen, “Approximation of structural optimization problems by means of designed numerical experiments,” *Structural and Multidisciplinary Optimization* **4**(3), pp. 206–212, 1992.
- [80] L. Etman, J. Adriaens, M. van Slagmaat, and A. Schoofs, “Crashworthiness design optimization using multipoint sequential linear programming,” *Structural and Multidisciplinary Optimization* **12**(4), pp. 222–228, 1996.
- [81] U. Schramm, H. Thomas, and D. Schneider, “Crashworthiness design using structural optimization,” in *AIAA-98-4729, 7th AIAA/USAF/NASA/ISSMO Symposium on Multidisciplinary Analysis and optimization, Missouri, AIAA Paper*, pp. 197–205, 1998.
- [82] K. Yamazaki and J. Han, “Maximization of the crushing energy absorption of tubes,” *Structural and Multidisciplinary Optimization* **16**(1), pp. 37–46, 1998.

- [83] J. Han and K. Yamazaki, “A Study on Maximization of Dynamic Crushing Energy Absorption of Square Tubes with and without Stiffener,” *JSME International Journal Series A* **43**(2), pp. 138–145, 2000.
- [84] J. Han and K. Yamazaki, “Crashworthiness optimisation of S-shape square tubes,” *International Journal of Vehicle Design* **31**(1), pp. 72–85, 2003.
- [85] P. O. Marklund and L. Nilsson, “Optimization of airbag inflation parameters for the minimization of out of position occupant injury,” *Computational Mechanics* **31**(6), pp. 496–504, 2003.
- [86] K. Craig, N. Stander, D. Dooge, and S. Varadappa, “Automotive crashworthiness design using response surface-based variable screening and optimization,” *Engineering Computations* **22**(1), pp. 38–61, 2005.
- [87] Y. Liu, “Optimum design of straight thin-walled box section beams for crashworthiness analysis,” *Finite Elements in Analysis and Design*, **44**(3), pp. 139–147, 2008.
- [88] Y. Liu, “Crashworthiness design of multi-corner thin-walled columns,” *Thin-Walled Structures* **46**(12), pp. 1329–1337, 2008.
- [89] J. Van Slycken, P. Verleysen, J. Degrieck, J. Bouquerel, and B. C. De Cooman, “Crashworthiness characterization and modelling of high-strength steels for automotive applications,” *Proceedings of the Institution of Mechanical Engineers, Part D: Journal of Automobile Engineering* **220**(4), pp. 391–400, 2006.
- [90] N. Peixinho and A. Pinho, “Study of viscoplasticity models for the impact behavior of high-strength steels,” *Journal of Computational and Nonlinear Dynamics* **2**(2), pp. 114–123, 2007.
- [91] W. D. Callister, *Materials Science and Engineering An Introduction.*, John Wiley & Sons Inc, 2007.

- [92] S. J. Hosseinipour and G. H. Daneshi, “Energy absorption and mean crushing load of thin-walled grooved tubes under axial compression,” *Thin-Walled Structures* **41**(1), pp. 31–46, 2003.
- [93] C. J. George, J. M. Starbuck, J. F. Fellers, S. Simunovic, and R. G. Boeman, “Crashworthiness of various random chopped carbon fiber reinforced epoxy composite materials and their strain rate dependence,” *Journal of Applied Polymer Science* **101**(3), pp. 1477–1486, 2006.
- [94] E. Mahdi, A. S. Mokhtar, N. A. Asari, F. Elfaki, and E. J. Abdullah, “Nonlinear finite element analysis of axially crushed cotton fibre composite corrugated tubes,” *Composite Structures* **75**(1), pp. 39–48, 2006.
- [95] A. I. Taub, P. E. Krajewski, A. A. Luo, and J. N. Owens, “The evolution of technology for materials processing over the last 50 years: The automotive example,” *JOM* **59**(2), pp. 48–57, 2007.
- [96] A. G. Caliskan, R. A. Jeryan, H. Mees, and S. Iregbu, “Experimental and analytical study of the crashworthiness for the 2005 Ford GT aluminum space-frame,” in *ASME International Mechanical Engineering Congress and Exposition*, Orlando, FL, United States, pp. 427–438, 2005.
- [97] R. Krauskopf, *Introduction to Geochemistry*, McGraw-Hill, 2003.
- [98] S. Das, “Magnesium for automotive applications: Primary production cost assessment,” *JOM Journal of the Minerals, Metals and Materials Society* **55**(11), pp. 22–26, 2003.
- [99] S. Das, “Primary magnesium production costs for automotive applications,” *JOM* **60**(11), pp. 63–69, 2008.
- [100] K. U. Kainer, *Magnesium Alloys and Technologies*, Wiley-VCH, 2003.
- [101] M. Nehan and R. Maloney, “Magnesium AM60B instrument panel structure for crashworthiness FMVSS 204 and 208 compliance,” *SAE Technical Paper 960419*, 1996.

- [102] C. A. Newland and M. T. Murray, “Strain rate dependent behavior of magnesium-based alloys,” in *Proceedings of the First Australasian Congress on Applied Mechanics: ACAM-96*, pp. 73–76, 1996.
- [103] T. Abbott, M. Easton, and R. Schmidt, “Magnesium for crashworthy components,” *JOM Journal of the Minerals, Metals and Materials Society*, pp. 227–230, 2003.
- [104] M. Easton, A. Beer, M. Barnett, C. Davies, G. Dunlop, Y. Durandet, S. Blacket, T. Hilditch, and P. Beggs, “Magnesium alloy applications in automotive structures,” *JOM* **60**(11), pp. 57–62, 2008.
- [105] S. S. Rao, *The finite element method in engineering*, Butterworth Heinemann, 2005.
- [106] O. Zienkiewicz, *The finite element method*, McGraw-Hill, 1977.
- [107] J. N. Reddy, *An introduction to nonlinear finite element analysis*, Oxford University Press, 2004.
- [108] T. Belytschko, W. K. Liu, and B. Moran, *Nonlinear Finite Elements for Continua and Structures*, Wiley, 2000.
- [109] R. D. Cook, D. S. Malkus, M. E. Plesha, and R. J. Witt, *Concepts and Applications of Finite Element Analysis*, Wiley, 2001.
- [110] J. O. Hallquist, *LS-DYNA Theory Manual*, Livermore Software Technology Corporation, 2006.
- [111] H. T. Y. Yang, S. Saigal, A. Masud, and R. K. Kapania, “A survey of recent shell finite elements,” *International Journal for Numerical Methods in Engineering* **47**(1-3), pp. 101–127, 2000.
- [112] T. Hughes and W. Liu, “Nonlinear Finite Element Analysis of Shells: Part I. Three-Dimensional Shells,” *Computer Methods in Applied Mechanics and Engineering* **26**(3), pp. 331–362, 1981.

- [113] T. Hughes and W. Liu, “Nonlinear finite element analysis of shells. Part II- Two-dimensional shells,” *Computer Methods in Applied Mechanics and Engineering* **27**, pp. 167–181, 1981.
- [114] LSTC, *LS-DYNA 971 manual*, Livermore Software Technology Company, 2007.
- [115] T. Belytschko and W. Bachrach, “Efficient implementation of quadrilaterals with high coarse-mesh accuracy.,” *Computer Methods in Applied Mechanics and Engineering* **54**(3), pp. 279–302, 1986.
- [116] A. H. Marchertas and T. B. Belytschko, *Nonlinear Finite Element Formulation for Transient Analysis of Three Dimensional Thin Structures, Technical Report ANL-8104*, Argonne National Laboratory, 1974.
- [117] J. Kennedy, T. Belytschko, and J. Lin, “Recent developments in explicit finite element techniques and their application to reactor structures.,” *Nuclear Engineering and Design* **97**(1), pp. 1–24, 1986.
- [118] T. Belytschko and I. Leviathan, “Projection schemes for one-point quadrature shell elements,” *Computer methods in applied mechanics and engineering* **115**(3-4), pp. 277–286, 1994.
- [119] T. Belytschko, B. Wong, and H. Chiang, “Improvements in low-order shell elements for explicit transient analysis,” *Analytical and computational models of shells* , pp. 383–398, 1989.
- [120] B. Engelmann, R. Whirley, and G. Goudreau, “A simple shell element formulation for large-scale elastoplastic analysis,” in *Winter annual meeting of the American Society of Mechanical Engineers*, 1989.
- [121] J. L. Batoz, K. J. Bathe, and L. W. Ho, “A study of three-node triangular plate bending elements,” *International Journal for Numerical Methods in Engineering* **15**, pp. 1771–1812, 1980.

- [122] L. S. D. Morley, “The constant-moment plate-bending element,” *The Journal of Strain Analysis for Engineering Design* **6**(1), pp. 20–24, 1971.
- [123] G. Wempner, “Finite elements, finite rotations and small strains of flexible shells,” *International Journal of Solids and Structures* **5**, pp. 117–153, 1969.
- [124] T. Belytschko and B. Hsieh, “Non-linear transient finite element analysis with convected co-ordinates,” *International Journal for Numerical Methods in Engineering* **7**(3), pp. 255–271, 1973.
- [125] J. M. Battini and C. Pacoste, “Plastic instability of beam structures using co-rotational elements,” *Computer Methods in Applied Mechanics and Engineering* **191**(51-52), pp. 5811–5831, 2002.
- [126] P. Khosravi, R. Ganesan, and R. Sedaghati, “Corotational non-linear analysis of thin plates and shells using a new shell element,” *International Journal for Numerical Methods in Engineering* **69**(4), pp. 859–885, 2007.
- [127] H. Stolarski, T. Belytschko, and S. H. O. Lee, “A review of shell finite elements and corotational theories,” *Computational mechanics advances* **2**(2), pp. 125–212, 1995.
- [128] N. Cristescu, *Dynamic plasticity.*, North-Holland Pub. Co., 1967.
- [129] L. Kollar and E. Dulacsha, *Buckling of Shells for Engineers*, John Wiley & Sons, 1984.
- [130] A. Otubushin, “Detailed validation of a non-linear finite element code using dynamic axial crushing of a square tube,” *International Journal of Impact Engineering*, **21**(5), pp. 349–368, 1998.
- [131] W. Abramowicz and N. Jones, “Dynamic axial crushing of square tubes,” *International Journal of Impact Engineering*, **2**(2), pp. 179–208, 1984.
- [132] M. Langseth, O. S. Hopperstad, and T. Berstad, “Crashworthiness of aluminium extrusions: validation of numerical simulation, effect of mass ratio and impact

- velocity,” *International Journal of Impact Engineering*, **22**(9-10), pp. 829–854, 1999.
- [133] K. Kormi, V. N. Wijayathunga, D. C. Webb, and S. T. . S. Al-Hassani, “FE investigation of a spirally slotted tube under axially compressive static and dynamic impact loading,” *International Journal of Crashworthiness* **8**(5), pp. 421–432, 2003.
- [134] L. Zheng and T. Wierzbicki, “Quasi-static crushing of s-shaped aluminum front rail,” *International Journal of Crashworthiness* **9**(2), pp. 155–173, 2004.
- [135] P. Hosseini-Tehrani and M. Nikahd, “Effects of ribs on s-frame crashworthiness,” *Proceedings of the Institution of Mechanical Engineers, Part D: Journal of Automobile Engineering* **220**(12), pp. 1679–1690, 2006.
- [136] P. Hosseini-Tehrani and M. Nikahd, “Two materials s-frame representation for improving crashworthiness and lightening,” *Thin-Walled Structures* **44**(4), pp. 407–414, 2006.
- [137] R. Hosseinzadeh, M. M. Shokrieh, and L. B. Lessard, “Parametric study of automotive composite bumper beams subjected to low-velocity impacts,” *Composite Structures* **68**(4), pp. 419–427, 2005.
- [138] M. Mao, E. Chirwa, and T. Chen, “Reinforcement of vehicle roof structure system against rollover occupant injuries,” *International Journal of Crashworthiness* **12**(1), pp. 41–55, 2007.
- [139] A. Zaouk, D. Marzougui, and N. Bedewi, “Development of a Detailed Vehicle Finite Element Model Part I: Methodology,” *International Journal of Crashworthiness* **5**(1), pp. 25–36, 2000.
- [140] A. Zaouk, D. Marzougui, and C. Kan, “Development of a Detailed Vehicle Finite Element Model Part II: Material Characterization and Component Testing,” *International Journal of Crashworthiness* **5**(1), pp. 37–50, 2000.

- [141] L. Kwasniewski, H. Li, R. Nimbalkar, and J. Wekezer, “Crashworthiness assessment of a paratransit bus,” *International Journal of Impact Engineering*, **32**(5), pp. 883–888, 2006.
- [142] W. Qi, X. L. Jin, and X. Y. Zhang, “Improvement of energy-absorbing structures of a commercial vehicle for crashworthiness using finite element method,” *The International Journal of Advanced Manufacturing Technology* **30**(11), pp. 1001–1009, 2006.
- [143] X. Zhang, X. Jin, W. Qi, and X. Hou, “Vehicle crash accident reconstruction based on fem and neural networks,” *Jixie Gongcheng Xuebao/Chinese Journal of Mechanical Engineering* **43**(3), pp. 143–147, 2007.
- [144] R. Maruthayappan, A. Rao, V. Gupta, and R. R. Samaha, “Improved finite element sid for in-vehicle simulation,” *SAE Technical Paper 1999-01-0716* , 1999.
- [145] P. J. Arnoux, S. Joonekindt, L. Thollon, and K. Kayvantash, “Radioss finite element model of the thor dummy,” *International Journal of Crashworthiness* **8**(6), pp. 529–541, 2003.
- [146] C. S. Shah, M. Maddali, S. A. Mungikar, P. D. Beillas, W. N. Hardy, K. H. Yang, P. Bedewi, K. H. Digges, and J. S. Augenstein, “Analysis of a real-world crash using finite element modeling to examine traumatic rupture of the aorta,” *SAE Technical Paper 2005-01-1293* , 2005.
- [147] Y. Kitagawa, T. Yasuki, and J. Hasegawa, “A study of cervical spine kinematics and joint capsule strain in rear impacts using a human FE model,” *SAE Technical Paper 2006-22-0020* , 2006.
- [148] J. Kim, “Influence of occupant restraint system on traumatic brain injuries,” *International Journal of Crashworthiness* **13**(1), pp. 25–40, 2008.

- [149] Y. Takahashi, Y. Kikuchi, A. Konosu, and H. Ishikawa, "Development and validation of the finite element model for the human lower limb of pedestrians," *SAE Technical Paper 2000-01-SC22*, 2000.
- [150] J. W. Lee, K. H. Yoon, Y. S. Kang, and G. J. Park, "Vehicle hood and bumper structure design to mitigate casualties of pedestrian accidents," in *The 19th International Technical Conference on The Enhanced Safety of Vehicles, Washington DC*, pp. 6–9, 2005.
- [151] T. Yasuki, "Mechanism analysis of pedestrian knee-bending angle by sedan-type vehicle using human fe model," *International Journal of Crashworthiness* **12**(4), pp. 329–340, 2007.
- [152] A. A. A. Alghamdi, "Collapsible impact energy absorbers: an overview," *Thin-Walled Structures*, **39**(2), pp. 189–213, 2001.
- [153] K. R. F. Andrews, G. L. England, and E. Ghani, "Classification of the axial collapse of cylindrical tubes under quasi-static loading," *International Journal of Mechanical Sciences*, **25**(9-10), pp. 687–696, 1983.
- [154] "Altair HyperMesh", <http://www.altairhyperworks.com/default.aspx>, accessed on May 2009.
- [155] E. A. Avallone and T. Baumeister, *Marks' Standard Handbook for Mechanical Engineers*, McGraw-Hill Professional, 1996.
- [156] S. R. Wu and N. Saha, "Some challenges to crashworthiness analysis," *SAE Technical Paper 2006-01-0669*, 2006.
- [157] N. El-Abbasi and S. Meguid, "A new shell element accounting for through-thickness deformation," *Computer Methods in Applied Mechanics and Engineering* **189**(3), pp. 841–862, 2000.
- [158] R. A. Fisher, *The Design of Experiments*, Macmillan Pub Co, 1971.

- [159] J. Antony, *Design of Experiments for Engineers and Scientists*, Butterworth-Heinemann, 2003.
- [160] G. D. Dandrock and A. G. Holms, “Statistical design and analysis of optimum seeking experiments to develop a gamma-prime strengthened cobalt-nickel base alloy,” Tech. Rep. AD0175306, National Aeronautics and Space Administration Cleveland Ohio Lewis Research Center, Washington, D. C., 1969.
- [161] D. C. Montgomery, *Design and Analysis of Experiments*, Wiley, 2008.
- [162] R. Koshal, “Application of the method of maximum likelihood to the improvement of curves fitted by the method of moments,” *Journal of the Royal Statistical Society, Series A* **96**, pp. 303–313, 1933.
- [163] R. H. Myers and D. C. Montgomery, *Response surface methodology : process and product optimization using designed experiments*, Wiley, 1995.
- [164] G. Venter and R. Haftka, “Minimum-Bias based experimental design for constructing surfaces in structural optimization,” in *Proceedings of the 38th AIAA/ASME/ASCE/AHS/ASC Structures, Structural Dynamics, and Materials Conference, Kissimmee, Florida*, **2**, pp. 1225–1238, 1997.
- [165] D. Ashlock, *Evolutionary Computation for Modeling and Optimization*, Springer, 2005.
- [166] T. J. Mitchell, “An algorithm for the construction of D-optimal experimental designs,” *Technometrics* **42**(1), pp. 48–54, 2000.
- [167] M. Redhe, J. Forsberge, T. Janssone, P. O. Marklund, and L. Nilsson, “Using the response surface methodology and the D-optimality criterion in crashworthiness related problems,” *Structural and Multidisciplinary Optimization* **24**(3), pp. 185–194, 2002.
- [168] M. McKay, R. Beckman, and W. Conover, “A Comparison of Three Methods for Selecting Values of Input Variables in the Analysis of Output from a Computer Code,” *Technometrics* **21**(2), pp. 239–245, 1979.

- [169] J. Sacks, W. J. Welch, T. J. Mitchell, and H. P. Wynn, “Design and Analysis of Computer Experiments,” *Statistical Science* **4**(4), pp. 409–435, 1989.
- [170] W. Welch, T. Yu, S. Kang, and J. Sacks, “Computer experiments for quality control by parameter design,” *Journal of Quality Technology* **22**(1), pp. 15–22, 1990.
- [171] J. Sacks, S. Schiller, and W. Welch, “Designs for computer experiments,” *Technometrics* **31**(1), pp. 41–47, 1989.
- [172] D. Van Campen, R. Nagtegaal, and A. Schoofs, “Approximation methods in structural optimization using experimental designs for multiple responses,” *Multicriteria Design Optimization-Procedures and Applications*, Springer-Verlag: Berlin, Heidelberg, New York , pp. 205–228, 1990.
- [173] A. Giunta, *Noisy Aerodynamic Response and Smooth Approximations in HSCT Design*. PhD thesis, Virginia Polytechnic Institute and State University, 1994.
- [174] W. Roux, *Structural Optimization using Response Surface Approximations*. PhD thesis, University of Pretoria, 1997.
- [175] Q. S. Xu, Y. Z. Liang, and K. T. Fang, “The effects of different experimental designs on parameter estimation in the kinetics of a reversible chemical reaction,” *Chemometrics and Intelligent Laboratory Systems* **52**(2), pp. 155–166, 2000.
- [176] W. J. Roux, N. Stander, and R. T. Haftka, “Response surface approximations for structural optimization,” *International Journal for Numerical Methods in Engineering* **42**(3), pp. 517–534, 1998.
- [177] F. Mistree, B. Patel, and S. Vadde, “On modeling multiple objectives and multi-level decisions in concurrent design,” *Advances in Design Automation* **69**(2), pp. 151–161, 1994.

- [178] G. Box and K. Wilson, "On the experimental attainment of optimum conditions," *Journal of the Royal Statistical Society - Series B* **13**, pp. 1–45, 1951.
- [179] G. Box and N. Draper, *Empirical Model-Building and Response Surfaces*, Wiley, 1987.
- [180] A. I. Khuri and J. A. Cornell, *Response Surfaces: Designs and Analyses*, CRC Press, 1996.
- [181] R. H. Myers, D. C. Montgomery, G. G. Vining, C. M. Borrer, and S. M. Kowalski, "Response surface methodology: A retrospective and literature survey," *Journal of quality technology* **36**(1), pp. 53–77, 2004.
- [182] D. C. Montgomery, E. A. Peck, and G. G. Vining, *Introduction to linear regression analysis*, J. Wiley & Sons, 2006.
- [183] D. Krige, "A statistical approach to some mine valuations and allied problem on the Witwatersrand, Unpubl," Master's thesis, University of Witwatersrand, 1951.
- [184] K. Gurney, *An Introduction to Neural Networks*, CRC, 1997.
- [185] T. Simpson, J. Poplinski, P. Koch, and J. Allen, "Metamodels for Computer-based Engineering Design: Survey and recommendations," *Engineering with Computers* **17**(2), pp. 129–150, 2001.
- [186] U. M. Fayyad, *Advances in knowledge discovery and data mining*, MIT Press, 1996.
- [187] H. Lu, R. Setiono, and H. Liu, "Effective Data Mining Using Neural Networks," *IEEE Transactions on Knowledge and Data Engineering* , pp. 957–961, 1996.
- [188] M. Kantardzic, *Data Mining: Concepts, Models, Methods, and Algorithms*, Wiley-IEEE Press, 2002.

- [189] M. El-Gindy and L. Palkovics, “Possible Application of Artificial Neural Networks to Vehicle Dynamics and Control: A Literature Review.,” *International Journal of Vehicle Design* **14**(5/6), pp. 592–614, 1993.
- [190] T. Omar, A. Eskandarian, and N. Bedewi, “Vehicle crash modelling using recurrent neural networks,” *Mathematical and Computer Modelling* **28**(9), pp. 31–42, 1998.
- [191] P. Hajela and E. Lee, “Topological optimization of rotorcraft subfloor structures for crashworthiness considerations,” *Computers and Structures* **64**(1-4), pp. 65–76, 1997.
- [192] T. W. Simpson, J. D. Peplinski, P. N. Koch, and J. K. Allen, “Metamodels for computer-based engineering design: survey and recommendations,” *Engineering with Computers* **17**(2), pp. 129–150, 2001.
- [193] M. Meckesheimer, R. R. Barton, T. Simpson, F. Limayem, and B. Yannou, “Metamodeling of combined discrete/continuous responses,” *AIAA Journal* **39**(10), pp. 1950–1959, 2001.
- [194] R. Jin, W. Chen, and A. Sudjianto, “On sequential sampling for global meta-modeling in engineering design,” in *ASME 2002 Design Engineering Technical Conferences and Computer and Information in Engineering Conference*, 2002.
- [195] N. Stander and K. J. Craig, “On the robustness of a simple domain reduction scheme for simulation-based optimization,” *Engineering Computations* **19**(4), pp. 431–450, 2002.
- [196] H. Kurtaran, A. Eskandarian, D. Marzougui, and N. E. Bedewi, “Crashworthiness design optimization using successive response surface approximations,” *Computational Mechanics* **29**(4), pp. 409–421, 2002.
- [197] N. Stander, W. J. Roux, M. Giger, M. Redhe, N. Fedorova, and J. Haarhoff, “Crashworthiness optimization in LS-OPT: Case studies in metamodeling and

- random search techniques,” in *Proceedings of the 4 th European LS-DYNA Conference, Ulm, Germany*, pp. 11–26, 2003.
- [198] H. H. Rosenbrock, “An automatic method for finding the greatest or least value of a function,” *The Computer Journal* **3**(3), pp. 175–184, 1960.
- [199] K. A. De Jong, *Analysis of the behavior of a class of genetic adaptive systems*. PhD thesis, University of Michigan, 1975.
- [200] R. M. Lewis, V. Torczon, and M. W. Trosset, “Direct search methods: then and now,” *Journal of Computational and Applied Mathematics* **124**(1-2), pp. 191–207, 2000.
- [201] J. C. Brown, A. J. Robertson, and S. T. Serpento, *Motor Vehicle Structures: Concepts and Fundamentals*, SAE International, 2001.
- [202] J. S. Arora, *Introduction to optimum design*, McGraw-Hill, New York, 1989.
- [203] “NCAC models, Finite Element Model Archive, <http://www.ncac.gwu.edu/vml/models.html>,” accessed on May 2009.
- [204] L. M. Patrick and T. B. Sato, “Methods of Establishing Human Tolerance Levels: Cadaver and Animal Research and Clinical Observations,” *Impact Injury and Crash Protection* , pp. 259–274, 1970.
- [205] A. King, J. Ruan, C. Zhou, W. Hardy, and T. Khalil, “Recent advances in biomechanics of brain injury research: a review,” *J Neurotrauma* **12**(4), pp. 651–658, 1995.
- [206] K. H. Yang, J. Hu, N. A. White, A. I. King, C. C. Chou, and P. Prasad, “Development of numerical models for injury biomechanics research: a review of 50 years of publications in the stapp car crash conference,” *Stapp Car Crash Journal* **50**, pp. 429–490, 2006.
- [207] J. Benedyk, “Light metals in automotive applications,” *Light metal age - Chicago* **58**, pp. 34–35, 2000.

- [208] R. Kurzweil, *Alan Turing: Life and Legacy of a Great Thinker (The law of accelerating returns)*, pp. 381–416. Springer, 2006.
- [209] P. Spethmann, S. H. Thomke, and C. Herstatt, “The Impact of Crash Simulation on Productivity and Problem-Solving in Automotive R&D,” in *The R&D Management Conference 2006, The challenges and opportunities of R&D management*, 2006.
- [210] “Data extracted from various sources from the published literature.”
- [211] V. Pareto, *Manuale di Economia Politica, Societa Editrice Libreria, Milano, Italy, 1906. Translated into English by AS Schwier as Manual of Political Economy*, Macmillan, 1971.
- [212] O. L. de Weck and M. B. Jones, “Isoperformance: Analysis and Design of Complex Systems with Known or Desired Outcomes,” in *14 th Annual International Symposium of the International Council on Systems Engineering (INCOSE)*, 2004.
- [213] J. Branke, *Multiobjective optimization : interactive and evolutionary approaches*, Springer, 2008.
- [214] K. E. Lewis, W. Chen, and L. C. Schmidt, *Decision making in engineering design*, ASME Press, 2006.
- [215] K. J. Cherkauer and J. W. Shavlik, “Growing simple decision trees to facilitate knowledge discovery,” in *Second International Conference on Knowledge Discovery and Data mining.*, pp. 315–318, 1998.
- [216] A. A. Freitas, “A critical review of multi-objective optimization in data mining: a position paper,” *ACM SIGKDD Explorations Newsletter* **6**(2), pp. 77–86, 2004.
- [217] C. A. Coello, “An updated survey of GA-based multiobjective optimization techniques,” *ACM Computing Surveys (CSUR)* **32**(2), pp. 109–143, 2000.

- [218] J. D. Schaffer, “Multiple objective optimization with vector evaluated genetic algorithms,” in *Proceedings of the 1st International Conference on Genetic Algorithms*, pp. 93–100, 1985.
- [219] D. E. Goldberg, *Genetic Algorithms in Search, Optimization and Machine Learning*, Addison-Wesley Longman Publishing Co., Inc. Boston, MA, USA, 1989.
- [220] K. Deb, “Evolutionary algorithms for multi-criterion optimization in engineering design,” *Evolutionary Algorithms in Engineering and Computer Science*, pp. 135–161, 1999.
- [221] C. A. Coello, D. A. Van Veldhuizen, and G. B. Lamont, *Evolutionary Algorithms for Solving Multi-Objective Problems*, Springer, 2002.
- [222] D. W. Corne, K. Deb, P. J. Fleming, and J. D. Knowles, “The good of the many outweighs the good of the one: evolutionary multi-objective optimization,” *IEEE Connections Newsletter* **1**(1), pp. 9–13, 2003.
- [223] C. Darwin, *On the Origin of Species: By Means of Natural Selection*, Dover Publications, 2006.
- [224] S. Erturk, D. Steglich, J. Bohlen, D. Letzig, and W. Brocks, “Modelling and simulation of extrusion of magnesium alloys,” *International Journal of Material Forming* **1**, pp. 419–422, 2008.
- [225] P. Venkataraman, *Applied optimization with MATLAB programming*, Wiley-Interscience, 2002.
- [226] D. Du and P. Pardalos, *Handbook of combinatorial optimization*, Kluwer Academic Publishers, 1998.
- [227] N. Jones, *Structural Crashworthiness*, Butterworth-Heinemann, 1983.
- [228] N. Sharpe, R. Vendrig, and K. Houtzager, “Improved design for frontal protection,” *SAE Technical Paper 2001-06-0137*, 2001.

- [229] Y. Motozawa and T. Kamei, “A new concept for occupant deceleration control in a crash,” *SAE Technical Paper 2000-01-0881*, 2000.
- [230] M. Yamaya and M. Tani, “Energy Absorption by the Plastic Deformation of Sheet Metal Columns with Box-Shaped Cross Section,” *Technical Review, Mitsubishi Heavy Industries, Ltd., Japan*, pp. 59–66, 1971.
- [231] T. Masanori and A. Funahashi, “Energy Absorption by the Plastic Deformation of Body Structural Members,” *SAE Technical paper 780368*, 1978.
- [232] M. D. White and N. Jones, “A theoretical analysis for the dynamic axial crushing of top-hat and double-hat thin-walled sections,” *Proceedings of the Institution of Mechanical Engineers, Part D: Journal of Automobile Engineering* **213**(4), pp. 307–325, 1999.
- [233] C. S. Cha, J. Y. Kang, and I. Y. Yang, “Axial Impact Collapse Analysis of Spot Welded Hat Shaped Section Members,” *KSME International Journal* **15**(2), pp. 180–191, 2001.
- [234] J. M. Starbuck, S. Simunovic, and G. C. Jacob, “Test Methodologies for Determining Energy-Absorbing Mechanisms of Automotive Composite Material Systems,” *SAE Transactions: Journal of Materials & Manufacturing* **109**, pp. 850–855, 2000.
- [235] C. Krauss, “A parametric study of crush initiators for a thin-walled tube,” *International Journal of Vehicle Design* **15**(3), pp. 385–401, 1994.